

Method Development towards Probing the Gut Metabolome using Reverse Phase Liquid  
Chromatography - Ion Mobility - Mass Spectrometry

By

James Christopher Poland

Dissertation

Submitted to the Faculty of the  
Graduate School of Vanderbilt University  
in partial fulfillment of the requirements  
for the degree of

DOCTOR OF PHILOSOPHY

in

Chemistry

May, 8<sup>st</sup>, 2020

Nashville, Tennessee

Approved:

John A. McLean

David E. Cliffl

Brian O. Bachmann

Melissa A. Farrow

Copyright © 2020 by James Poland  
All Rights Reserved

## ACKNOWLEDGEMENTS

I would like to thank my dissertation advisor, Dr. John A. McLean for the opportunity to work in his group while allowing me to explore my personal scientific curiosity. The interdisciplinary nature of the research the McLean lab and the collaborative spirit allowed me to flourish as a scientist. I am grateful for his mentoring, both in and out of the lab, and guidance. It has been a true honor to complete my dissertation research in the McLean group.

I would also like to thank my dissertation committee members, Dr. David E. Cliffler, Dr. Brian O. Bachmann, and Dr. Melissa A. Farrow for their insight and direction. Their advice helped to broaden my scope while reminding me to stay focus on the bigger picture.

This research would be impossible without the many collaborators that pushed me to be a better scientist. This includes Dr. Charles Robb Flynn, Dr. Sean Davies, and Dr. Seth Bordenstein. Their work in the microbiome sparked such a deep curiosity in me that it shaped the rest of my dissertation research. They allowed me to work with them to determine how the metabolome fits into this growing area of research.

I would also like to thank the Fisk-Vanderbilt Bridge Program for not only being a source of strength, but providing financial support for a portion of this research. This includes Dr. Keivan Stassun, Dr. Dina Stroud, Dr. Natalie Arnett, and Dr. Lauren Campbell for giving me the confidence to persevere when I would lose confidence in myself.

Additionally, I would like to thank my colleagues in the McLean group throughout the years for continued support, motivation, and stimulating discussion. The instrumentation expertise offered by Dr. Stacy Sherrod allowed me to develop many of the methods discussed in this work. In particular, I would like to acknowledge Dr. Sarah M. Stow and Dr. Nichole M. Lareau

for their continued support. The friendship, willingness to help, and experience laid the ground work for the direction of my thesis work and graduate experience. I would also like to thank Berkley M. Ellis, Rachel A. Harris, and Jacqueline A. Picache, for the insightful discussions and comradery.

I would like to thank my family for their support and encouragement throughout my time as a graduate student. My parents provided a great deal of understanding when I would choose science over visitation. To my father, you have taught me respect and patience and how to wait until the time is right. You became a sounding board when I needed to vent and a source of strength when I felt weak. I am forever grateful. To my mother, I watched as you overcome odds at every step, and it resonated with me when I needed it the most. To my Grandmother Linda, I hear your voice with every decision that I make; It never fails to put a smile on my face. Your contagious laugh can be heard no matter how far away from home I am.

I would also like to thank my Nashville family. My church community at Glendale United Methodist and the rugby community provided by the Nashville Grizzlies gave me an outlet away from lab. The Adair family and Hosford clan gave me food and warmth during holidays. I would like to give a special thank you to Justin Hosford, Sharee Burneen, Michael Cochran, and Scott Kelly for always being there for me, regardless of the hour. They provided an amazing support system while I was so far from home. Our vigorous debates kept my mind sharp and reminded me of my family. I am eternally grateful for all that you have provided.

Lastly, I would like to acknowledge the funding sources for this research: the Vanderbilt Institute of Chemical Biology, the College of Arts and Science, the Center for Innovative Technologies, the Vanderbilt Chemical Biology Interface training program, and the Fisk-Vanderbilt Master to PhD. Bridge Program.

## TABLE OF CONTENTS

	Page
ACKNOWLEDGEMENTS.....	iii
LIST OF TABLES.....	vii
LIST OF FIGURES.....	viii
Chapter	
I. FUNDAMENTALS OF ION MOBILITY-MASS SPECTROMETRY FOR THE ANALYSIS OF BIOMOLECULES.....	1
1.1. Origins of Biomolecular Analysis by Ion mobility-Mass Spectrometry.....	1
1.2. Biomolecular Separation and Analytical Utility of IM-MS.....	4
1.3. Instrumentation Considerations.....	8
1.3.1. Chromatography.....	8
1.3.2. Ion Sources.....	8
1.3.3. Time-Dispersive Ion Mobility Techniques.....	11
1.3.4. Mass Spectrometry Considerations.....	13
1.4. Introduction to Current Trends.....	15
1.5. Integrating Ion Mobility for Omics Analysis.....	15
1.5.1. Proteomics.....	17
1.5.2. Lipidomics.....	18
1.5.3. Metabolomics.....	22
1.6. Continuing Advancements in IM-MS Technology.....	26
1.7. Future Remarks on IM-MS in Multi-omics Studies.....	32
1.8. Acknowledgements.....	34
1.9. references.....	35
II. INTEGRATED, HIGH-THROUGHPUT, MULTIOMICS PLATFORM ENABLES DATA-DRIVEN CONSTRUCTION OF CELLULAR RESPONSES AND REVEALS GLOBAL DRUG MECHANISM OF ACTION.....	50
2.1. Introduction.....	50
2.2. Experimental Details.....	52
2.2.1. Metabolite Extraction.....	52
2.2.2. Metabolomic Mass Spectrometry Analysis.....	53
2.2.3. Metabolite Data Processing and Analysis.....	54
2.3. Results and Discussion.....	55
2.3.1. Metabolomic Analysis.....	57
2.4. Remarks and Perspective.....	60
2.5. Acknowledgements.....	61

2.6 References .....	61
III. COLLISION CROSS SECTION CONFORMATIONAL ANALYSES OF BILE ACIDS VIA ION MOBILITY-MASS SPECTROMETRY .....	64
3.1. Introduction .....	64
3.2. Methods .....	67
3.2.1. Standards and Chemicals.....	67
3.2.2. Measurements of CCS of Bile Acids .....	67
3.3. Discussion .....	68
3.4. Conclusion.....	75
3.5. Acknowledgements .....	77
3.6. References .....	77
IV. UTILIZING UNTARGETED ION MOBILITY-MASS SPECTROMETRY TO PROFILE CHANGES IN THE GUT METABOLOME FOLLOWING BILIARY DIVERSION SURGERY .....	80
4.1. Introduction .....	80
4.2. Experimental Methods .....	83
4.2.1. Standards and Chemicals.....	83
4.2.2. Surgery and Fecal Collection .....	85
4.2.3. Fecal Metabolite Extraction and Preparation .....	85
4.2.4. Data Analysis.....	88
4.3. Results and Discussions .....	89
4.3.1. Bile Acids Separation Optimization.....	89
4.3.2. Global, Untargeted Analysis of Fecal Metabolite Profiling.....	90
4.3.3. Application of the Untargeted LC-IM-MS Method to Mouse Feces following Bile Diversion Surgery.....	91
4.4. Conclusion .....	97
4.5. Acknowledgements.....	97
4.6. References.....	97
V. CONCLUSION AND FUTURE DIRECTIONS FOR ION MOBILITY-MASS SPECTROMETRY BASED METHODS TO PROBE MICROBIOME-HOST INTERACTIONS.....	101
5.1. Summary .....	101
5.2. Future Direction .....	104
5.3. Conclusions .....	106
5.4. References .....	108
APPENDIX	
A. APPENDIX A: REFERENCES OF ADAPTATION FOR CHAPTERS .....	109
B. APPENDIX B: SUPPLEMENTARY MATERIAL FOR CHAPTER II .....	110
C. APPENDIX C: SUPPLEMENTARY MATERIAL FOR CHAPTER III .....	113
D. APPENDIX D: CURRICULUM VITAE.....	126

## LIST OF TABLES

Table	Page
1. Table 1.1 Three Key Analytical Uses of Ion Mobility .....	5
2. Table 3.1. A list of negative mode CCS measurements for [M-H] <sup>-</sup> .....	71
3. Table B.1. Bile acid CCS values.....	111
4. Table C.1. Supplemental table showing name, <i>m/z</i> , retention time adduct type, CCS, and relative standard deviation of bile acid standards .....	116
5. Table C.2. Truncated tentative annotations of the top 30 abundant compounds of fecal compounds.....	117
6. Table C.3. Annotations of positive mode significant compounds between DIO and GBIL <sub>prox</sub> .....	118
7. Table C.4. Annotations of negative mode significant compounds between DIO and GBIL <sub>prox</sub> .....	120
8. Table C.5. Annotations of the 30 most significant compounds between DIO and GBIL <sub>dist</sub> in positive mode .....	121
9. Table C.6. Annotations of the 30 most significant compounds between DIO and GBIL <sub>dist</sub> in negative mode.....	123
10. Table C.7. Affected pathways as predicted with <i>Mummichog</i> .....	125

## LIST OF FIGURES

Figure	Page
1. Figure 1.1. Histogram of the number of publications published per year in ion mobility.....	2
2. Figure 1.2. Bubble plot projecting the number of CCS values reported over time .....	3
3. Figure 1.3. Cartoon depiction of biological molecules in conformation space .....	7
4. Figure 1.4. Nesting of Analytical Timescales.....	9
5. Figure 1.5. Temporally-Dispersive Ion Mobility Techniques .....	12
6. Figure 1.6. Schematic of IMMS analysis workflow with different front-end separation techniques.....	16
7. Figure 1.7. Ion mobility-mass spectrometry data acquisition and basic principles .....	19
8. Figure 1.8. Schematic visualization of acquisition using data-independent acquisition with and without ion mobility coupling .....	21
9. Figure 1.9. An example of 2D image showing mobility separation of plasma samples.....	24
10. Figure 1.10. Schematic diagram of the multipass SLIM SUPER IM-MS instrument.....	28
11. Figure 1.11. Schematic diagram illustrating a spatial multiplexing strategy for DTMS.....	29
12. Figure 1.12 Mitochondrial shuttles .....	33
13. Figure 2.1. Multiomics platform for MOA construction .....	56
14. Figure 2.2. Figure displaying detected features from HILIC and RPLC.....	58
15. Figure 2.3. Graph demonstrating metabolomic coverage observed with HILIC and RPLC...59	
16. Figure 3.1. Skeletal structure of bile acids.....	65
17. Figure 3.2. Representative IM-MS spectrum of $\beta$ -muricholic acid.....	70
18. Figure 3.3. A conformation space CCS vs $m/z$ plot of the $[M-H]^-$ adduct of bile acids.....	72



19. Figure 3.4. Ball and stick model of cholic acid and glycocholic acid .....	74
20. Figure 3.5. Comparison of saturated and unsaturated bile acids .....	76
21. Figure 4.1 Schematic of the distal and proximal bile diversion surgeries .....	82
22. Figure 4.2. Flowchart depicting the individual steps for metabolite analysis .....	84
23. Figure 4.3 Overlay of the negative-polarity extracted ion chromatography of bile acids .....	87
24. Figure 4.4. Unsupervised PCA and volcano plots of mouse fecal samples.....	92
25. Figure 4.5. Observed bile acids and their normalized intensities .....	94
26. Figure 4.6. Top predicted pathways altered by GB-IL <sub>prox</sub> .....	95
27. Figure 5.1. Self-organizing maps of metabolomic profiles after diet change.....	107
28. Figure C.1. Arrival time distribution of bile acids in negative ion mode .....	113
29. Figure C.2. Principal component analysis and volcano plots of fecal samples both in negative and positive ion mode.....	114
30. Figure C.3. Overview of the steroid hormone biosynthesis pathway .....	115

## CHAPTER I

# INTRODUCTION TO ION MOBILITY – MASS SPECTROMETRY TO ANALYZE BIOLOGICAL MATERIAL

### 1.1 Origins of Biomolecular Analysis by Ion Mobility-Mass Spectrometry

Ion mobility-mass spectrometry (IM-MS) is an integrated chemical separation technique which combines complementary size- and mass-selective separations into a single analytical platform. IM-MS can separate individual chemical compounds on the millisecond time scale; as such is considered a high-throughput technique. IM-MS is currently used in numerous chemical analysis applications including those of biological origin. Historically, IM traces its roots back to experiments by Rutherford and Thomson in the late 1890s (1), and was further improved by Tyndall in the 1920s using pure drift gases (2-3), before being paired with mass spectrometry in the 1960s (4) (**Figure 1.1**) (5). Electrospray ionization (ESI) and laser ionization were first used with IM in 1968 (6,7) and 1982 (8), respectively, with Bowers demonstrating matrix assisted laser desorption/ionization (MALDI) with IM-MS in the mid-1990s.(9) In the late 1990s onward, both MALDI and ESI ionization techniques were utilized with custom and home-built IM-MS instruments by several laboratories, establishing IM-MS as highly-sensitive technique for biomolecular analysis.(10,11,12,13,14) These soft ionization techniques readily paired with IM-MS and enabled the analysis of large, intact molecules.(15) The application of IM-MS to biomolecules growth is illustrated in the timeline in **Figure 1.2**.(16) In 2006, a commercially available ion mobility-mass spectrometer well suited for biomolecular analysis was developed by Waters Corporation, named the Synapt HDMS (“High Definition” MS), which combined the soft

## Historical Developments in Ion Mobility (IM) Technologies

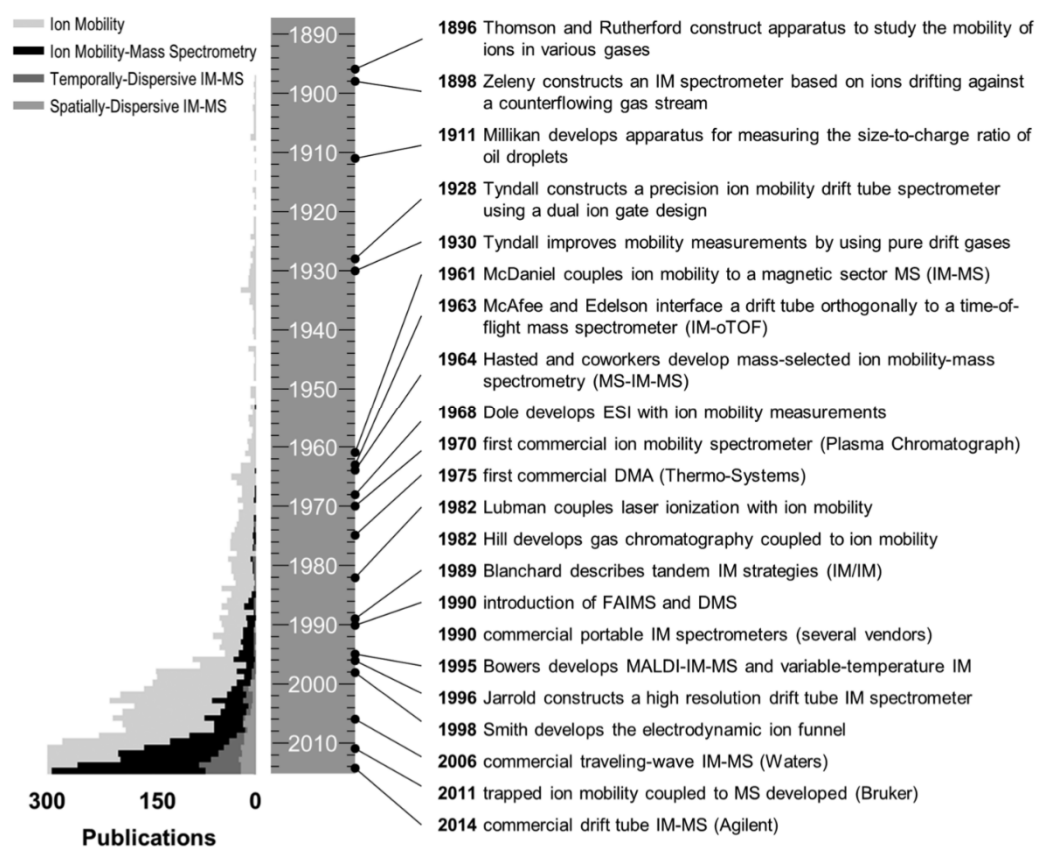


**Figure 1.1** (Left) Histogram of the number of publications published per year in ion mobility and ion mobility-mass spectrometry. Note that the scale is truncated at 300 to highlight the number of publications specifically utilizing IM-MS. Further distinction is made to discriminate the frequency of publication for both time and space-dispersive IM-MS publications. (Right) Historical milestones in the development of ion mobility and IM-MS instrumentation. (Figure and legend from May, et. al.) (5)

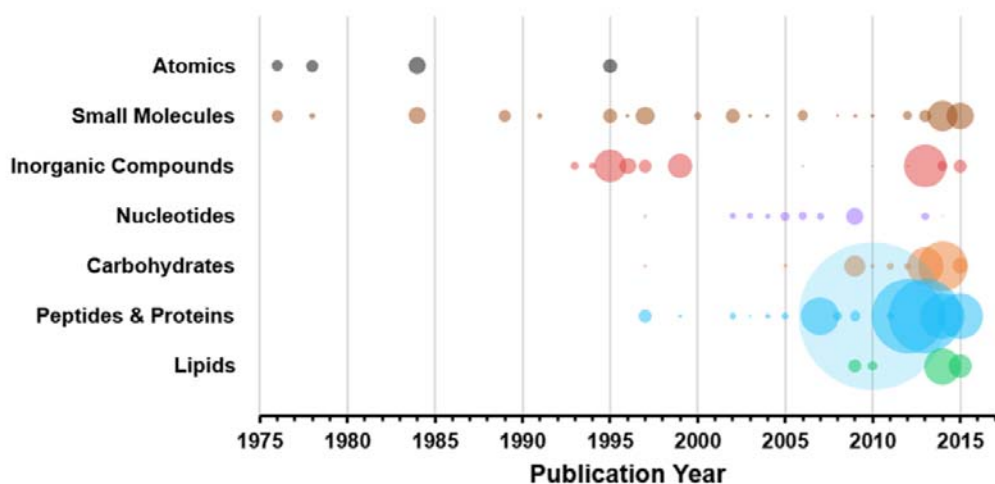


**Figure 1.2** Bubble plot reporting the number of CCS values reported over time for the top 7 chemical classes (each uniquely colored) represented. The size of each bubble encodes the relative number of CCS values for each respective year. (Figure and legend from May, et. al.) (12)

ionization of ESI and liquid chromatography-ESI with the rapid separation of traveling wave-based IM technology and time-of-flight MS. The traveling wave IM technique was improved significantly in 2011 and the platform subsequently supported other optional analytical capabilities including MALDI and MS imaging, as well as integration with a variety of other ion sources and accessories (17,18,19). This first commercial offering enabled a larger scientific community access to IM-MS which otherwise was only available to researchers with the capability to build their own instruments. Subsequently, other vendors entered the market with their own commercial IM-MS offerings, including Agilent Technologies in 2014 (drift tube IM) (20) and Bruker Corporation in 2016 (trapped IM) (21). With the availability of versatile commercial instrumentation, biomolecular analysis using IM-MS flourished and continues to be a rapidly growing field, providing fundamental insight into some of our most important biological questions.

## **1.2 Biomolecular Separation and Analytical Utility of IM-MS**

IM-MS has found great utility for biomolecular separation due to its broad sample compatibility, resolution, and sensitivity. It has been used to separate and analyze a wide range of masses, from small molecules to large protein complexes (22-29). The analytical importance of IM is summarized in **Table 1.1**.(12) IM provides a broad range of analytically valuable enhancements, including increasing peak capacity when coupled with other separation stages (chromatography, MS, etc), and enhancing low abundance signals of importance by reducing interference from chemical noise. In addition, it allows for the structural characterization of analytes through the measurement of their gas-phase cross-sectional area. In particular, it has been observed that biomolecular classes maintain different molecular packing efficiencies in the gas phase, which results in class-specific correlations (i.e., “trend lines”) to develop in 2-dimensional

**Table 1.1** Three Key Analytical Uses of Ion Mobility (Adapted from May, et. al.(12))

analytical use of ion mobility	description	additional requirements	example application areas
1. chemical separation	partition signal from chemical noise and increase peak capacity of the analysis	none	detection of illicit compounds (e.g., drugs and explosives) and screening of exogenous metabolites (e.g., pesticides and industrial chemicals)
2. analyte identification and characterization	use CCS measurement to characterize unknowns by correlation	reference values from databases and libraries incorporating normalized drift times, reduced mobilities, and/or CCS	emerging omic and small molecule discovery initiatives
3. structural analysis	utilize the experimental CCS to infer structural information	computational methods to link theoretical structure(s) to the experimental CCS	insights into protein complex arrangements and structure

IM-MS spectra (**Figure 1.3**) (16,30,31). Notably, the canonical biochemical classes (lipids, peptides, carbohydrates, and nucleotides) align themselves into unique regions of IM-MS analytical space which reflect their conformational preferences. Within each broad class trend, subclass trends may also exist. As a prominent example, lipids have a characteristic behavior in IM-MS indicative of their primary class and structures. (32) Specifically, lipid packing efficiency is affected by both headgroup identity and modifications within their acyl tail(s), forming differing trendlines in maps of gas-phase collision cross section (CCS) versus mass. Current research is considering the effects of degree of unsaturation and carbon chain length on lipid packing efficiency and trendline behavior in IM.(33,34,35) A novel approach, ozonolysis paired with IM-MS is now being applied to lipidomics to allow for determination of double bond location in lipids.(36,37) For broad scale identification of unknowns, empirically-derived databases of mass and CCS are being assembled for a variety of biomolecular compounds. (12,20,25,38-44) In addition to specific chemical class information, IM can address the challenge of resolving and identifying isobaric compounds that are unresolvable by conventional MS. In many cases, isobaric species including isomers and conformers can be distinguished in the IM dimension due to the different conformations they adopt in the gas-phase, observed both across and within peptides, carbohydrates, or lipids classes.(45-50) Collectively, the capability to rapidly resolve biochemicals based on both structure and  $m/z$  has made IM-MS an invaluable analytical tool for biomolecular analysis.

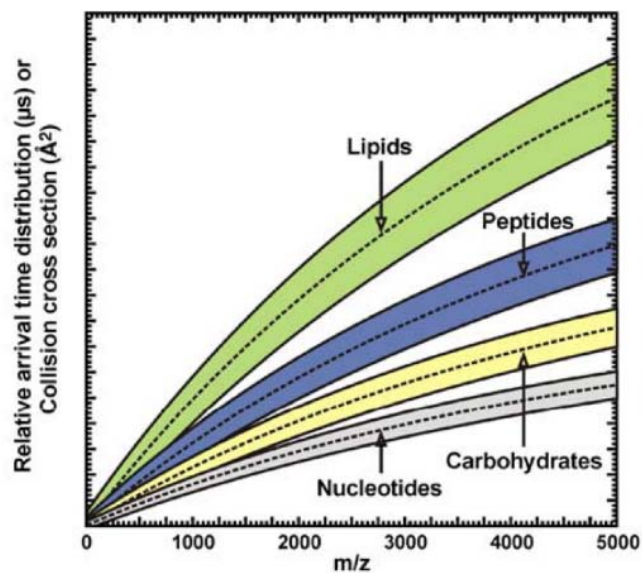


**Figure 1.3** A cartoon depiction of where singly charged analytes (e.g., produced by MALDI) of different molecular classes are observed in IM-MS conformation space. (Figure and legend from Fenn, et. al.) (26)



## 1.3 Instrumentation Considerations

### 1.3.1 Chromatography

The inclusion of a front end chromatographic separation prior to IM-MS provides added peak capacity while enhancing the analytical sensitivity of both the IM and MS stages by reducing ion suppression resulting from the simultaneous infusion of multiple analytes. Liquid chromatography (LC) is commonly implemented with IM-MS due to its ability to use a wide variety of flow rates, column choices, and solvents that pair well with ESI ion generation.(51,52) Since the IM separation occurs post-ionization, all of the LC conditions which work in LC-MS are also compatible with IM-MS, including both normal and reverse phase LC columns and numerous solvent systems.(53) Autosampler systems are also commonly utilized with LC to facilitate automated, high throughput LC-IM-MS workflows.(54) Other chromatographic separation techniques such as gas chromatography (GC) and supercritical fluid chromatography (SFC) have also been demonstrated with IM-MS (55,56,57), although these are less common due to the more limited analytical space that these techniques encompass (e.g., volatile and nonpolar analytes, respectively). **Figure 1.4** illustrates the compatibility of timescales for chromatography with IM-MS.(5) While chromatography operates on a timescale of minutes, the downstream analytical strategies such as IM and MS operate on the order of milliseconds to microseconds, allowing further separation of components eluting from the chromatographic dimension without affecting the overall sample throughput.

### 1.3.2 Ion Sources

Two of the most common methods for ionization of biomolecules are MALDI and ESI. These so called “soft” ionization techniques impart minimal energy to molecules during the

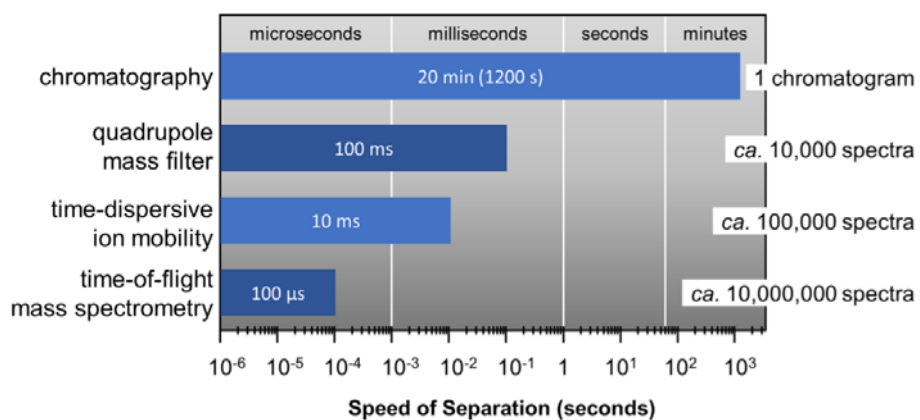


**Figure 1.4** Nesting of analytical time scales based on speed of separation is shown for the analytical strategies on the left combined with the total number of potential spectra obtained through nesting the subsequent analytical separation dimensions shown to the right. (Figure and legend adapted from May, et. al.) (5)

ionization process, which helps to maintain the analyte's structural integrity during transfer to the gas-phase, which is crucial for the analysis of fragile biomolecules.(9,15) MALDI is performed on solid samples using a laser to desorb and generate ions and tends to generate low charge states in a narrow distribution, which simplifies the mass spectra.(58,59) The use of a laser also facilitates operating MALDI in an imaging mode, allowing spatially-resolved mass information to be obtained.(60) MALDI-based MS imaging (MSI) has been utilized to determine analyte location in tissue samples (61), and MSI has also been coupled with IM-MS to provide a highly-dimensional separation technique that can simultaneously separate analytes based on spatial location, size, and mass.(62,63) MALDI, however, is not conducive to direct analysis of liquid samples such as the effluent stream originating from LC, which requires offline sample fraction collection for MALDI analysis. Liquid sample analysis is, however, readily facilitated by ESI, which generates a continuous flow of ions from liquid-phase samples. ESI has enabled high-throughput LC-MS experiments and has been used to combine LC with IM-MS. In contrast to the low charge states observed in MALDI, ESI typically generates multiply charged ions. Since mass spectrometers measure ions as a mass-to-charge ratio, higher charge states effectively increase the practical mass range accessible to a mass spectrometer, facilitating analysis of proteins and other high mass analytes alongside small molecules in a complex biological sample.(64,65) Multiply charged ions have also improved detection limits for Fourier transform MS (FTMS) techniques (66,67), improved the ion fragment yields for traditional collisional activation experiments (collision-induced dissociation, CID) (68), and have enabled electron-induced fragmentation techniques such as electron capture dissociation (ECD) and electron transfer dissociation (ETD) to be implemented (69,70). Specifically, for IM analysis the various charge states generated from ESI are readily

resolved into distinct trendlines in mobility versus mass space, which facilitates the separation and identification of multiply charged species.(10)

### 1.3.3 Time-Dispersive Ion Mobility Techniques

Two ion mobility techniques that are used in commercially, available instruments are drift tube ion mobility spectrometry (DTIMS) and traveling wave ion mobility spectrometry (TWIMS) (**Figure 1.5**) (5). TWIMS was the first IM technique to be used in a commercially available IM-MS platform. In TWIMS, ion separations result from a series of dynamically-pulsed voltages (an electrodynamic field) which creates a traveling wave potential that transfers ions through the drift region in a mobility-selective mode. TWIMS separations are typically faster than DTIMS while accessing similar resolving powers (71), and because the traveling wave does not require high voltage operation, TWIMS is easier to implement on existing MS platforms. Although DTIMS combined with MS was implemented commercially several years after TWIMS, it is an older technique and considered the standard and most accurate method for CCS determination. Unlike TWIMS, DTIMS separates ions using a constant voltage gradient (a uniform electric field) which allows the measured ion drift times to be related directly to CCS via the fundamental ion mobility equation, commonly referred to as the Mason-Schamp relationship (72,73). On the other hand, TWIMS-derived CCS values are determined via an empirical calibration relationship between TWIMS measured drift times and known CCS values obtained from DTIMS (27,32,74). Due to the fact that TWIMS does not require high voltages to operate, it is readily scalable to longer path lengths, which fundamentally improves instrument resolution. In contrast, high operational voltages must be utilized in order to increase the path length in DTIMS. Next generation TWIMS instruments are taking advantage of this scalability, producing high resolving power platforms

### Temporally-Dispersive Ion Mobility Techniques

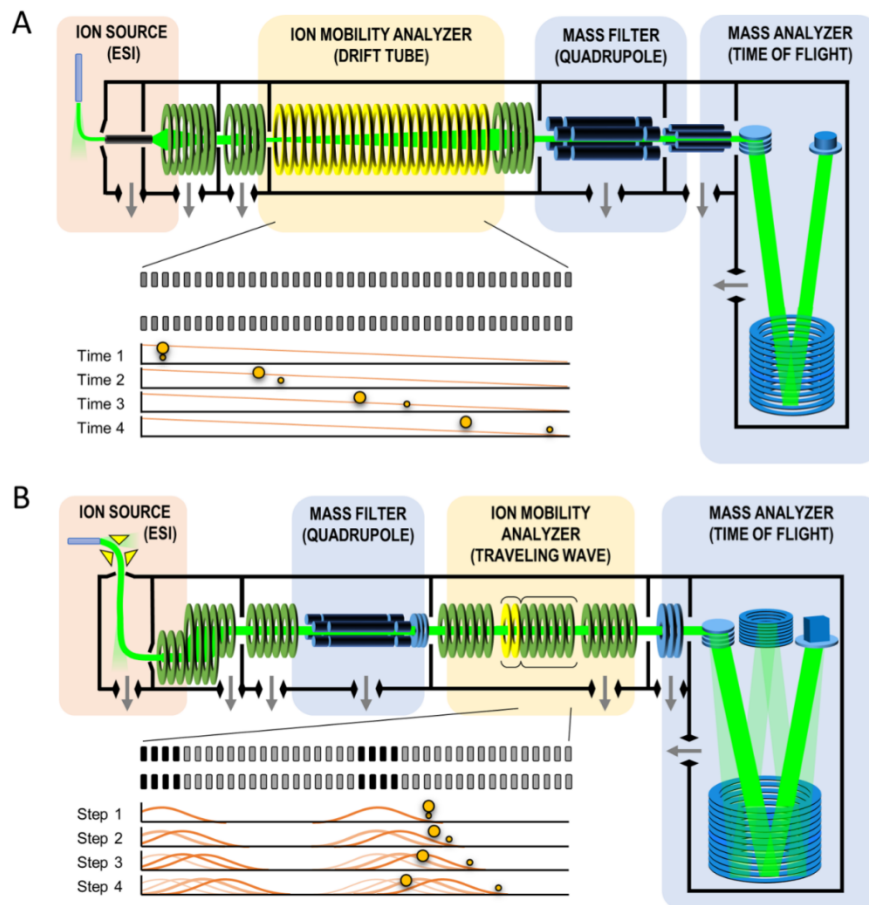


**Figure 1.5** Two representative schematic diagrams for contemporary time-dispersive IM-MS instrumentation. (A) An electrostatic drift tube (DTIMS) arrangement similar to that described by Smith and co-workers. (B) An electrodynamic drift tube (TWIMS) arrangement similar to that described by Giles and co-workers. In both arrangements, hypothetical time courses are shown to illustrate the temporal separation of smaller and larger collision cross section ions. (Figure and legend from May, et. al.) (5)

based on cyclic designs.(41,75)

### **1.3.4 Mass Spectrometry Considerations**

Mass spectrometry is routinely conducted after IM separations to provide mass measurement on mobility separated ions. In this IM-MS configuration, most of the chemical separation occurs in the mass dimension due to the high resolving power (>10,000) accessible by modern mass spectrometers, however, the added IM dimension provides improved peak capacity and the capability for resolving isomeric compounds based on structural differences (76). IM is commonly coupled with time-of-flight (TOF) mass spectrometry due to its ability to rapidly analyze a wide mass range simultaneously and with high resolution. The timescale of the TOF is on the order of microseconds, pairing well with an upstream IM which is on the order of milliseconds per analysis. Quadrupole MS is also commonly used with IM-MS as an added mass filtering stage for tandem MS/MS experiments, which can further aid in analyte identification and characterization.

Fragmentation methods have been utilized with great success in tandem mass spectrometry and continue to be used in IM-MS, where it can be initiated between the IM and MS stages (IM/MS) or prior to IM-MS either with a front-end mass filter (MS/IM-MS) or without, as is the case with in-source ion activation (/IM-MS) (77). Collision induced dissociation (CID) is commonly used to fragment ions as it is readily implemented with existing ion optics. CID is implemented by inducing ion collisions with an inert background gas (such as nitrogen or argon) under elevated voltage conditions, and CID is considered an ergodic process whereby energy is distributed across the entire analyte, causing the lowest energy bonds to break first. This leads to reproducible fragmentation of ions and the analysis of CID fragmentation spectra has been used

with IM-MS to identify isobaric species which exhibit different bond energies. The CID method is commonly used in proteomics to determine the amino acid sequence of peptides. While highly predictable, CID does not preserve weak bonds such as noncovalent complexes and post-translational modifications, and is less effective at fragmenting large molecules, such as intact proteins. To address these deficiencies, electron capture dissociation (ECD) and electron transfer dissociation (ETD) have been used, both of which fragment the ion in a non-ergodic process, breaking bonds CID would not, and thus creating different but informative fragments compared to CID. ECD requires simultaneous trapping of ions and free electrons, and has only been implemented in ion cyclotron resonance MS. ETD and CID have been used simultaneously with IM-MS for glycoproteomics (78,79,80). This allows a variety of fragments to be determined for a given precursor ion, with CID fragmenting the glycan portion and ETD fragmenting the peptide portion. Combining the ion drift time, precursor mass, and fragment mass information allows for confident identification of the precursor.

IM-MS holds an important role in biomolecular analysis. The ability of IM-MS to integrate with a wide variety of chromatographic techniques, ion generation methods, fragmentation methods, and mass analyzers results in a versatile and powerful technique for biomolecular analysis, particularly in the omic sciences (proteomics, lipidomics, metabolomics, etc.) where deriving biological answers requires high sensitivity and confident identifications. Additionally, IM improves peak capacity compared to standalone MS and is compatible with other analytical stages such as LC separations and tandem ion fragmentation. In this context, IM can differentiate isobaric species and provides an additional descriptor (ion drift times or gas-phase CCS) for the identification of unknowns. The next few sections discuss some specific applications of IM-MS to biomolecular analysis.

## 1.4 Introduction to Current Trends

The confident identification of small molecules continues to be one of the most difficult challenges in omic studies. While advancements in proteomics have streamlined MS-based identification efforts for peptides, metabolomic and lipidomic identification capabilities have generally lagged behind (34,81-84). One reason for this is that while the structure of peptides consist of rationally-assembled amino acid building blocks which can be elucidated through ion fragmentation strategies, metabolites and lipids are not biopolymers with predicable sub-structural units. Additionally, the prevalence of isobaric species in lipidomics complicates feature identification, and metabolomics studies often encounter features of redundant mass that lack unique fragmentation patterns, further confounding attempts at identification by MS. Therefore, a combination of analytical techniques is required for high-confidence lipidomics and metabolomics. As shown in **Figure 1.6**, gas chromatography, liquid chromatography, or another front end separation can be readily combined with IM and MS analysis to provide highly-dimensional datasets which can be partitioned into specific omic workflows (80,53). The IM analysis provides charge state and chemical class-specific separations based on differences in intrinsic gas-phase packing, as well as quantitative size information via the CCS measurement which can be used as a reproducible measurement for identification purposes (80).

## 1.5 Integrating Ion Mobility for Omic Analysis

IM-MS provides a fast separation of chemically-unique biological groups with the added benefit of measuring collision cross section concurrently with mass-to-charge ratio (27,78,85). This capability is important for omics studies utilizing complex biological samples which routinely



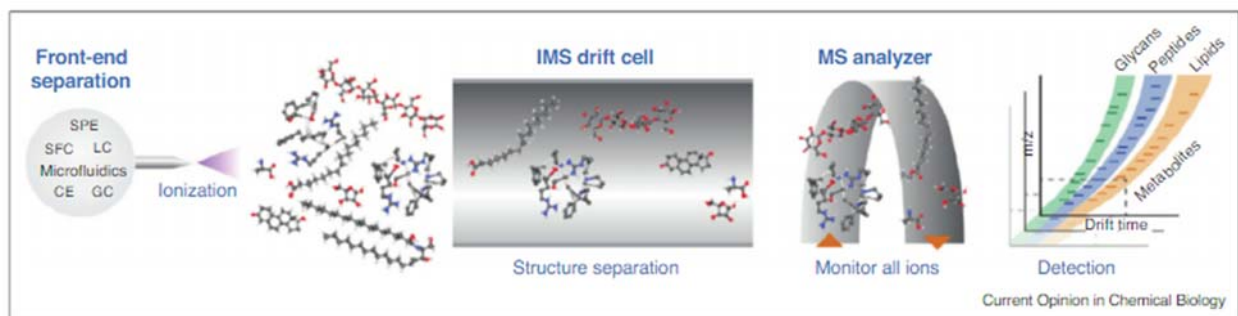


**Figure 1.6** Schematic of IMMS analysis workflow with different types of front-end separation techniques. Abbreviations: SPE, solid phase extraction; SFC, super critical fluidic chromatography; LC, liquid chromatography; CE, capillary electrophoresis; GC, gas chromatography. (Figure and Caption from Zhang et al.) (84)

require extensive sample purification strategies to isolate molecules of interest from undesirable compounds that would otherwise make MS analysis difficult (e.g., salts, detergents, and other types of chemical noise) (77,86). Sample preparation strategies have the potential to chemically alter molecules of interest, for example, by oxidation, reduction, conversion to a secondary metabolite, or loss of a post-translational modification in peptides. Integrating IM with MS can help offset some of the burden of chemical separation and alleviate the need for extensive sample handling. In certain cases where fragmentation occurs post-mobility, either intrinsically or intentionally, IM-MS also allows the alignment of precursor and product ions which can further aid in identification (79,87). The following sections provide examples of how ion mobility has been integrated in proteomic, lipidomic, and metabolomic analyses. Although each analysis is discussed separately, it should be noted that ion mobility allows for simultaneous analysis of these individual omic fields via chemical class separation, providing a truly integrated multi-omic experiment.

### **1.5.1 Proteomics**

Proteomics, the large-scale study of proteins, has been a driving force in systems biology and has increased our understanding of diseases and human health. Proteins serve as the machines for all cellular processes, thus proteomic studies are one of the most crucial tasks in systems biology. MS-based proteomics is a major component to the advancements in the field (88,89). Proteins encompass a large dynamic range of concentrations, necessitating separation techniques to enhance lower abundance species prior to mass analysis. Common separation methods for proteomics include gel electrophoresis, liquid chromatography, and, in a growing number of instances, ion mobility (90,91,92).

Ion mobility has been utilized extensively in structural proteomics (78,93). Proteins of similar or exact mass, such as protein conformers, can be separated by IM due to differences in their gas-phase size (94). **Figure 1.7** illustrates an IM separation for protein ions of different sizes but similar mass-to-charge ratio (88). The majority of multiprotein complexes have been analyzed on TWIMS instruments, and it has been demonstrated that incorporation of TWIMS with MS analysis can increase proteome coverage by up to 60% (95).

In addition to separating proteins, IM is used to probe structural information (88). Temperature-controlled ESI sources and heated ion transfer capillaries have been used prior to IM-MS to rapidly heat proteins and monitor their controlled denaturation (11,96,97). In addition, thermally-induced protein conformational transformations as well as protein-ligand interactions are observed. In these ways and others, IM-MS progresses from a separation strategy to a structural measurement technique to broaden our understanding of how protein clusters are formed and stabilized (91,92).

### 1.5.2 Lipidomics

Lipids comprise a large portion of the small molecules extracted from organisms. They have three major functions in biological systems: energy storage, cellular signaling, and structural functions. Lipids can be divided into eight major categories (fatty acids, glycerolipids, glycerophospholipids, sphingolipids, sterols, prenols, saccharolipids, and polyketides) with many different structural motifs ranging from fused cyclic molecules to long chain fatty acids. Lipids cover a large range of  $m/z$  ratios and while mass spectrometry has been a powerful tool in lipidomics, the numerous isomeric lipid species which can exist makes lipid structural characterization by MS challenging (98-100). Contributing to lipid structural complexity are the

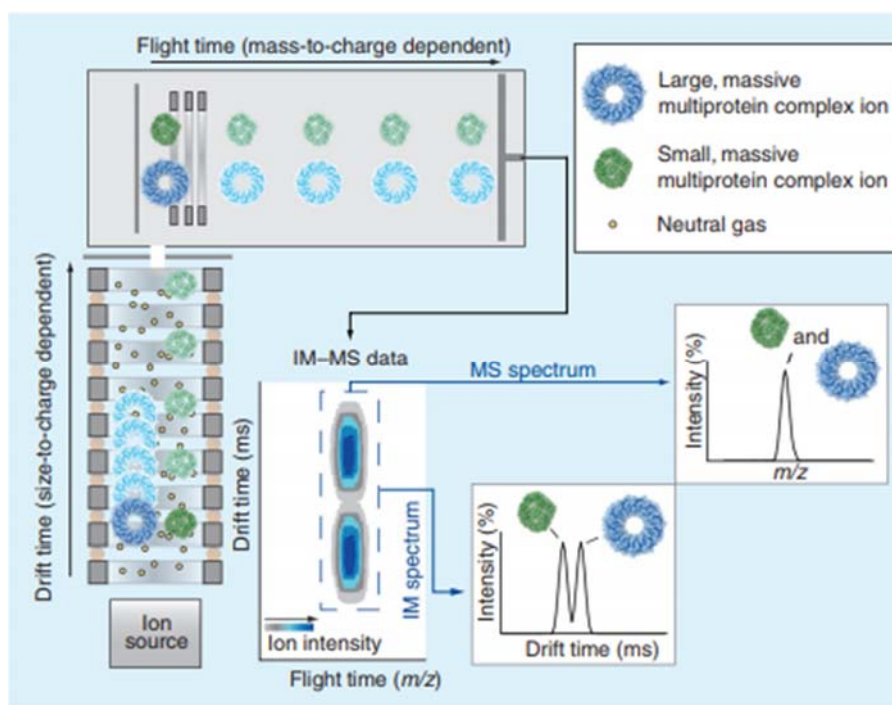


**Figure 1.7** Ion mobility-mass spectrometry data acquisition and basic principles. Ions are generated at the ion source (lower left) and are allowed to drift in an ion guide filled with neutral gas molecules under the influence of an electric field. The ions migrate through this region according to their size-to-charge ratio. They are then injected into a ToF mass analyzers under vacuum for  $m/z$  analysis. The resulting data are 3D, containing ion intensity, size and mass information. The various dimensions of the data can be shown as a contour plot (middle, bottom), or 2D selections in drift time of  $m/z$  (lower right). A key for the diagram is shown (upper right). (Figure and Caption from Zhang et al.) (93)

numerous potential double bond positions, geometric (cis/trans), constitutional (linear and branched) and stereochemical orientations that a lipid can adopt which are all isobaric in mass. Identifying complex lipid structures has been a struggle in the field of lipidomics; one that ion mobility is well-suited to address (94,95,101,102). Lipid identifications in MS-based lipidomics utilize the exact mass measurement as well as characteristic fragmentation patterns obtained from tandem MS/MS experiments to assign confidence to structural identifications. As many lipids are chemically and structurally similar, lipids can be challenging to separate using LC alone, making it difficult to correlate fragment ions with their precursor ion forms. As demonstrated by Paglia et al., ion mobility can be used to align fragmentation spectra with precursor parent ions to increase the confidence in lipid identification (**Figure 1.8**). In this study, ion mobility was also demonstrated to be useful in separating co-eluting lipid structures with the same  $m/z$  ratios (103).

Ozone-induced dissociation has been recently demonstrated with IM-MS to elucidate the location of double bonds in the acyl tail region of lipids. Two separate strategies have been described: solution-phase ozonolysis of lipids prior to being introduced to the mass spectrometer (104), and gas-phase ozonolysis of lipid ions within the MS, the latter technique termed OzID. These ozonolysis strategies have been shown to be useful for locating the position of double bonds within lipids, however, one shortcoming with this approach is that it does not provide any information about the geometry (cis/trans) of the double bond prior to ozonolysis (99,105). This emphasizes the strength of IM-MS analysis, where ion mobility allows for the differentiation of some geometric lipid isomers, such as cis versus trans, even when present in a complex biological mixture. Groessl et al. demonstrated that CCS differences of 1% or more are sufficient to baseline separate lipids in DTIMS (96). Although the possibility to use IM for identification purposes was also discussed, it was noted that high precision and accuracy are needed to create and populate

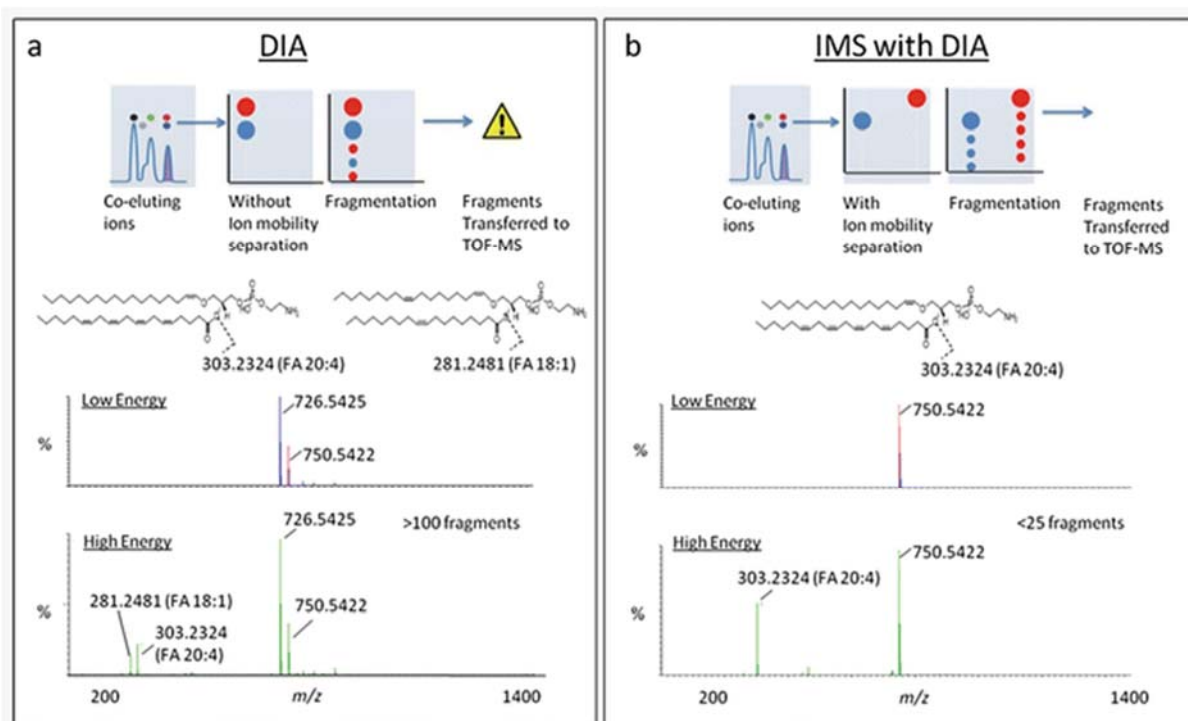


**Figure 1.8** Schematic visualization of acquisition using data-independent acquisition (MSE) and MSE coupled with IM (HDMSE). Combined with IM separation, fragmentation offers unique capabilities to increase specificity and confidence in identifying complex lipid structures. (Figure and Caption from Paglia et al.) (98)

reliable reference data libraries. Recently, Leaptrot et al. reported on an empirical CCS database of various sphingolipids and phospholipids incorporating 456 high-precision DTIMS measurements (global average RSD of 0.18%), which provides a quantitative means of identifying unknown lipids, including isomers, by IM-derived CCS information (33). As these CCS libraries become more available, it is expected that lipidomics using IM-MS will continue to grow.

### 1.5.3 Metabolomics

Metabolomics is the measurement of the thousands of small molecules in a biological system. Unlike genomics and proteomics, metabolomics encompasses a large amount of chemical diversity as it consists of molecules from many different biological classes, such as carbohydrates, amino acids, hormones, and lipids (106). There are generally two approaches to MS-based metabolomics: (1) targeted analysis, in which a panel of metabolites are selected for chemical analysis, and (2) untargeted analysis, in which all small molecules present in the sample are analyzed simultaneously (101). Both approaches have their advantages. Targeted studies allow for semi-quantitative analysis of small molecules on a curated list. Isotope standards can be analyzed concurrently with unknowns and calibrated against empirically-measured response curves (calibration curves) in order to determine the concentration of specific metabolites within a sample. Since only a small number of  $m/z$  values are prioritized, targeted studies are commonly conducted on MS instrumentation with selective ion monitoring capabilities, such as triple quadrupole and ion trap instruments where a select  $m/z$  can be tuned and monitored in a continuous duration, greatly increasing the instrument sensitivity and response reproducibility, which improves quantitative results. While targeted approaches provide quantitative information regarding metabolites of interest, these studies do not provide detailed information for other small molecules

present in the sample. Untargeted approaches, on the other hand, focuses on separating and comprehensively measuring all of the small molecules present in the sample, but lacks robust means of quantifying these signals. Also, untargeted studies generally utilize analytical methods and settings that attempt to measure a large breadth of molecules, and thus can be less sensitive to a specific class or pool of analytes (101,107,108). While untargeted studies can detect a large number of molecules present in a sample, identifying the oftentimes thousands of metabolites observed in a single untargeted study can be an arduous task. For a single  $m/z$  feature, there can be hundreds of matches to known compounds in various metabolomic databases, making an absolute identification difficult (102,103,109). Thus in order to improve confidence in metabolite identification, multiple dimensions of analytical information are generally obtained in untargeted experiments, which can include measurements from front end chromatographic separations (analyte polarity and retention times), as well as post-ionization techniques such as ion mobility (likely chemical class and collision cross sections) and tandem MS (ion stability and fragmentation information). Ion mobility in particular can provide additional peak capacity, isomeric differentiation, and an additional molecular descriptor (CCS) which can help to alleviate some of the difficulties associated with confident metabolite identification (110,111,102-104).

As noted in the previous section, IM can improve fragmentation identification in lipidomics, and this advantage applies to metabolomics as well. With such chemical diversity found in the metabolome, ion isolation is complicated by co-eluting species, and thus aligning precursor ions with their fragments originating from ion activation experiments is challenging. Using IM prior to ion fragmentation allows co-eluting small molecules to be further resolved following chromatography (102-104). For example, Wickramasekara et al. classified co-eluting lipid species based on the differences in their IM drift times (**Figure 1.9**) (112). In addition, the



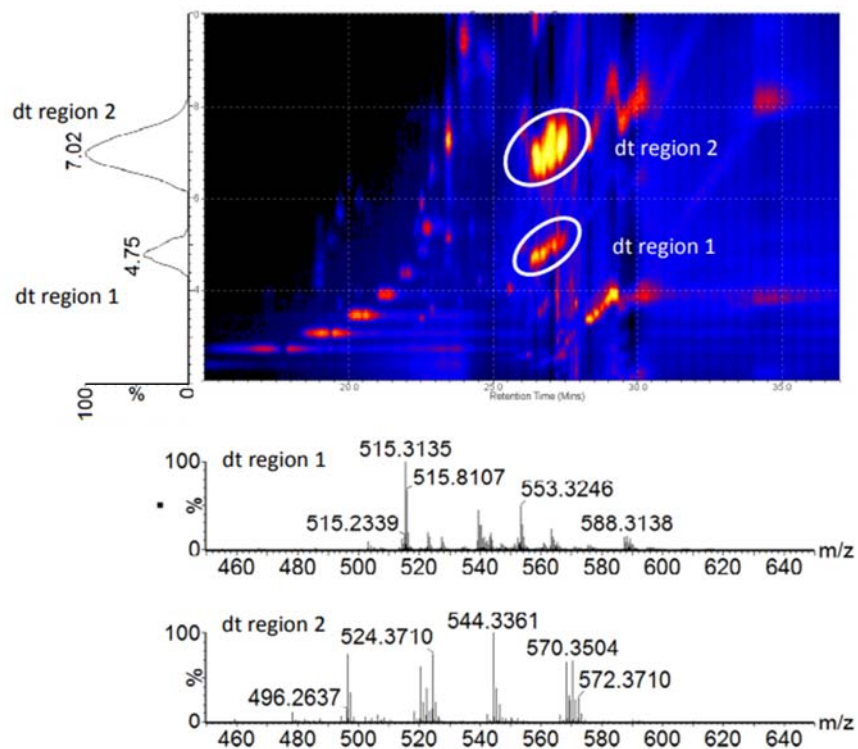


**Figure 1.9** An example of a 2D image (drift time vs retention time) showing the ion mobility separation of different compound classes in rat plasma samples. The encircled regions mark the compound classes that eluted within a similar retention time window (26-28 min). Drift time-extracted spectra (bottom) show that these two clusters belong to different lipid classes, namely Lyso-PC and SM lipids (sphingosine phosphocholines) that have drift time distributions centered around 7.02 ms and 4.75 ms, respectively. (Figure and Caption from Wickramasekara et al.) (112)

drift time extracted spectra can be used to align fragment ions to the corresponding parent ion, as these signals have identical drift times when conducting the fragmentation post-mobility. This capability to mobility-align ion precursors and fragments can help to collate specific ion fragment information which can then be used with the accurate mass measurement to match unknowns to database entries, thus increasing the confidence in assigning metabolite identifications.

In addition to utilizing the enhanced separation and fragment alignment capabilities from IM, CCS measurements derived from IM experiments can improve metabolite validation (26). CCS is linked to an intrinsic molecular property of the analyte (the microscopic molecular cross section) and thus is considered more robust than other conditional measurement parameters such as the chromatographic retention time. This property makes CCS useful as an additional molecular descriptor that can be used in metabolomic studies along with accurate mass and fragmentation information. Currently, there are several laboratories attempting to use CCS in metabolite identification workflows. For example, Paglia et al. has described a robust analytical workflow incorporating CCS for both metabolite and lipid identifications, and report a ca. 2% inter-laboratory reproducibility of the TWIMS derived CCS (42,84). Stow et al. utilized standardized DTIMS instrumentation deployed across several laboratories to achieve an inter-laboratory CCS reproducibility of better than 0.5%, and recent work by Nichols et al. describes the utility of DTIMS CCS measurements as a molecular descriptor in untargeted studies of primary human metabolites (113,114). As more research shifts towards incorporating CCS into metabolomic analysis, there is a need for databases to propagate likewise. Recent efforts for developing CCS databases to support metabolite identifications have included pesticides, pollutants, xenobiotics, and steroids (115-118). Leveraging the standardization efforts for DTIMS, Picache et al. has recently described a “Unified CCS Compendium” which compiles over 3,800 CCS measurements

obtained from different studies into a single, self-consistent resource with a global average CCS precision of 0.25% RSD (43). These and other efforts will allow rapid and reliable metabolite identification and quantification, which becomes increasingly important as the field shifts towards comprehensively characterizing individual metabolomic pathways.

## **1.6 Continuing Advancements in IM-MS Technology**

Innovation in IM-MS instrumentation continues at a rapid pace. Various improvements have been suggested and novel IM-MS technologies now being described allow for ingenious solutions for challenges encountered in biomolecular analysis. For example, a novel instrument design approach now being actively developed for IM-MS utilizes a scalable ion optical architecture consisting of electrode pads on a printed circuit board (PCB) and driven with electrodynamic (RF) fields that confine ions to a predefined ion optical path. This approach, named by the authors as “structures for lossless ion manipulations” (SLIM), utilizes a 2-dimensional electrode geometry that is both modular and scalable such that various experiments can be achieved on the same instrument platform (41,119,120-122). In SLIM, two PCBs with a mirrored electrode symmetry are placed above and below one another to create the ion path of travel in between the boards, and a dynamic electric fields are used to both contains and guides the ions through the SLIM device (123). SLIM allows high transmission ion transfer through elevated pressure regions, and SLIM-based ion mobility separations based on both DTIMS and TWIMS have been demonstrated (124,125). The ability to print electrodes on a two-dimensional surface allows for various ion manipulation modules to be fabricated, including modules to move ions at 90-degree angles (elbows and tees) (118,126). This facilitates cyclic racetrack and serpentine geometries to be fabricated for long path-length, high-resolution ion mobility separations, and

incorporation of “tee” junctions allows selection of a discrete ion mobility region for further tandem analysis by either IM or MS. An example of SLIM-based ion mobility instrumentation is shown in **Figure 1.10** (119). Current designs have created instruments with some of the highest IM resolution currently available (72).

In addition to TWIMS and DTIMS, a relatively new ion mobility technique called trapped ion mobility spectrometry (TIMS) is currently available in commercial instrumentation (127,128). TIMS performs ion mobility separations by selectively releasing ions trapped in a mobility “analyzer” cell combining a gas flow and an opposing electric field (129,130). The ions trapped in TIMS are released slowly by lowering the electric field barrier, which allows a mobility spectrum to be obtained and subsequent MS analysis to be performed. The rate at which the electric field is lowered corresponds with IM resolution, with slower scan rates leading to higher resolution. TIMS instruments are capable of high IM resolutions and are very versatile due to its variable scan rate (131). Either high throughput or high resolution scan rates may be chosen as needed, or a scan rate may be variable during analysis to allow high resolution only for certain range of mobilities, enabling targeted high resolution experiments to be conducted. This is in contrast to current high resolution approaches based on cyclic or racetrack IM technologies, which relies on selecting a narrow population of mobilities for high resolution analysis, at a cost of rejecting other ions outside of this mobility window.

While most efforts have focused on improving IM resolution, some approaches have sought to improve sensitivity and throughput. An example of such an approach is a multi-channel IM spectrometer shown in **Figure 1.11** (5). This instrument utilizes eight discrete ion optical paths to perform eight ion mobility separations in parallel (132,5). Each ion channel can act independently, analyzing eight unique samples at a time, improving throughput. Alternatively, the

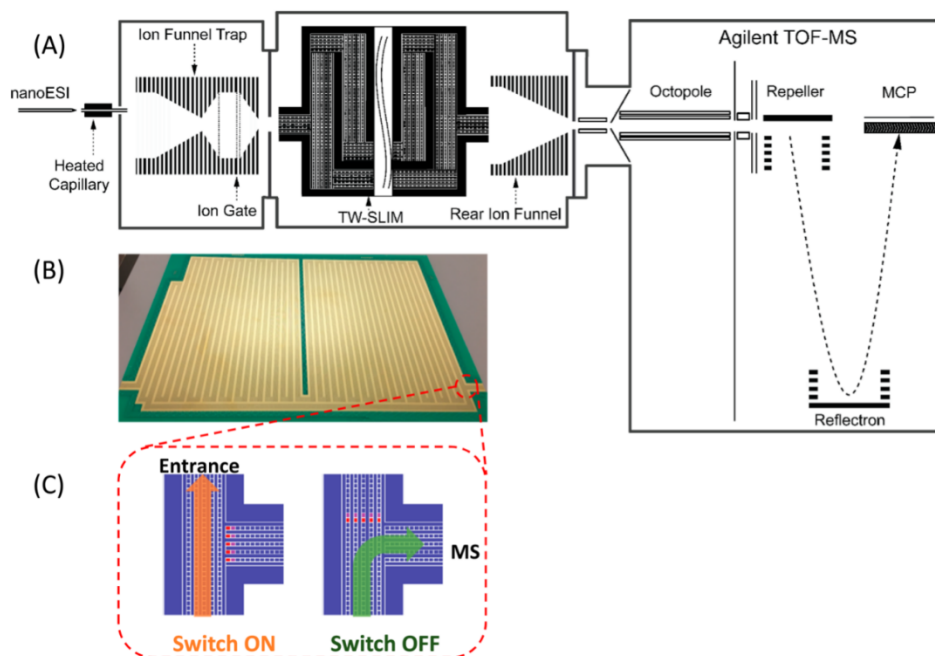


**Figure 1.10** (A) Schematic diagram of the multipass SLIM SUPER IM-MS instrument used in this work; (B) photo of one of the two SLIM module surfaces; and (C) illustration of an ion switch (switch on, ion cycling; switch off, transmit ion to MS). (Figure and legend from Deng, et. al.) (120)

### Spatial Multiplexing

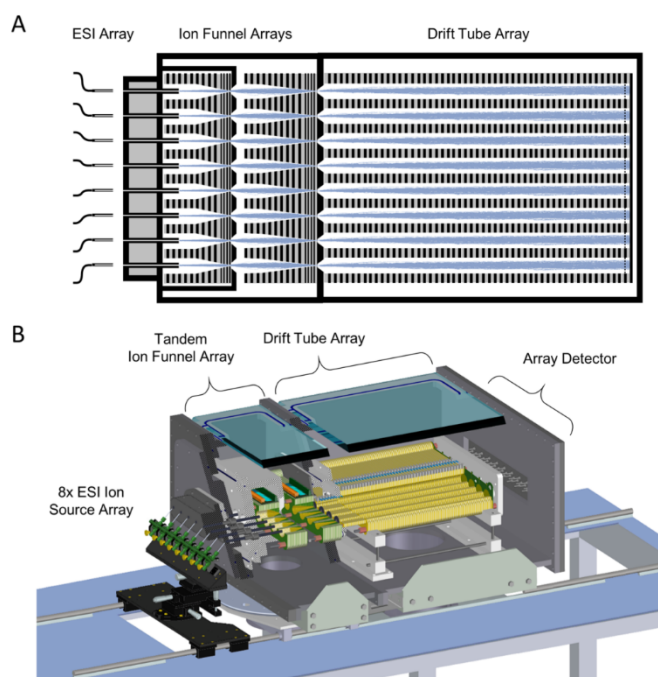


**Figure 1.11** Schematic diagram illustrating a spatial multiplexing strategy for DTIMS through combining eight individual IM channels: (A) diagram showing ion simulations through the interfacing ion funnels and the drift tube array and (B) cutaway showing component details of the spatially multiplexed instrument. (Figure and legend from May, et. al.) (5)

multi-channel instrument can analyze the same sample simultaneously across the eight ion optical paths, increasing the sensitivity of the instrument. As the analytical community pushes for rapid extraction of more information from complex samples, advancements in high throughput instrument designs remain crucial.

Additional strategies for improving the mobility separation have focused on increasing the chemical selectivity of existing IM instrument by using alternate drift gases (133). The understanding and application of the effect of drift gas on IM separations and the associated CCS measurement is still in early development, but there is now mounting evidence that the use of more polarizable drift gases (e.g., CO<sub>2</sub>, N<sub>2</sub>O, NO<sub>2</sub>) can increase the resolution for certain ion species (128,134). While the hard-sphere interactions between the ion and drift gas tend to predominate the mobility of ions in the IM experiment (135), long-range interactions also play a role in the observed IM separations and are exploited by varying the drift gas polarizability. Improved selectivity can occur between certain ionic species depending upon their susceptibility to long-range interactions (136). The effect on separation efficiency by varying the drift gas composition is similar to the effect of varying the solvent conditions in capillary electrophoresis to affect separation selectivity. It is common to alter the drift gas in some high-field IM techniques, such as high-field asymmetric waveform ion mobility spectrometry (FAIMS) and differential mobility spectrometry (DMS) (137,138,139-142). In low-field IM techniques, this is less common, but there have been a number of significant examples (143,144). Using an ambient pressure drift tube, Hill and coworkers showed that varying the drift gas polarizability could improve selectivity for various small molecules including drugs, carbohydrates, and peptides (128,129,145-146). Using a reduced pressure drift tube, Yost and coworkers reported that carbon dioxide improved resolving power for several isobaric steroids (147). Eberlin and coworkers demonstrated that replacing

nitrogen with carbon dioxide in a TWIMS instrument could improve separation of a number of analytes such as carbohydrates and isomeric haloanilines (46,148,149-150). However, it is common for observations of more polarizable drift gases to report minimal improvement to overall IM peak capacity or resolution compared to nitrogen on helium (131,151-153). For example, Fjeldsted and coworkers investigated the separation of various small molecule pesticides, isomeric carbohydrates, and fluoroalkyl phosphazenes in a wide variety of drift gases, including helium, nitrogen, argon, carbon dioxide, nitrous oxide, and sulfur hexafluoride. Generally, it was observed that helium and nitrogen had the highest resolution and resolving power, with some of the more polarizable drift gases demonstrating better selectivity when comparing certain analyte pairs (133). To fully evaluate drift gas effect, a broader range of masses and biological classes needs to be reported in a variety of drift gases across multiple platforms and laboratories. Recently, Morris et al. utilized DTIMS operated in a variety of drift gases (helium, nitrogen, argon, and carbon dioxide) to study several different classes of compounds (quaternary ammoniums, phosphazenes, polypeptides, and carbohydrates) and provided recommended experimental parameters that allow for comparable CCS values to be determined among multiple laboratories (154). Currently, the majority of CCS measurements have been reported in either helium or nitrogen, hindering the evaluation of IM separation performance in other alternate drift gases (12), though as the methods and parameters to perform these variable drift gas experiments become standardized, normalized measurements such as CCS will be vital for allowing direct comparison of separations conducted on different platforms (e.g. drift tube or traveling wave) (121). The potential analytical importance of drift gas composition on improving IM resolution and separation selectivity is significant, and currently this area of research is largely unexplored.



## 1.7 Future Remarks on IM-MS in Multi-Omic Studies

When utilized in various omics studies, IM has been used primarily to partition analytes of interest from chemical noise originating from complex samples, resolve ambiguities within co-eluting features, and align precursor and fragmentation data acquired in data independent strategies. While the majority of IM-MS applications in biomolecular analysis have focused on specific omic fields (e.g., proteomics, lipidomics, metabolomics), there is increasing interest in utilizing IM-MS for untargeted, multi-omic studies which examine a large breadth of molecule types simultaneously (155). A truly, multi-omic analytical workflow will facilitate the development of system maps which connect relationships between molecule types and allow perturbed pathways to be highlighted. To illustrate this concept, **Figure 1.12** displays work from Paglia et al. on building pathway maps to track metabolites being shuttled between mitochondria and the cytosol (156). An area that can benefit from this type of analysis is the microbiome field. The microbiome has experienced recent and significant attention aimed at understanding the integral role that commensal bacteria plays on human health (157-159). This focus, in large part, is due to advancements in sequencing of bacterial communities allowing for whole populations to be analyzed simultaneously, facilitating the comparison of healthy versus disease states (158,159). One challenge that remains in microbiome research is the understanding of the mechanisms that lead to disease, which can be addressed at least in part by building biochemical inventories of small molecule metabolites observed within the samples. MS-based metabolomics can be applied to a variety of sample types, can measure thousands of metabolites, and requires very little sample quantities, and thus has high potential for integration into multi-omic study. In particular, the ability of IM-MS experiments to separate and detect multiple biological classes and chemical motifs simultaneous, can allow perturbed metabolites to be observed along with changes in the

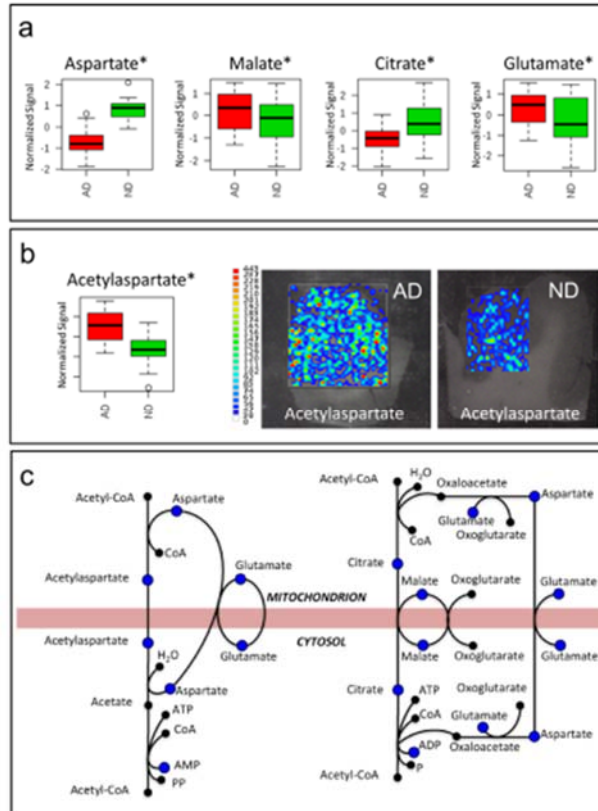


**Figure 1.12** Mitochondrial shuttles. (a) Bar Charts of aspartate, malate, citrate, and glutamate obtained from normalized signals in AD (red) and ND control subjects (green). (b) Bar chart of N-acetylaspartate (NAA) obtained from normalized signals in AD (red) and control subjects (green) and MS imaging of AD and control subjects brain sections. (c) Mitochondrial shuttles and metabolites quantified in his experiment (blue dots). \* $p < 0.05$  (t test). Targeted data used for bar charts were normalized by mean centering, scaled by unit variance, and log-transformed. (Figure and Caption from Paglia et al.) (156)

bacterial community. Uncovering changes in the metabolomic profile can provide insight into the role that particular bacteria plays within the complex interplay of biomolecules associated with the microbiome.

Throughout this chapter, biomolecular analysis by various IM-MS technologies have been highlighted. Currently, IM is used primarily to enhance the separation of molecules present within complex samples. However, with the higher quality IM measurements now being reported (39), the role of IM for supporting biomolecular identifications is poised to make a significant impact in the omics sciences, particularly within the metabolomics and lipidomics communities. As high resolutions, precisions, and multi-stage tandem experiments become available, IM-MS will play an increasingly important role in providing deeper levels of information in large-scale biomolecular analysis initiatives including biological pathway analysis, systems, and synthetic biology.

## **1.8. Acknowledgements**

This chapter contains the invited book chapter for Ion Mobility Mass Spectrometry Mass Spectrometry – Methods and Protocols in the Methods in Molecular Biology: “Fundamentals of Ion Mobility-Mass Spectrometry for the Analysis of Biomolecules,” by Caleb B. Morris, James C. Poland, Jody C. May, and John A. McLean.

This work was supported in part using the resources of the Center for Innovative Technology at Vanderbilt University. The authors gratefully acknowledge financial support for this work provided by the National Institutes of Health (NIH NIGMS R01GM092218 and NCI R03CA222452) and the U.S. Environmental Protection Agency under Assistance Agreement No. 83573601. This work has not been formally reviewed by the EPA. The views expressed in this document are solely those of the authors and do not necessarily reflect those of the funding

agencies and organizations. The U.S. Government does not endorse any products or commercial services mentioned in this publication.

## 1.9. References

1. Thomson, J. J., Rutherford, E.; On the passage of electricity through gases exposed to Roentgen rays. *Philosophical Magazine Series 5* **1896**, 42 (258), 392 - 407.
2. Tyndall, A. M., Powell, C. F.; The Mobility of Ions in Pure Gases. *Proceedings of the Royal Society of London. Series A, Containing Papers of a Mathematical and Physical Character* **1930**, 129 (809), 162-180.
3. Tyndall, A. M.; Starr, L. H.; Powell, C. F., The Mobility of Ions in Air. Part IV. Investigations by Two New Methods. *Proceedings of the Royal Society of London. Series A, Containing Papers of a Mathematical and Physical Character* **1928**, 121 (787), 172-184.
4. Barnes, W. S., Martin, D. W., McDaniel, E. W.; Mass Spectrographic Identification of the Ion Observed in Hydrogen Mobility Experiments. *Physical Review Letters* **1961**, 6 (3), 110-111.
5. May, J. C., McLean, J. A.; Ion Mobility-Mass Spectrometry: Time-Dispersive Instrumentation. *Analytical Chemistry* **2015**, 87 (3), 1422-1436.
6. Dole, M., Mack, L. L., Hines, R. L., Mobley, R. C., Ferguson, L. D., Alice, M. B.; Molecular Beams of Macroions. *The Journal of Chemical Physics* **1968**, 49 (5), 2240-2249.
7. Dole, M., Hines, R. L., Mack, L. L., Mobley, R. C., Ferguson, L. D., Alice, M. B.; Gas Phase Macroions. *Macromolecules* **1968**, 1 (1), 96-97.
8. Lubman, D. M., Kronick, M. N.; Plasma chromatography with laser-produced ions. *Analytical Chemistry* **1982**, 54 (9), 1546-1551.
9. von Helden, G., Wyttenbach, T., Bowers, M. T.; Inclusion of a MALDI ion source in the ion chromatography technique: conformational information on polymer and biomolecular ions. *International Journal of Mass Spectrometry and Ion Processes* **1995**, 146-147, 349-364.
10. Wittmer, D., Chen, Y. H., Luckenbill, B. K., Hill, H. H., Jr.; Electrospray Ionization Ion Mobility Spectrometry. *Analytical Chemistry* **1994**, 66 (14), 2348-2355.
11. Clemmer, D.E., and Jarrold, M.F.; 1997. Ion mobility measurements and their applications to clusters and biomolecules. *Journal of Mass Spectrometry* **1997**, 32(6), 577-592.

12. Hoaglund, C.S., Valentine, S.J., Sporleder, C.R., Reilly, J.P. and Clemmer, D.E.; Three-dimensional ion mobility/TOFMS analysis of electrosprayed biomolecules. *Analytical Chemistry* **1998**, *70*(11), 2236-2242.
13. Henderson, S.C., Valentine, S.J., Counterman, A.E. and Clemmer, D.E.; ESI/ion trap/ion mobility/time-of-flight mass spectrometry for rapid and sensitive analysis of biomolecular mixtures. *Analytical Chemistry* **1999**, *71*(2), 291-301.
14. Gillig, K.J., Ruotolo, B., Stone, E.G., Russell, D.H., Fuhrer, K., Gonin, M. and Schultz, A.J.; Coupling high-pressure MALDI with ion mobility/orthogonal time-of-flight mass spectrometry. *Analytical Chemistry* **2000**, *72*(17), 3965-3971.
15. Smith, R. D.; Loo, J. A.; Loo, R. R. O.; Busman, M.; Udseth, H. R.; Principles and practice of electrospray ionization - mass spectrometry for large polypeptides and proteins. *Mass Spectrometry Reviews* **1991**, *10* (5), 359-452.
16. May, J. C.; Morris, C. B.; McLean, J. A.; Ion Mobility Collision Cross Section Compendium. *Analytical Chemistry* **2017**, *89* (2), 1032-1044.
17. Giles, K.; Williams, J. P.; Campuzano, I., Enhancements in travelling wave ion mobility resolution. *Rapid Communications in Mass Spectrometry* **2011**, *25* (11), 1559-1566.
18. Giles, K.; Pringle, S. D.; Worthington, K. R.; Little, D.; L., W. J.; Bateman, R. H.; Applications of a Traveling Wave-Based Radio-Frequency-Only Stacked Ring Ion Guide. *Rapid Communications in Mass Spectrometry* **2004**, *18* (20), 2401-2414.
19. Pringle, S. D.; Giles, K.; Wildgoose, J. L.; Williams, J. P.; Slade, S. E.; Thalassinos, K.; Bateman, R. H.; Bowers, M. T.; Scrivens, J. H.; An investigation of the mobility separation of some peptide and protein ions using a new hybrid quadrupole/travelling wave IMS/oa-ToF instrument. *International Journal of Mass Spectrometry* **2007**, *261* (1), 1-12.
20. May, J. C., Goodwin, C. R., Lareau, N. M., Leaptrot, K. L., Morris, C. B., Kurulugama, R. T., Mordehai, A., Klein, C., Barry, W., Darland, E., Overney, G., Imatani, K., Stafford, G. C., Fjeldsted, J. C., McLean, J. A.; Conformational Ordering of Biomolecules in the Gas Phase: Nitrogen Collision Cross Sections Measured on a Prototype High Resolution Drift Tube Ion Mobility-Mass Spectrometer. *Analytical Chemistry* **2014**, *86* (4), 2107-2116.
21. Silveira, J.A., Ridgeway, M.E. and Park, M.A.; 2014. High resolution trapped ion mobility spectrometry of peptides. *Analytical chemistry*, **2014**, *86*(12), pp.5624-5627.
22. Zhang, F., Guo, S., Zhang, M. Y., Zhang, Z. X., Guo, Y. L.; Characterizing ion mobility and collision cross section of fatty acids using electrospray ion mobility mass spectrometry. *Journal of Mass Spectrometry* **2015**, *50* (7), 906-913.

23. Kurulugama, R. T., Darland, E., Kuhlmann, F., Stafford, G., Fjeldsted, J.; Evaluation of drift gas selection in complex sample analyses using a high performance drift tube ion mobility-QTOF mass spectrometer. *Analyst* **2015**, *14* (20), 6834-6844.
24. Paglia, G., Williams, J. P., Menikarachchi, L., Thompson, J. W., Tyldesley-Worster, R., Halldorsson, S., Rolfsson, O., Moseley, A., Grant, D., Langridge, J., Palsson, B. O., Astarita, G.; Ion Mobility Derived Collision Cross Sections to Support Metabolomics Applications. *Analytical Chemistry* **2014**, *86* (8), 3985-3993.
25. Allen, S. J., Schwartz, A. M., Bush, M. F.; Effects of Polarity on the Structures and Charge States of Native-Like Proteins and Protein Complexes in the Gas Phase. *Analytical Chemistry* **2013**, *85* (24), 12055-12061.
26. Campuzano, I., Bush, M. F., Robinson, C. V., Beaumont, C., Richardson, K., Kim, H., Kim, H. I.; Structural Characterization of Drug-like Compounds by Ion Mobility Mass Spectrometry: Comparison of Theoretical and Experimentally Derived Nitrogen Collision Cross Sections. *Analytical Chemistry* **2012**, *84* (2), 1026-1033.
27. Bush, M. F., Campuzano, I. D. G., Robinson, C. V.; Ion Mobility Mass Spectrometry of Peptide Ions: Effects of Drift Gas and Calibration Strategies. *Analytical Chemistry* **2012**, *84* (16), 7124-7130.
28. Shah, A. R., Agarwal, K., Baker, E. S., Singhal, M., Mayampurath, A. M., Ibrahim, Y. M., Kangas, L. J., Monroe, M. E., Zhao, R., Belov, M. E., Anderson, G. A., Smith, R. D.; Machine learning based prediction for peptide drift times in ion mobility spectrometry. *Bioinformatics* **2010**, *26* (13), 1601-1607.
29. Forsythe, J.G., Stow, S.M., Nefzger, H., Kwiecien, N.W., May, J.C., McLean, J.A. and Hercules, D.M.; Structural characterization of methylenedianiline regioisomers by ion mobility-mass spectrometry, tandem mass spectrometry, and computational strategies: I. Electrospray spectra of 2-ring isomers. *Analytical Chemistry*, **2014**, *86*(9), pp.4362-4370.
30. Fenn, L. S., McLean, J. A.; Biomolecular structural separations by ion-mobility-mass spectrometry. *Analytical and Bioanalytical Chemistry* **2008**, *391* (3), 905-909.
31. Fenn, L. S., Kliman, M., Mahsut, A., Zhao, S. R., McLean, J. A.; Characterizing ion mobility-mass spectrometry conformation space for the analysis of complex biological samples. *Analytical and Bioanalytical Chemistry* **2009**, *394* (1), 235-244.
32. Hines, K. M., May, J. C., McLean, J. A., Xu, L. B.; Evaluation of Collision Cross Section Calibrants for Structural Analysis of Lipids by Traveling Wave Ion Mobility-Mass Spectrometry. *Analytical Chemistry* **2016**, *88* (14), 7329-7336.
33. Leaptrot, K. L., May, J. C., Dodds, J. N., McLean, J. A.; Ion Mobility Conformational Lipid Atlas for High Confidence Lipidomics. *Nature Communications* **2019**, *10*(1), 985.

34. Baker, E. S., Burnum-Johnson, K. E., Jacobs, J. M., Diamond, D. L., Brown, R. N., Ibrahim, Y. M., Orton, D. J., Piehowski, P. D., Purdy, D. E., Moore, R. J., Danielson, W. F., Monroe, M. E., Crowell, K. L., Slysz, G. W., Gritsenko, M. A., Sandoval, J. D., LaMarche, B. L., Matzke, M. M., Webb-Robertson, B.-J. M., Simons, B. C., McMahon, B. J., Bhattacharya, R., Perkins, J. D., Carithers, R. L., Strom, S., Self, S. G., Katze, M. G., Anderson, G. A., Smith, R. D.; Advancing the High Throughput Identification of Liver Fibrosis Protein Signatures Using Multiplexed Ion Mobility Spectrometry. *Molecular & Cellular Proteomics* **2014**, *13* (4), 1119-1127.
35. Liu, X., Plasencia, M., Ragg, S., Valentine, S. J., Clemmer, D. E.; Development of high throughput dispersive LC--ion mobility--TOFMS techniques for analysing the human plasma proteome. *Briefings in Functional Genomics and Proteomics* **2004**, *3* (2), 177-186.
36. Poad, B. L. J., Zheng, X. Y., Mitchell, T. W., Smith, R. D., Baker, E. S., Blanksby, S. J.; Online Ozonolysis Combined with Ion Mobility-Mass Spectrometry Provides a New Platform for Lipid Isomer Analyses. *Analytical Chemistry* **2018**, *90* (2), 1292-1300.
37. Harris, R. A., May, J. C., Stinson, C. A., Xia, Y., McLean, J. A.; Determining Double Bond Position in Lipids Using Online Ozonolysis Coupled to Liquid Chromatography and Ion Mobility-Mass Spectrometry. *Analytical Chemistry* **2018**, *90* (3), 1915-1924.
38. Valentine, S. J., Counterman, A. E., Clemmer, D. E.; A database of 660 peptide ion cross sections: use of intrinsic size parameters for bona fide predictions of cross sections. *Journal of the American Society for Mass Spectrometry* **1999**, *10* (11), 1188-1211.
39. Tao, L., McLean, J. R., McLean, J. A., Russell, D. H.; A collision cross-section database of singly-charged peptide ions. *Journal of the American Society for Mass Spectrometry* **2007**, *18* (9), 1727-1728.
40. Dilger, J. M., Valentine, S. J., Glover, M. S., Ewing, M. A., Clemmer, D. E.; A database of alkali metal-containing peptide cross sections: Influence of metals on size parameters for specific amino acids. *International Journal of Mass Spectrometry* **2012**, *330-332* (0), 35-45.
41. Dilger, J. M., Valentine, S. J., Glover, M. S., Clemmer, D. E.; A Database of Alkaline-Earth-Coordinated Peptide Cross Sections: Insight into General Aspects of Structure. *Journal of the American Society for Mass Spectrometry* **2013**, *24* (5), 768-779.
42. Paglia, G., Angel, P., Williams, J. P., Richardson, K., Olivos, H. J., Thompson, J. W., Menikarachchi, L., Lai, S., Walsh, C., Moseley, A., Plumb, R. S., Grant, D. F., Palsson, B. O., Langridge, J., Geromanos, S., Astarite, G.; Ion Mobility-Derived Collision Cross Section As an Additional Measure for Lipid Fingerprinting and Identification. *Analytical Chemistry* **2015**, *87* (2), 1137-1144.
43. Picache, J.A., Rose, B.S., Balinski, A., Leaptrot, K.L., Sherrod, S.D., May, J.C., and McLean, J.A.; Collision cross section compendium to annotate and predict multi-omic compound identities. *Chemical Science* **2019**, *10*(4), pp.983-993.

44. Ellis, H. W., Thackston, M. G., McDaniel, E. W., Mason, E. A.; Transport Properties of Gaseous Ions Over a Wide Energy Range. Part III. *Atomic Data and Nuclear Data Tables* **1984**, *31* (1), 113-151.
45. Deng, L. L., Ibrahim, Y. M., Baker, E. S., Aly, N. A., Hamid, A. M., Zhang, X., Zheng, X. Y., Garimella, S. V. B., Webb, I. K., Prost, S. A., Sandoval, J. A., Norheim, R. V., Anderson, G. A., Tolmachev, A. V., Smith, R. D.; Ion Mobility Separations of Isomers based upon Long Path Length Structures for Lossless Ion Manipulations Combined with Mass Spectrometry. *Chemistry Select* **2016**, *1* (10), 2396-2399.
46. Dodds, J. N., May, J. C., McLean, J. A.; Investigation of the Complete Suite of the Leucine and Isoleucine Isomers: Toward Prediction of Ion Mobility Separation Capabilities. *Analytical Chemistry* **2017**, *89* (1), 952-959.
47. Dwivedi, P., Bendiak, B., Clowers, B. H., Hill Jr, H. H.; Rapid Resolution of Carbohydrate Isomers by Electrospray Ionization Ambient Pressure Ion Mobility Spectrometry-Time-of-Flight Mass Spectrometry (ESI-APIMS-TOFMS). *Journal of the American Society for Mass Spectrometry* **2007**, *18* (7), 1163-1175.
48. Fenn, L. S., McLean, J. A.; Structural resolution of carbohydrate positional and structural isomers based on gas-phase ion mobility-mass spectrometry. *Physical Chemistry Chemical Physics* **2011**, *13* (6), 2196-2205.
49. Groessl, M.; Graf, S.; Knochenmuss, R., High resolution ion mobility-mass spectrometry for separation and identification of isomeric lipids. *Analyst* **2015**, *14* (20), 6904-6911.
50. Lalli, P. M., Corilo, Y. E., Fasciotti, M., Riccio, M. F., de Sa, G. F.; Daroda, R. J., Souza, G. H. M. F., McCullagh, M., Bartberger, M. D., Eberlin, M. N., Campuzano, I. D. G.; Baseline resolution of isomers by traveling wave ion mobility mass spectrometry: investigating the effects of polarizable drift gases and ionic charge distribution. *Journal of Mass Spectrometry* **2013**, *48* (9), 989-997.
51. Valentine, S.J., Kulchania, M., Barnes, C.A.S., and Clemmer, D.E.; Multidimensional separations of complex peptide mixtures: a combined high-performance liquid chromatography/ion mobility/time-of-flight mass spectrometry approach. *International Journal of Mass Spectrometry* **2001**, *212*(1-3), 97-109.
52. Matz, L.M., Dion, H.M., and Hill Jr, H.H.; Evaluation of capillary liquid chromatography–electrospray ionization ion mobility spectrometry with mass spectrometry detection. *Journal of Chromatography A* **2002**, *946*(1-2), 59-68.
53. Lareau, N.M., May, J.C. and McLean, J.A.; Non-derivatized glycan analysis by reverse phase liquid chromatography and ion mobility-mass spectrometry. *Analyst*, **2015**, *140*(10), pp.3335-3338.



54. Nichols, C.M., May, J.C., Sherrod, S.D. and McLean, J.A.; Automated flow injection method for the high precision determination of drift tube ion mobility collision cross sections. *Analyst*, **2018**, *143*(7), pp.1556-1559.
55. Gerhardt, N., Schwolow, S., Rohn, S., Perez-Cacho, P. R., Galan-Soldevilla, H., Arce, L., Weller, P.; Quality assessment of olive oils based on temperature-ramped HS-GC-IMS and sensory evaluation: Comparison of different processing approaches by LDA, kNN, and SVM. *Food Chemistry* **2019**, *278*, 720-728.
56. Donato, P., Giuffrida, D., Oteri, M., Inferrera, V., Dugo, P., Mondello, L.; Supercritical Fluid Chromatography x Ultra-High Pressure Liquid Chromatography for Red Chilli Pepper Fingerprinting by Photodiode Array, Quadrupole-Time-of-Flight and Ion Mobility Mass Spectrometry (SFC x RP-UHPLC-PDA-Q-ToF MS-IMS). *Food Analytical Methods* **2018**, *11* (12), 3331-3341.
57. Hill, H. H., Stlouis, R. H., Morrissey, M. A., Shumate, C. B., Siems, W. F., McMinn, D. G.; A Detection Method for Unified Chromatography-Ion Mobility Monitoring. *HRC-Journal of High Resolution Chromatography* **1992**, *15* (7), 417-422.
58. Hillenkamp, F., Karas, M., Beavis, R.C. and Chait, B.T.; Matrix-assisted laser desorption/ionization mass spectrometry of biopolymers. *Analytical Chemistry*, **1991**, *63*(24), pp.1193A-1203A.
59. Karas, M., Bahr, U., and Gießmann, U.; Matrix-assisted laser desorption ionization mass spectrometry. *Mass Spectrometry Reviews*, **1991**, *10*(5), pp.335-357.
60. Stoeckli, M., Chaurand, P., Hallahan, D.E., and Caprioli, R.M.; Imaging mass spectrometry: a new technology for the analysis of protein expression in mammalian tissues. *Nature Medicine*, **2001**, *7*(4), p.493.
61. Cornett, D.S., Reyzer, M.L., Chaurand, P., and Caprioli, R.M.; MALDI imaging mass spectrometry: molecular snapshots of biochemical systems. *Nature Methods*, **2007**, *4*(10), p.828.
62. McLean, J. A., Ridenour, W. B., Caprioli, R. M.; Profiling and imaging of tissues by imaging ion mobility-mass spectrometry. *Journal of Mass Spectrometry* **2007**, *42* (8), 1099-1105.
63. Jackson, S.N., Ugarov, M., Egan, T., Post, J.D., Langlais, D., Albert Schultz, J., and Woods, A.S.; MALDI-ion mobility-TOFMS imaging of lipids in rat brain tissue. *Journal of Mass Spectrometry*, **2007**, *42*(8), pp.1093-1098.
64. Fenn, J.B., Mann, M., Meng, C.K., Wong, S.F., and Whitehouse, C.M.; Electrospray ionization for mass spectrometry of large biomolecules. *Science*, **1989**, *246*(4926), pp.64-71.
65. Fenn, J.B., Mann, M., Meng, C.K., Wong, S.F., and Whitehouse, C.M.; Electrospray ionization—principles and practice. *Mass Spectrometry Reviews*, **1990**, *9*(1), pp.37-70.

66. Belov, M.E., Gorshkov, M.V., Udseth, H.R., Anderson, G.A., and Smith, R.D.; Zeptomole-sensitivity electrospray ionization– fourier transform ion cyclotron resonance mass Spectrometry of proteins. *Analytical Chemistry*, **2000**, 72(10), pp.2271-2279.
67. Hardman, M. and Makarov, A.A., Interfacing the orbitrap mass analyzer to an electrospray ion source. *Analytical Chemistry*, **2003**, 75(7), pp.1699-1705.
68. Tang, X.J., Thibault, P., and Boyd, R.K.; Fragmentation reactions of multiply-protonated peptides and implications for sequencing by tandem mass spectrometry with low-energy collision-induced dissociation. *Analytical Chemistry*, **1993**, 65(20), pp.2824-2834.
69. Zubarev, R.A., Kelleher, N.L., and McLafferty, F.W.; Electron capture dissociation of multiply charged protein cations. A nonergodic process. *Journal of the American Chemical Society*, **1998**, 120(13), pp.3265-3266.
70. Syka, J.E., Coon, J.J., Schroeder, M.J., Shabanowitz, J., and Hunt, D.F.; Peptide and protein sequence analysis by electron transfer dissociation mass spectrometry. *Proceedings of the National Academy of Sciences*, **2004**, 101(26), pp.9528-9533.
71. Dodds, J.N., May, J.C., and McLean, J.A.; Correlating resolving power, resolution, and collision cross section: unifying cross-platform assessment of separation efficiency in ion mobility spectrometry. *Analytical Chemistry*, **2017**, 89(22), pp.12176-12184.
72. Mason, E. A., McDaniel, E. W.; *Transport Properties of Ions in Gases*. John Wiley & Sons: New York, **1988**; p 560.
73. Siems, W.F., Viehland, L.A., and Hill Jr, H.H.; Improved momentum-transfer theory for ion mobility. 1. Derivation of the fundamental equation. *Analytical Chemistry* **2012**, 84(22), 9782-9791.
74. Bush, M.F., Hall, Z., Giles, K., Hoyes, J., Robinson, C.V. and Ruotolo, B.T., Collision cross sections of proteins and their complexes: a calibration framework and database for gas-phase structural biology. *Analytical Chemistry* **2010**, 82(22), 9557-9565.
75. Deng, L. L.; Ibrahim, Y. M.; Hamid, A. M.; Garimella, S. V. B.; Webb, I. K.; Zheng, X. Y.; Prost, S. A.; Sandoval, J. A.; Norheim, R. V.; Anderson, G. A.; Tolmachev, A. V.; Baker, E. S.; Smith, R. D., Ultra-High Resolution Ion Mobility Separations Utilizing Traveling Waves in a 13 m Serpentine Path Length Structures for Lossless Ion Manipulations Module. *Analytical Chemistry* **2016**, 88 (18), 8957-8964.
76. May, J. C., McLean, J. A.; Advanced Multidimensional Separations in Mass Spectrometry: Navigating the Big Data Deluge. In *Annual Review of Analytical Chemistry, Vol 9*, Bohn, P. W.; Pemberton, J. E., Eds. Annual Reviews: Palo Alto, **2016**; Vol. 9, 387-409.

77. May, J.C., Goodwin, C.R., and McLean, J.A.; Gas-Phase Ion Mobility-Mass Spectrometry (IM-MS) and Tandem IM-MS/MS Strategies for Metabolism Studies and Metabolomics. *Encyclopedia of Drug Metabolism and Interactions*, **2011**, 1-29.
78. Kolli, V., Schumacher, K. N., Dodds, E. D.; Ion mobility-resolved collision-induced dissociation and electron transfer dissociation of N-glycopeptides: gathering orthogonal connectivity information from a single mass-selected precursor ion population. *Analyst* **2017**, *142* (24), 4691-4702.
79. Lermyte, F., Verschueren, T., Brown, J. M., Williams, J. P., Valkenburg, D., Sobott, F.; Characterization of top-down ETD in a travelling-wave ion guide. *Methods* **2015**, *89*, 22-29.
80. Williams, J. P., Pringle, S., Richardson, K., Gethings, L., Vissers, J. P. C., De Cecco, M., Houel, S., Chakraborty, A. B., Yu, Y. Q., Chen, W. B., Brown, J. M.; Characterisation of glycoproteins using a quadrupole time-of-flight mass spectrometer configured for electron transfer dissociation. *Rapid Communications in Mass Spectrometry* **2013**, *27* (21), 2383-2390.
81. Ruotolo B. L., Benesch J. L. P., Sandercock A. M., Hyung S., Robinson C.; Ion mobility-mass spectrometry analysis of large protein complexes. *Nature Protocols*, **2008**, *3*, 1139-1152
82. McLean J. A., Ruotolo B. T., Gillig K. J., Russel D. H.; Ion mobility-mass spectrometry: a new paradigm for proteomics. *International Journal of Mass Spectrometry*. **2005**, *240*, 3, 301-315
83. Paglia, G., Astarita, G.; Metabolomics and lipidomics using traveling-wave ion mobility mass spectrometry. *Nature Protocols*, **2017**, *12*, 797-813
84. Zhang X., Quinn K., Cruickshank-Quinn C., Reisdorph R., Reisdorph N.; "The application of Ion Mobility Mass Spectrometry to metabolomics" *Current Opinion in Chemical Biology*, **2018**, *42*, 60-66
85. May, J. C., Goodwin, C. R., McLean, J. A.; Ion mobility mass spectrometry strategies for untargeted systems, synthetic, and chemical biology. *Current Opinion in Biotechnology* **2015**, *31*, 117-121
86. Dunn, W. B., Broadhurst D., Begley, P., Zelena E., Francis-McIntyre S., Anderson, N., Brown, M., Knowles, J. D., Halsall, A., Haselden, J. N., Nicholls, A. W., Wilson, I. D., Kell, D. B., Goodacre, R.; The Human Serum Metabolome Consortium; Procedures for large-scale metabolic profiling of seruma and plasma using gas chromatography and liquid chromatraphy coupled to mass spectrometry. *Nature Protocols* **2011**, *6*, 1060-1083
87. Hoaglund-Hyzer, C.S., Li, J. and Clemmer, D.E.; Mobility labeling for parallel CID of ion mixtures. *Analytical Chemistry*, **2000** *72*(13), 2737-2740.
88. Taguchi, F., Solomon, B., Gregorc, V., Roder, H., Gray, R., Kashara, K., Nisho, M., Brahmer, J., Spreafico, A., Ludovini, V., Massion, P. P., Dziadziuszho, R., Schiller, J., Grigorieva, J.,

- Tsy-pin, M., Hunsucker, S. W., Caprioli R., Duncan, M. W., Hirsch, F. R., Bunn, P. A., Carbone, D. P.; Mass spectrometry to classify non-small-lung cell lung cancer patients for clinical outcome after treatment with epidermal growth factor receptor tyrosine kinase inhibitors: a multicohort cross-institutional study. *Journal of the National Cancer Institute* **2007**, 99, 11, 838-846
89. Mori, H., Takio, K., Ogawara, M., Selkoe D. J.; mass spectrometry of purified amyloid beta protein in Alzheimer's disease. *Journal of Biochemical Chemistry* **1992**, 17082-17086
90. Djidja, M. C., Francese, S., Loadman, P. M., Sutton, C. W., Scriven, P., Claude, E., Snel, M. F., Franck, J., Salzet, M., Clench, M. R.; Detergent addition to tryptic digests and ion mobility separation prior to MS/MS improves peptide yield and protein identification for *in situ* proteomics investigation of frozen and formalin-fixed paraffin-embedded adenocarcinoma tissue sections. *Proteomics*, **2009**, 9, 10, 2750-2763
91. Moon, M. H., Myung, S., Plasencia, M., Hilderbrand, A. E., Clemmer, D. E.; Nanoflow LC/Ion mobility/CID/TOF for proteomics: analysis of a human urinary proteome. *Journal of Proteome Research*. **2003**, 2(6), 589-597
92. Thalassinos, K., Grabenauer, M., Slade, S. E., Hilton G. R., Bowers, M. T., Scrivens, J. H.; Characterization of phosphorylated peptides using traveling wave-based and drift cell ion mobility mass spectrometry. **2009** 81, 1, 248-254
93. Zhong, Y., Hyung, S., Ruotolo, B. T.; Ion mobility-mass spectrometry for structural proteomics. *Expert Review of Proteomics*. **2012**, 9, 1, 47-58
94. May, J.C., McLean, J.A.; A uniform field ion mobility study of melittin and implications of low-field mobility for resolving fine cross-sectional detail in peptide and protein experiments. *Proteomics* **2015**, 15(16), pp.2862-2871.
95. Shliaha, P. V., Bond, N. J., Gatto, L., Liley, K. S.; Effects of traveling wave ion mobility separation of data independent acquisition in proteomics studies. *Journal of Proteome Research*. **2013**, 12, 6, 2323-2339
96. Wang, G., Abzalimov, R. R., Kaltashov, I. A.; Direct monitoring of heat-stressed biopolymers with temperature-controlled electrospray ionization mass spectrometry. *Analytical Chemistry* **2011**, 83, 8, 2870-2876
97. El-Baba, T. J., Woodall, D. W., Raab, S. A., Fuller, D. R., Langanowsky, A., Russell, D. H., Clemmer, D. E.; Melting Proteins: evidence for multiple stable structures upon thermal denaturation of native ubiquitin from ion mobility spectrometry-mass spectrometry measurements. *Journal of the American Chemical Society*. **2017**, 139(18), 6306-6309
98. Han, X., Yang, K., Gross, R. W.; Multi-dimensional mass spectrometry-based shotgun lipidomics and novel strategies for lipidomic analysis. *Mass Spectrometry Reviews*. **2011**, 31, 1, 134-178

99. Kliman, M., May, J. C., McLean, J. A.; Lipid analysis and lipidomics by structurally selective ion mobility-mass spectrometry. *Biochimica et Biophysica Acta (BBA)- Molecular and Cell Biology of Lipids* **2011**, 1811, 11, 935-945
100. Paglia, G., Kliman, M., Claude, E., Geromanos, S., Astarita G.; Application of ion-mobility mass spectrometry for lipids. *Analytical and Bioanalytical Chemistry* **2015**, 407, 17, 4995-5007
101. Gressel, M., Graf, S., Knochenmuss, R.; High resolution ion mobility-mass spectrometry for separation and identification of isomeric lipids. *Analyst* **2015**, 140
102. Di Giovanni, J. P., Barkley, R. M., Jones, D. N. M., Hankins, J. A., Murphy, R. C.; Tandem mass spectrometry and ion mobility reveals structural insight into eicosanoid product ion formation. *Journal of The American Society for Mass Spectrometry*. **2018**, 29, 6, 1231-1241
103. Paglia G., Shrestha B., Astarita G.; Ion-Mobility Mass Spectrometry for Lipidomics Applications. In *Lipidomics*, **2017**, pp 61-79. Humana Press, New York, NY
104. Thomas, M. C., Mitchell, T. W., Harman, D. G., Deeley, J. M., Murphy, R. C., Blanksby, S. J.; Elucidation of double bond position in unsaturated lipids by ozone electrospray ionization mass spectrometry. *Analytical Chemistry*. **2007**, 79, 13, 5013-5022
105. Sun, C., Zhao, Y., Curtis, J. M.; Elucidation of phosphatidylcholine isomers using two dimensional liquid chromatography coupled in-line with ozonolysis mass spectrometry. *Journal of Chromatography A*. **2014**, 1351, 37-45
106. Dettmer, K., Aronov, P. A., Hammock, B. D.; Mass Spectrometry-based metabolomics. *Mass Spectrometry Reviews*. **2007**, 26, 1, 51-78
107. Zhang, X., Quinn, K., Cruickshank-Quinn, C., Reisdorph, R., Reisdorph N.; Applications of ion mobility mass spectrometry to metabolomics. *Current Opinion in Chemical Biology*. **2018**, 42, 60-66
108. Sinclair, E., Hollywood, K. A., Yan, C., Blankley, R., Rainer, B., Barran P.; Mobilising ion mobility mass spectrometry for metabolomics. *Analyst*, **2018**, 19
109. Schrimpe-Rutledge, A. C., Codreanu S. G., Sherrod, S. D., McLean, J. A.; Untargeted metabolomics strategies- challenges and emerging directions. *Journal of American Society of Mass Spectrometry*. **2016**, 27, 12, 1897-1905
110. May, J.C., Gant-Branum, R.L., McLean, J.A.; Targeting the untargeted in molecular phenomics with structurally-selective ion mobility-mass spectrometry. *Current Opinion in Biotechnology* **2016**, 39, pp.192-197.

111. Nichols, C.M., Dodds, J.N., Rose, B.S., Picache, J.A., Morris, C.B., Codreanu, S.G., May, J.C., Sherrod, S.D., McLean, J.A.; 2018. Untargeted Molecular Discovery in Primary Metabolism: Collision Cross Section as a Molecular Descriptor in Ion Mobility-Mass Spectrometry. *Analytical Chemistry* **2018**, 90(24), pp.14484-14492.
112. Wickramasekara, S.I., Zandkarimi, F., Morr e, J., Kirkwood, J., Legette, L., Jiang, Y., Gombart, A.F., Stevens, J.F., Maier, C.S; Electrospray Quadrupole Travelling Wave Ion Mobility Time-of-Flight mass Spectrometry for the Detection of Plasma Metabolome Changes Caused by Xanthohumol in Obese Zucker (fa/fa) Rats, *Metabolites*, **2013**, 3, 701-717
113. Stow, M. S., Causon T. J., Zheng X., Kurulugama R. T., Mairinger, T., May, J. C., Rennie E. E., Smith R. D., McLean, J. A., Hann, S., Fjeldsted, J. C.; An Interlaboratory Evaluation of Drift Tube Ion Mobility-Mass Spectrometry Collision Cross Section Measurements. *Analytical Chemistry* **2017**, 89, 17, 9048-9055
114. Nichols, C. M., Dodds, J. N., Rose, B. S., Picache J. A., Morris C. B., Codreanu, S., G., May, J. C., Sherrod, S. D., McLean, J. A.; Untargeted Molecular Discovery in Primary Metabolism: Collision Cross Section as a Molecular Descriptor in Ion Mobility- Mass Spectrometry. *Analytical Chemistry*, **2018**, 90, 24, 14484-14492
115. Regueiro J., Negreira N., Berntssen M.H.; Ion-mobility-derived collision cross section as an additional identification point for multiresidue screening of pesticides in fish feed. *Analytical chemistry*. **2016** Nov 4;88(22):11169-77.
116. Stephan S., Hippler J., K hler T., Deeb A.A., Schmidt T.C., Schmitz O.J.; Contaminant screening of wastewater with HPLC-IM-qTOF-MS and LC+ LC-IM-qTOF-MS using a CCS database. *Analytical and Bioanalytical Chemistry*. **2016**, 408, 24, 6545-55
117. Zheng X., Aly N.A., Zhou Y., Dupuis K.T., Bilbao A., Paurus V.L., Orton D.J., Wilson R., Payne S.H., Smith R.D., Baker E.S.; A structural examination and collision cross section database for over 500 metabolites and xenobiotics using drift tube ion mobility spectrometry. *Chemical Science*. **2017**, 8, 11, 7724-36
118. Hern andez-Mesa M., Le Bizec B., Monteau F., Garc a-Campa a A.M., Dervilly-Pinel G.; Collision Cross Section (CCS) database: An additional measure to characterize steroids. *Analytical chemistry*. **2018**,90, 7, 4616-25
119. Chen, T. C., Ibrahim, Y. M., Webb, I. K., Garimella, S. V. B., Zhang, X., Hamid, A. M., Deng, L. L., Karnesky, W. E., Prost, S. A., Sandoval, J. A., Norheim, R. V., Anderson, G. A., Tolmachev, A. V., Baker, E. S., Smith, R. D.; Mobility-Selected Ion Trapping and Enrichment Using Structures for Lossless Ion Manipulations. *Analytical Chemistry* **2016**, 88 (3), 1728-1733.

120. Ibrahim, Y. M., Hamid, A. M., Deng, L. L., Garimella, S. V. B., Webb, I. K.; Baker, E. S., Smith, R. D.; New frontiers for mass spectrometry based upon structures for lossless ion manipulations. *Analyst* **2017**, *142* (7), 1010-1021.
121. Zhang, X. Y., Garimella, S. V. B., Prost, S. A., Webb, I. K., Chen, T. C., Tang, K. Q., Tolmachev, A. V., Norheim, R. V., Baker, E. S., Anderson, G. A., Ibrahim, Y. M., Smith, R. D.; Ion Trapping, Storage, and Ejection in Structures for Lossless Ion Manipulations. *Analytical Chemistry* **2015**, *87* (12), 6010-6016.
122. Chouinard, C. D., Nagy, G., Webb, I. K., Shi, T. J., Baker, E. S., Prost, S. A., Liu, T., Ibrahim, Y. M., Smith, R. D.; Improved Sensitivity and Separations for Phosphopeptides using Online Liquid Chromatography Coupled with Structures for Lossless Ion Manipulations Ion Mobility-Mass Spectrometry. *Analytical Chemistry* **2018**, *90* (18), 10889-10896.
123. Garimella, S. V. B., Ibrahim, Y. M., Webb, I. K., Tolmachev, A. V., Zhang, X. Y., Prost, S. A., Anderson, G. A., Smith, R. D.; Simulation of Electric Potentials and Ion Motion in Planar Electrode Structures for Lossless Ion Manipulations (SLIM). *Journal of the American Society for Mass Spectrometry* **2014**, *25* (11), 1890-1896.
124. Webb, I. K., Garimella, S. V. B., Tolmachev, A. V., Chen, T. C., Zhang, X. Y., Cox, J. T., Norheim, R. V., Prost, S. A., LaMarche, B., Anderson, G. A., Ibrahim, Y. M., Smith, R. D.; Mobility-Resolved Ion Selection in Uniform Drift Field Ion Mobility Spectrometry/Mass Spectrometry: Dynamic Switching in Structures for Lossless Ion Manipulations. *Analytical Chemistry* **2014**, *86* (19), 9632-9637.
125. Deng, L. L., Webb, I. K., Garimella, S. V. B., Hamid, A. M., Zheng, X. Y., Norheim, R. V., Prost, S. A., Anderson, G. A., Sandoval, J. A., Baker, E. S., Ibrahim, Y. M., Smith, R. D.; Serpentine Ultralong Path with Extended Routing (SUPER) High Resolution Traveling Wave Ion Mobility-MS using Structures for Lossless Ion Manipulations. *Analytical Chemistry* **2017**, *89* (8), 4628-4634.
126. Garimella, S. V. B., Ibrahim, Y. M., Webb, I. K., Ipsen, A. B., Chen, T. C., Tolmachev, A. V., Baker, E. S., Anderson, G. A., Smith, R. D.; Ion manipulations in structures for lossless ion manipulations (SLIM): computational evaluation of a 90 degrees turn and a switch. *Analyst* **2015**, *14* (20), 6845-6852.
127. Fernandez-Lima, F. A., Kaplan, D. A., Suetering, J., Park, M. A.; Gas-phase separation using a trapped ion mobility spectrometer. *International Journal for Ion Mobility Spectrometry* **2011**, *14* (2-3), 93-98.
128. Adams, K.J., Montero, D., Aga, D., Fernandez-Lima, F.; Isomer separation of polybrominated diphenyl ether metabolites using nanoESI-TIMS-MS. *International Journal for Ion Mobility Spectrometry* **2016**, *19* (2-3), 69-76.

129. Michelmann, K., Silveira, J. A., Ridgeway, M. E., Park, M. A.; Fundamentals of Trapped Ion Mobility Spectrometry. *Journal of the American Society for Mass Spectrometry* **2015**, *26* (1), 14-24.
130. Hernandez, D. R., DeBord, J. D., Ridgeway, M. E., Kaplan, D. A., Park, M. A., Fernandez-Lima, F.; Ion dynamics in a trapped ion mobility spectrometer. *Analyst* **2014**, *139* (8), 1913-1921.
131. Silveira, J. A., Danielson, W., Ridgeway, M. E., Park, M. A.; Altering the mobility-time continuum: nonlinear scan functions for targeted high resolution trapped ion mobility-mass spectrometry. *International Journal for Ion Mobility Spectrometry* **2016**, *19* (2-3), 87-94.
132. May, J. C., Leaptrot, K. L., Sundarapandian, S., McLean, J. A.; *In Theoretical Evaluation and Performance Characterization of an 8-Channel Spatially Multiplexed Ion Mobility-Mass Spectrometer*, 60th Annual ASMS Conference on Mass Spectrometry and Allied Topics, Vancouver, BC, May **2012**; Vancouver, BC.
133. Asbury, G. R., Hill, H. H.; Using different drift gases to change separation factors ( $\alpha$ ) in ion mobility spectrometry. *Analytical Chemistry* **2000**, *72* (3), 580-584.
134. Matz, L. M., Hill, H. H., Jr. Beegle, L. W., Kanik, I.; Investigation of drift gas selectivity in high resolution ion mobility spectrometry with mass spectrometry detection. *Journal of the American Society for Mass Spectrometry* **2002**, *13* (4), 300-307.
135. Berant, Z., Karpas, Z.; Mass-mobility correlation of ions in view of new mobility data. *Journal of the American Chemical Society* **1989**, *111* (11), 3819-3824.
136. Howdle, M. D., Eckers, C., Laures, A. M. F., Creaser, C. S.; The effect of drift gas on the separation of active pharmaceutical ingredients and impurities by ion mobility-mass spectrometry. *International Journal of Mass Spectrometry* **2010**, *298* (1-3), 72-77.
137. Purves, R. W., Ozog, A. R., Ambrose, S. J., Prasad, S., Belford, M., Dunyach, J. J.; Using Gas Modifiers to Significantly Improve Sensitivity and Selectivity in a Cylindrical FAIMS Device. *Journal of the American Society for Mass Spectrometry* **2014**, *25* (7), 1274-1284.
138. Waraksa, E., Perycz, U., Namiesnik, J., Sillanpaa, M., Dymerski, T., Wojtowicz, M., Puton, J.; Dopants and gas modifiers in ion mobility spectrometry. *TrAC-Trends Anal. Chem.* **2016**, *82*, 237-249.
139. Schneider, B. B., Covey, T. R., Nazarov, E. G.; Investigation of the chemical orthogonality effect of transport gas modifiers on DMS separations. *Abstracts of Papers of the American Chemical Society* **2013**, *246*, 1.
140. Kafle, A., Coy, S. L., Wong, B. M., Fornace, A. J., Glick, J. J., Vouros, P.; Understanding Gas Phase Modifier Interactions in Rapid Analysis by Differential Mobility-Tandem Mass



- Spectrometry. *Journal of the American Society for Mass Spectrometry* **2014**, 25 (7), 1098-1113.
141. Levin, D. S., Vouros, P., Miller, R. A., Nazarov, E. G., Morris, J. C.; Characterization of gas-phase molecular interactions on differential mobility ion behavior utilizing an electrospray ionization-differential mobility-mass spectrometer system. *Analytical Chemistry* **2006**, 78 (1), 96-106.
142. Porta, T., Varesio, E., Hopfgartner, G.; Gas-Phase Separation of Drugs and Metabolites Using Modifier-Assisted Differential Ion Mobility Spectrometry Hyphenated to Liquid Extraction Surface Analysis and Mass Spectrometry. *Analytical Chemistry* **2013**, 85 (24), 11771-11779.
143. Fernandez-Maestre, R., Wu, C., Hill, H. H.; Buffer gas modifiers effect resolution in ion mobility spectrometry through selective ion-molecule clustering reactions. *Rapid Communications in Mass Spectrometry* **2012**, 26 (19), 2211-2223.
144. Garabedian, A., Leng, F. F., Ridgeway, M. E., Park, M. A., Fernandez-Lima, F.; Tailoring peptide conformational space with organic gas modifiers in TIMS-MS. *International Journal for Ion Mobility Spectrometry* **2018**, 21 (1-2), 43-48.
145. Beegle, L. W., Kanik, I., Matz, L., Hill, H. H.; Electrospray ionization nigh-resolution ion mobility spectrometry for the detection of organic compounds, 1. Amino acids. *Analytical Chemistry* **2001**, 73 (13), 3028-3034.
146. Beegle, L. W., Kanik, I., Matz, L., Hill, H. H.; Effects of drift-gas polarizability on glycine peptides in ion mobility spectrometry. *International Journal of Mass Spectrometry* **2002**, 216 (3), 257-268.
147. Chouinard, C. D., Beekman, C. R., Kemperman, R. H. J., King, H. M., Yost, R. A.; Ion mobility-mass spectrometry separation of steroid structural isomers and epimers. *International Journal for Ion Mobility Spectrometry* **2017**, 20 (1-2), 31-39.
148. Fasciotti, M., Lalli, P. M., Klitzke, C. F., Corilo, Y. E., Pudenzi, M. A., Pereira, R. C. L., Bastos, W., Daroda, R. J., Eberlin, M. N.; Petroleomics by Traveling Wave Ion Mobility–Mass Spectrometry Using CO<sub>2</sub> as a Drift Gas. *Energy & Fuels* **2013**, 27 (12), 7277-7286.
149. Fasciotti, M., Sanvido, G. B., Santos, V. G., Lalli, P. M., McCullagh, M., de Sá, G. F., Daroda, R. J., Peter, M. G., Eberlin, M. N.; Separation of isomeric disaccharides by traveling wave ion mobility mass spectrometry using CO<sub>2</sub> as drift gas. *Journal of Mass Spectrometry* **2012**, 47 (12), 1643-1647.
150. Bataglioni, G. A., Souza, G., Heerdt, G., Morgon, N. H., Dutra, J. D. L., Freire, R. O., Eberlin, M. N., Tata, A.; Separation of glycosidic cationomers by TWIM-MS using CO<sub>2</sub> as a drift gas. *Journal of Mass Spectrometry* **2015**, 50 (2), 336-343.

151. Ruotolo, B. T., McLean, J. A., Gillig, K. J., Russell, D. H.; Peak capacity of ion mobility mass spectrometry: the utility of varying drift gas polarizability for the separation of tryptic peptides. *Journal of Mass Spectrometry* **2004**, *39* (4), 361-367.
152. Jurneczko, E., Kalapothakis, J., Campuzano, I. D. G., Morris, M., Barran, P. E.; Effects of Drift Gas on Collision Cross Sections of a Protein Standard in Linear Drift Tube and Traveling Wave Ion Mobility Mass Spectrometry. *Analytical Chemistry* **2012**, *84* (20), 8524-8531.
153. Davidson, K. L., Bush, M. F.; Effects of Drift Gas Selection on the Ambient-Temperature, Ion Mobility Mass Spectrometry Analysis of Amino Acids. *Analytical Chemistry* **2017**, *89* (3), 2017-2023.
154. Morris, C. B., May, J. C., Leaptrot, K. L., McLean, J. A.; Evaluating Separation Selectivity and Collision Cross Section Measurement Reproducibility in Helium, Nitrogen, Argon, and Carbon Dioxide Drift Gases for Drift Tube Ion Mobility-Mass Spectrometry. *Journal of the American Society of Mass Spectrometry* **2019** (in press)
155. Norris, J. L., Farrow, M. A., Gutierrez, D. B., Palmer, L. D., Muszynski, N., Sherrod, S. D., Pino, J. C., Allen, J. L., Spraggins, J. M., Lubbock A. L. R., Jordan, A., Burns, W., Poland, J. C., Romer, C., Manier M. L., Nei, Y., Prentice, B. M., Rose, K. L., Hill, S., Van de Plas, R., Tsui, T., Braman, N. M., Keller, M. R., Rutherford, S. A., Lobdell, N., Lopez, C. F., Lacy, D. B., McLean, J. A., Wikswo, J. P., Skaar, E. P., and Caprioli, R. M.; Integrated, High-Throughput, Multiomics Platform Enables Data-Driven Construction of Cellular Responses and Reveals Global Drug Mechanisms of Action. *Journal of Proteome Research* **2017**, *16*, 3, 1364-1375
156. Paglia G., Stocchero M., Cacciato S., Lai S., Angel P., Alam M.T., Keller M., Ralser M., Astarita G.; Unbiased Metabolomic Investigation of Alzheimer's Disease Brain Points to Dysregulation of Mitochondrial Aspartate Metabolism, *J. Proteome Res.*, 2016, *15*, 608-618
157. Morgan, X. C., Segata N., Huttenhower C.; Biodiversity and functional genomics in the human microbiome. *Trends in Genetics*, **2013**, *29*, 1, 51-58
158. Weir, T. L., Manter D. K., Brittany B. A., Heuberger A. L., Ryan E. P.; Stool microbiome and metabolome differences between colorectal cancer patients and healthy adults. *PLOS ONE*, **2013**
159. Raman, M., Ahmed, I., Gillevet, P. M., Probert, C. S., Ratcliffe, N. M., Smith, S., Greenwood, R., Sikaroodi, M., Lam, V., Crotty, P., Bailey, J., Meyes, R. P., Rioux, K. P.; Fecal microbiome and volatile organic compound metabolome in obese humans with nonalcoholic fatty liver disease. *Clinical Gastroenterology and Hepatology*. **2013**, *11*, 7, 868-875

## CHAPTER II

# INTEGRATED, HIGH-THROUGHPUT, MULTIOMICS PLATFORM ENABLES DATA-DRIVEN CONSTRUCTION OF CELLULAR RESPONSES AND REVEALS GLOBAL DRUG MECHANISMS OF ACTION

### 2.1. Introduction

The total and complete understanding of cellular responses at the molecular level requires an appreciation for of the complexity and dynamic nature of cellular pathways. While many primary studies of exposure to exogenous compounds often reveal immediate mechanism of actions (MOA), many secondary MOAs are not understood or even explored until several years after the initial discovery. This can lead to devastating effects for compounds being administered to patients. An example of this is the identification of thalidomide's target of toxicity 50 years after observance of the teratogenic properties.(1) Even therapeutic compounds designed for specific targets, for example statins, often induce multifaceted effects.(2) This highlights the need to identify initial MOAs as well as downstream effects that result from these changes.

Drug development strategies largely focus on the interaction of a drug candidate with a single molecular target, assuming that optimization of affinity to a target produces the most effective outcomes. Despite preclinical research being optimized and automated to ensure the rapid generation of suitable drug candidates, the failure rate remains high. Recent estimates suggest that as few as one in ten developed drug candidates succeed.(3–5) Factors leading to failure include safety concerns and effects that are difficult to predict with targeted assays.(3,5) These undesirable

side effects may not manifest until late stages of clinical trials, after investing billions of dollars into a lead compound.(6,7)

The decline in drug development research and efficiency has been well-documented.(8–10) Of the many contributing factors, a major one is that current technologies do not provide a systems-level evaluation of the candidate drug,(11) instead focusing on targeted studies to demonstrate efficacy. It has been noted that drug development was more effective in the era when animals (e.g., systems) were primarily used in the initial stages of development,(8) emphasizing the tradeoffs in using a reductionist approach to drug development. Clearly, there is an urgent need to fundamentally change the way we analyze cellular responses and evaluate potential therapeutic drugs and threatening toxins. A comprehensive approach to understanding cellular response to drug candidates can contribute to both the efficacy and safety of the final product, elucidate pathways of adaptive tolerance and resistance, and highlight possible polypharmacological applications. Additionally, a complete understanding of the molecular landscape allows for the screening of pre-existing mutations that dispose patients to therapeutic failure.

Understand the complex cellular response up front requires exhaustive molecular profiling, a task well-suited to multiomics approaches. The prevailing thought for these technologies is that they are not applicable to programs requiring high throughput results.(12,13) However, recent advances in the technologies used for transcriptomics, proteomics, and metabolomics provide unprecedented molecular specificity and speed while maintaining high standards for data quality. Integration of these technologies facilitates a cohesive analysis of cellular response, and increases in analytical efficiency coupled with modern computational capabilities make it feasible to rapidly obtain comprehensive data of a compound's MOA. Of equal importance, this approach enables

the discovery of cellular processes outside of targeted pathways, providing molecular information and insight into complex cellular responses.

Although this is a multi-omic study that includes transcriptomics, proteomics, and metabolomics, for the purpose of this dissertation, I focus solely on the development of the metabolomic portion in which I personally contributed. Presented here is the development and applications of these techniques using ion mobility-mass spectrometry for improved metabolite separation and identification, in the aim of a more complex multiomic investigation.

## **2.2. Experimental Details**

### **2.2.1. Metabolite Extraction**

All solvents used for metabolite extraction and analysis (MeOH, H<sub>2</sub>O, ACN, FA, ammonium formate and ammonium acetate) were LC/MS grade (Fisher Scientific, Fair Lawn, NJ). Cell slides (~6-7 x 10<sup>3</sup> cells/slide) were kept at -80°C or on dry ice until ready for metabolomic sample processing. Intracellular metabolites were extracted by scraping individual cell slides in 350 µL of cooled (4°C) 2:2:1 (v:v:v) ACN:MeOH:H<sub>2</sub>O. Individual samples were dried in vacuo just until dried and reconstituted in 1 mL of 75:25 (v:v) ACN:H<sub>2</sub>O (dry ice cooled), vortexed for 30 s, sonicated (five 1 s pulses at 30% amplitude while on ice) and incubated at -80°C for 2 h. After incubation, samples were cleared by centrifugation at 15,000 rpm for 15 min, and the resulting supernatant was removed, halved in volume and evaporated to dryness in a vacuum concentrator. Dried extracts were reconstituted in 100µL of reverse phase reconstitution solvent mixture containing 98:2 (v:v) H<sub>2</sub>O:ACN with 0.1% FA for reverse phase analysis or 100µL of normal phase reconstitution solvent mixture containing 80:20 (v:v) ACN:H<sub>2</sub>O for normal phase analysis; followed by centrifugation for 60 s at 5,000 rpm to remove insoluble debris. Quality

control samples were prepared by combining equal volumes (20  $\mu\text{L}$ ) of each sample type and samples were transferred to HPLC vials prior to IMMS analysis.

### **2.2.2. Metabolomic Mass Spectrometry Analysis**

UPLC-IM-MS and data-independent acquisition ( $\text{MS}^E$ ) were performed on a Synapt G2 HDMS (Waters Corporation, Milford, MA) mass spectrometer equipped with a nanoAcquity UPLC system and autosampler (Waters Corporation, Milford, MA). Chromatographic separations were achieved using both hydrophilic-interaction liquid chromatography (HILIC) and reverse phase liquid chromatography (RPLC). A 1.7  $\mu\text{m}$  (1 mm x 100 mm) ACQUITY BEH amide column (Waters Corporation) was used for HILIC analysis and reverse phase liquid chromatography was performed using a 1.8  $\mu\text{m}$  (1 mm X 100 mm) HSS T3 ACQUITY column fitted with a 1.8  $\mu\text{m}$  HSS C18 pre-column (2.1 mm X 5 mm). Samples were analyzed three times each in UPLC-HILIC-HDMSE and UPLC-RPLC-HDMSE in positive ionization mode. For HILIC analysis, mobile phase A was 9:1 (v:v)  $\text{H}_2\text{O}$ :ACN and mobile phase B was 9:1 (v:v) ACN: $\text{H}_2\text{O}$ , both with 0.1% FA and 10mM ammonium acetate. The following elution gradient was used for HILIC analysis: 0 min, 12.5% A; 1 min, 12.5% A; 4 min, 62.5% A; 10 min, 37.5% A; 11 min, 80% A; 13 min, 80% A; 14 min, 12.5% B. Flow rates for HILIC analysis were 90  $\mu\text{L}/\text{min}$  with a column temperature at 30°C and an injection volume of 5  $\mu\text{L}$ . For RPLC analysis, mobile phase A was  $\text{H}_2\text{O}$  and mobile phase B was ACN, both with 0.1% FA. The following elution gradient was used for RPLC analysis: 0 min, 99% A; 1 min, 99% A; 10 min, 40% A; 20 min, 99% A; 22 min, 99% A; 25 min, 1% A. Flow rates for RPLC analysis were 75  $\mu\text{L}/\text{min}$  with a column temperature of 45°C and an injection volume of 5  $\mu\text{L}$ .

HDMS<sup>E</sup> analyses were run using resolution mode, with a capillary voltage of 3 kV, source temperature at 120°C, sample cone voltage at 35V, source gas flow of 300 mL min<sup>-1</sup>, desolvation gas temperature of 325°C, He cell flow of 180 mL min<sup>-1</sup>, and an IM gas flow of 90 mL min<sup>-1</sup>. The data were acquired in positive ion mode from 50 to 2000 Da with a 1 s scan time; leucine enkephalin was used as the lock mass (*m/z* 556.2771). All runs were analyzed using HDMS<sup>E</sup> with an energy ramp from 10 to 40 eV.

### 2.2.3. Metabolite Data Processing and Analysis

The acquired UPLC-IM-MS<sup>E</sup> data were imported, processed, normalized and interpreted in Progenesis QI v.2.1 (Non-linear Dynamics, Newcastle, UK). Briefly, each UPLC-IM-MS<sup>E</sup> data file was imported as an ion intensity map (used for visualization in both *m/z* and retention time dimensions) and underwent retention time alignment and peak picking. Peak picking was performed on individual aligned runs by matching peaks in an aggregate data set that is created from all aligned runs. Following peak picking, the features (retention time and *m/z* pairs) were reduced using both adduct ([M+H]<sup>+</sup>, [M+Na]<sup>+</sup>, [M+K]<sup>+</sup>, etc.) and isotope deconvolution. Data were normalized to all compounds. Statistically significant changes were identified using multivariate statistical analysis including principal component analysis (PCA) and *p*-values generated using analysis of variance (ANOVA) or pairwise comparisons. Pairwise comparisons were performed for each cisplatin treatment (1, 6, 24 or 48 hr) vs. its matched control (1, 6, 24 or 48 hr). Three biological and three technical replicates from each sample type were used to calculate both fold change and *p*-value and features were considered for identification only if they met both significance criteria of fold change >|1.5| and *p*≤0.1; we have termed this list ‘prioritized metabolites’. Prioritized metabolites or features were assigned tentative structural identifications

using accurate mass measurements ( $< 10$  ppm error) and isotope distribution by searching the Human Metabolome Database (HMDB).(37) Following tentative structural identifications for both chromatography methods (HILIC and RPLC), spreadsheets were merged for further data processing. In particular, metabolites associated with drugs, plants, food, and microbial origin were eliminated. Metabolites with a tentative structural identification (met the dual significance criteria of fold change at an absolute value of 1.5 or above and a p-value of  $\leq 0.1$ ) were used in the mechanism of action. In an effort to increase the confidence in metabolite assignment, fragmentation spectra of metabolites that met significance criteria were searched in HMDB (14), METLIN (15), MassBank (16), and NIST (17). Metabolite peak identifications were putatively S-24 assigned using product ions observed in the fragment ion spectra analyzed in HDMSE mode. Ion mobility separations were used to isolate precursor ions and correlate product ions.

### **2.3. Results and Discussion**

This study demonstrates a multiomics platform designed to assess a comprehensive MOA of exogenous compounds in 30 days. Taken into consideration is the selection of cell type, exposure methods, and analytical modalities by evaluating stability, reproducibility, utility, and feasibility within 30 days. For this study, we used A549 cells; however, our platform is amenable to various adherent and suspension cell lines. The sponsoring agency selected cisplatin as the test compound and revealed its identity on the first day of the 30 day period.

**Figure 2.1** graphically illustrates the three phases of our procedure: (1) molecular screening (days 0-3), (2) discovery analytics (days 4-25), and (3) mechanism construction (days 26-30). Phase 1 screens a wide range of cisplatin dose and exposure times to establish the treatment protocol for discovery experiments. This preliminary screen deduces dosing conditions that



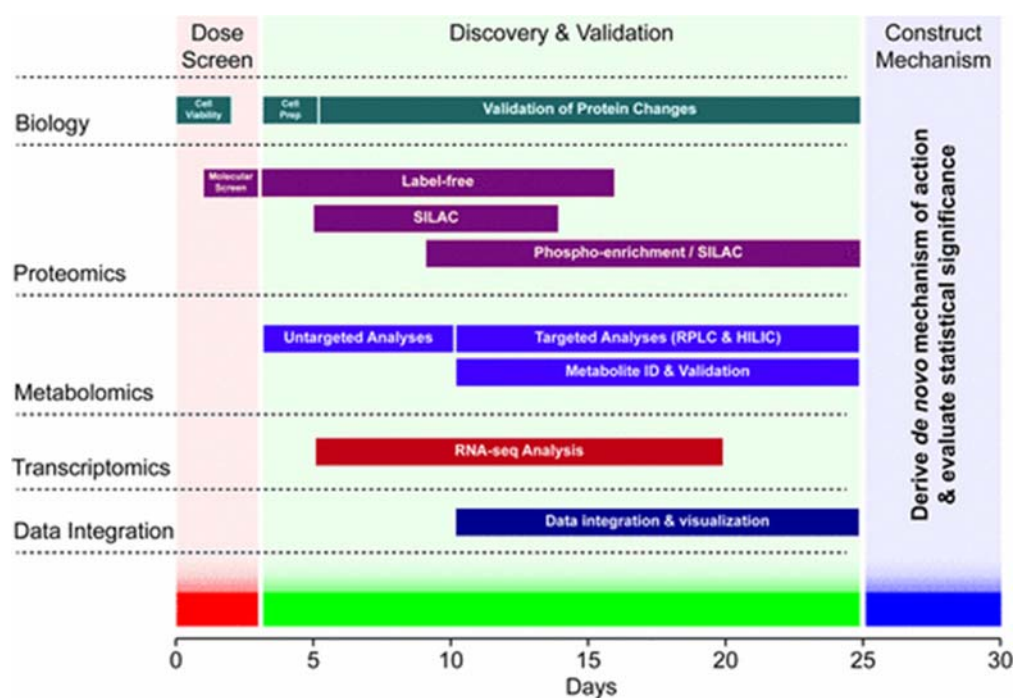


**Figure 2.1** Multiomics platform for MOA construction. The 30 day procedure has three distinct phases: dose screen (days 0–3), discovery and validation (days 4–25), and mechanism construction (days 26–30). Phase 1 incorporates cell viability and molecular screens to establish protocols for the discovery phase. Phase 2 integrates proteomics, metabolomics, and transcriptomics to determine molecular changes correlated with compound dose. In Phase 3, network analysis of all statistically significant changes drives construction of a comprehensive MOA.

provide relevant data for the MOA, allowing the application of this protocol to uncharacterized compounds. During Phase 2, transcriptomics, proteomics, and metabolomics determine changes in molecular expression correlated with exposure to the compound. In Phase 3, data integration and analysis drive mechanism construction.

For the purpose of this dissertation, the metabolomics workflow will be explained in greater detail in how it attributes to the determination of the MOA. In addition, the influence that this study has on developing methods for various applications, including the gut microbiome, will also be discussed at the end.

### **2.3.1. Metabolomic Analysis**

This method combined hydrophobic and hydrophilic chromatography techniques. Both hydrophilic interaction liquid chromatography (HILIC) and reversed-phased chromatography (RPLC) generated a similar number of identified features with IM-MS analysis, approximately 7,000 for HILIC and 8,000 for RPLC. Less than half of these molecules are observed across both LC methods (**Figure 2.2**). The additional coverage afforded by combining HILIC and RPLC analysis allowed for 46% and 70% more identifications than using either technique alone, illustrating the importance of using multiple separation techniques (**Figure 2.3**). This is due to the ability to separate molecules based on their chemical affinities and detect a greater diversity of species, improving the identification and quantification of significantly altered species. Furthermore, 51% of the total number of statistically significant metabolite species identified were not represented in more than a single time point (**Figure 2.3**). The large number of unique metabolites observed at 24 hours suggests that as exposure time of cisplatin increases, the metabolism of the cell is altered. It is important to note that the global metabolomics data shown represent only those species identified through database correlation and statistically prioritized

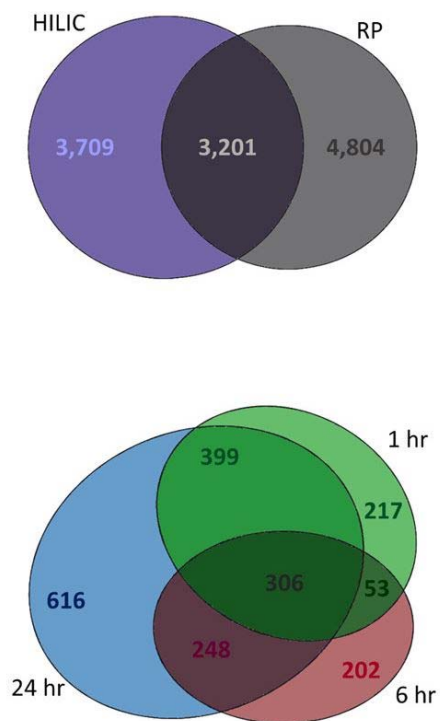


**Figure 2.2.** Figure displaying detected features detected from HILIC and RPLC. Approximately 7,000 features are detected with HILIC and 8,000 features detected in RPLC (top). Significantly altered changed metabolites are show the overlap across the modalities and time. For visual simplicity, 3 out of 4 time points are shown (bottom).

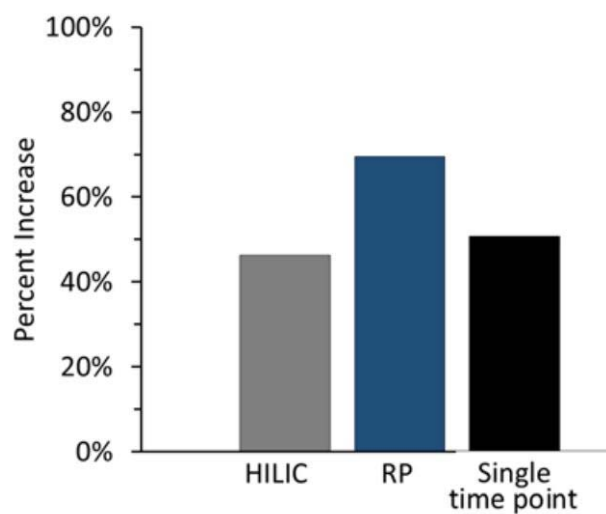


**Figure 2.3.** A graph demonstrating the metabolomic coverage observed using HILIC and RPLC. The additional coverage afforded by combining these techniques allow for 46% (gray bar) and 70% (blue bar) more identifications. Furthermore 51% of the total number of statistically significant metabolite species identified were not represented in more than a single time point (black bar).

based on the significance criteria of the study.

The proteomic and biology assays provided evidence that suggested apoptosis. The proteomic and biological methods are outside of the scope of this dissertation. These analyses along with the transcriptomic data, the pathway that lead to this apoptosis is explored. When compared to the literature-derived canonical MOA, it was determined to be in agreement for both the network and on a time-resolved basis. The capture of 32 out of 33 species from >53,000 unique measurements tested less than 0.1% of the collected data. Although many metabolites identified supported findings from the other omic fields, many metabolites were a part of pathways outside of the canonical one. The metabolomic data supported these findings while expanding beyond the current literature.

#### **2.4. Remarks and Perspective**

The platform provides proof-of-concept for how to utilize a multiomic study to provide a MOA. The method described herein utilizes technologies for large-scale measurement of molecular events to generate a comprehensive picture of the cellular response to an exogenous compound. Using cisplatin, we demonstrate that this platform can identify primary MOA and pathways important for side effects and resistance. This platform provides several key developments in MOA determination. First, a 3 day screening platform determines relevant exposure and dose using MS to determine the maximal molecular changes. Second, comprehensive molecular data are collected within 2-3 weeks, including post translational modifications and metabolomics. These data can generate a tunable output of the final network or mechanism based on statistical confidence in empirical measurements. Finally, this platform provides high-throughput, comprehensive MOA assessment.

The applications for this platform are diverse and span various fields of study. Assessment of pharmaceutical compounds can rapidly uncover MOA and potential off-target effects as well as improve the selection of drug candidates likely to succeed. This platform could promote rapid MOA assessment for unknown compounds, environmental pollutants, and infectious agents. The metabolomic aspect of this investigation demonstrates the speed in which metabolites can be validated and used to generate biological information. LC-IM-MS methods are explored further in this dissertation as the focus shift to the gut microbiome.

## **2.5 Acknowledgements**

This chapter contains portions of the published research article: Jeremy L. Norris, Melissa A. Farrow, Danielle B. Gutierrez, Lauren D. Palmer, Nicole Muszynski, Stacy D. Sherrod, James C. Pino, Jamie L. Allen, Jeffrey M. Spraggins, Alex L. R. Lubbock, Ashley Jordan, William Burns, James C. Poland, Carrie Romer, M. Lisa Manier, Yuan-wei Nei, Boone M. Prentice, Kristie L. Rose, Salisha Hill, Raf Van de Plas, Tina Tsui, Nathaniel M. Braman, M. Ray Keller, Stacey A. Rutherford, Nichole Lobdell, Carlos F. Lopez, D. Borden Lacy, John A. McLean, John P. Wikswo, Eric P. Skaar, and Richard M. Caprioli, “Integrated, High-Throughput, Multiomics Platform Enables Data-Driven Construction of Cellular Responses and Reveals Global Drug Mechanisms of Action,” *Journal of Proteome Research*, **2017**, 16 (3) 1364-1375

Financial support for aspects of this research was provided by the U.S. Army Research Office and the Defense Advanced Research Projects Agency and was accomplished under Cooperative Agreement no. W911 NF-14-2-0022. The views and conclusions contained in this document are those of the authors and should not be interpreted as representing the official policies, either expressed or implied, of the Army Research Office, DARPA, or the U.S. Government. The U.S.

Government purposes notwithstanding any copyright notation herein. This work was supported by the National Science Foundation grant MCB-1411482 (C.F.L., J.C.P.) and the VICC Young Ambassador Awards (C.F.L.). The authors acknowledge Jerry Holman for assistance in custom coding informatics tools, Randi Grant-Branum for providing valuable feedback to manuscript revisions and the MSRC Proteomics Core at Vanderbilt University for sample services.

## 2.6. References

- (1) Kim, C. Y., Kim, S. K., Phi, J. H., Lee, M. M., Kim, I. A., Kim, I. H., Wang, K. C., Jung, H. L., Lee, M. J., Cho, B. K.; A prospective study of Temozolomide plus thalidomide during and after radiation therapy for pediatric diffuse pontine gliomas: preliminary results of the Korean Society for Pediatric Neuro-Oncology study. *J. Neuro-Oncol.* **2010**, 100 (2), 193–198.
- (2) Zhou, Q., Liao, J. K.; Statins and cardiovascular diseases: From cholesterol lowering to pleiotropy. *Curr. Pharm. Des.* **2009**, 15 (5), 467– 478
- (3) Hay, M., Thomas, D. W., Craighead, J. L., Economides, C., Rosenthal, J.; Clinical development success rates for investigational drugs. *Nat. Biotechnol.* **2014**, 32 (1), 40–51
- (4) DiMasi, J. A., Feldman, L., Seckler, A., Wilson, A.; Trends in risks associated with new drug development: success rates for investigational drugs. *Clin. Pharmacol. Ther.* **2010**, 87 (3), 272–27712
- (5) Kola, I., Landis, J.; Can the pharmaceutical industry reduce attrition rates? *Nat. Rev. Drug Discovery* **2004**, 3 (8), 711–715
- (6) DiMasi J.A., Grabowski H.G., Hansen R.W.; Cost to Develop and Win Marketing Approval for a New Drug Is \$2.6 Billion. *Tufts Center for the Study of Drug Development* **2014**
- (7) Crawford, M.; State of the Industry. *News Magazine* **2010**, 34– 39.
- (8) Scannell, J. W., Blanckley, A., Boldon, H., Warrington, B.; Diagnosing the decline in pharmaceutical R&D efficiency. *Nat. Rev. Drug Discovery* **2012**, 11 (3), 191–200
- (9) Pammolli, F., Magazzini, L., Riccaboni, M.; The productivity crisis in pharmaceutical R&D. *Nat. Rev. Drug Discovery* **2011**, 10 (6), 428– 438.
- (10) Paul, S. M., Mytelka, D. S., Dunwiddie, C. T., Persinger, C. C., Munos, B. H., Lindborg, S. R., Schacht, A. L.; How to improve R&D productivity: the pharmaceutical industry’s grand challenge. *Nat. Rev. Drug Discovery* **2010**, 9 (3), 203–214

- (11) Ahuja, V., Sharma, S.; Drug safety testing paradigm, current progress and future challenges: an overview. *J. Appl. Toxicol.* **2014**, 34 (6), 576–594
- (12) Kim, M.-S.; Proteomics equipped with multiplexing toward ultra high throughput. *Proteomics* **2015**, 15 (2–3), 183–184
- (13) Sereni, M. I., Pierobon, M., Angioli, R., Petricoin, E. F., Frederick, M. J.; Reverse phase protein microarrays and their utility in drug development. *Methods Mol. Biol.* **2013**, 986, 187–214.
- (14) Chimento, A., Sirianni, R., Casaburi, I., Ruggiero, C., Maggiolini, M., Ando, S., Pezzi, V.; 17 $\beta$ -Estradiol activates GPER- and ESR1- dependent pathways inducing apoptosis in GC-2 cells, a mouse spermatocyte-derived cell line. *Mol. Cell. Endocrinol.* **2012**, 355 (1), 49–59.
- (15) Wilson, H. L., McFie, P. J., Roesler, W. J.; Characterization of domains in C/EBPalpha that mediate its constitutive and cAMPinducible activities. *Mol. Cell. Endocrinol.* **2001**, 181 (1–2), 27–34.
- (16) Rotinen, M., Villar, J., Celay, J., Serrano, I., Notario, V., Encío, I.; Transcriptional regulation of type 11 17 $\beta$ -hydroxysteroid dehydrogenase expression in prostate cancer cells. *Mol. Cell. Endocrinol.* **2011**, 339 (1–2), 45–53.
- (17) Panchanathan, R., Shen, H., Zhang, X., Ho, S.-M., Choubey, D.; Mutually positive regulatory feedback loop between interferons and estrogen receptor-alpha in mice: implications for sex bias in autoimmunity. *PLoS One* **2010**, 5 (5), e10868.



## CHAPTER III

### COLLISION CROSS SECTION CONFORMATIONAL ANALYSES OF BILE ACIDS VIA ION MOBILITY-MASS SPECTROMETRY

#### 3.1. Introduction

Bile acids are compounds that are essential for human health. These compounds primarily assist in the solubilization of dietary lipids and promote their absorption through the digestive tract.(1) Bile acids are the primary mechanism governing the elimination of cholesterol, aid in the motility of bacteria in the small intestine, and act as signaling molecules for the mitogen-activated protein kinase (MAPK) pathways, nuclear hormone receptors (FXR $\alpha$ ), and the G-protein-coupled receptor (GPCR) TGR5.(1,2) The function of any individual compound from this class of molecules is dictated by its specific structure, so the accurate identification of these molecules is of growing importance. However, the separation of bile acids remains challenging due to their structural similarities, often resulting in indistinguishable MS/MS fragmentation patterns and similar chromatographic retention times.

Bile acids are derived from cholesterol and possess a fused four ring core with four primary substitution sites (typically on carbon 3, 6, 7, and 12 as shown in red in **Figure 3.1**). Bile acids are characterized by conjugation at carbon 24 (designated in blue in **Figure 3.1**) and the functionalization of these substitution sites.(3) The most common modification, a hydroxyl group, can vary in position and/or orientation, and often determines molecular function. For example, chenodeoxycholic acid (CDCA) and deoxycholic acid (DCA) are two bile acids that differ in the position of the hydroxyl group. Both compounds solubilize lipids as part of the enterohepatic

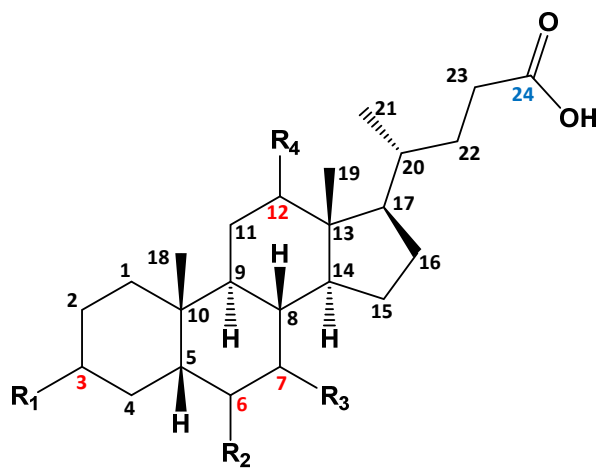


**Figure 3.1.** Four ring structure common to all bile acids. Carbons are numbered with substituents located at carbon 3, 6, 7 and 12, highlighted in red font. R groups are -H, -OH, or  $-\text{HSO}_4\text{e}$  groups. Carbon 24, highlighted in blue font, is conjugated with glycine or taurine to yield glycocholates and taurocholates, respectively.

circulatory system, but DCA additionally acts as a hepatotoxin and oncometabolite.(4,5)

Bile acids are difficult to distinguish from each other using liquid chromatography-mass spectrometry (LC-MS) methods alone, due in part to their similar polarities.(6) One example, the isomeric pair  $\alpha$ - and  $\beta$ -muricholic acid, only differ in the orientation of the hydroxyl group on carbon 6. Zheng et al. recently demonstrated that  $\alpha$ - and  $\beta$ -muricholic acid could be resolved using ion mobility (IM), despite these minor structural differences.(8) This validates the utility of IM as an additional dimension of separation, in conjunction with LC for improved resolution of isomers.(7,8)

Picache et al. recently published and released the Unified Collision Cross Section (CCS) Compendium containing a myriad of compounds including lipids, carbohydrates, amino acids, peptides and other small molecules.(9) The motivation for the Unified CCS Compendium is to provide an open source database for the IM community to collect and compare CCS values that meet specific criteria for precision and accuracy. CCS values can then be used as an additional descriptor for omic studies to aid in the identification and validation of unknown small molecules. It has been demonstrated that molecules with similar chemical motifs tend to exhibit correlations in conformational space.(10-12) Compounds of a given biomolecular class that adopt similar gas phase structures fall along specific mass-mobility trendlines. Using both CCS values and mass-to-charge ( $m/z$ ) ratios, it is possible to increase confidence in metabolite annotation to identify unknown molecules and predict biomolecular class when performing global untargeted metabolomic studies.(10,12-19) The Unified CCS Compendium previously contained a limited number of bile acid entries, with proton loss  $[M-H]^-$  being the most reported ion state. In this report, we expand on previously obtained CCS values of bile acids by analyzing adding conjugated, unsaturated, and sulfated bile acids in both positive and negative ionization mode. While  $[M-H]^-$  was

the predominant ion in negative mode, positive mode analyses contained a variety of observed adducts, including  $[M+Na]^+$ ,  $[M+H-H_2O]^+$ ,  $[M+H-2H_2O]^+$ ,  $[M+H-H_2SO_4]^+$ ,  $[M+H-H_2SO_4-H_2O]^+$ , and  $[M+H-H_2SO_4-2H_2O]^+$  ion species.

## 3.2. Methods

### 3.2.1. Standards and Chemicals

Optima grade acetonitrile and water were purchased from Fisher Scientific (Loughborough, UK). Ammonium acetate was purchased from Sigma Aldrich (Dorset, UK). Formic acid was purchased from Fluka (Buchs, Switzerland). Bile acid standards were purchased from Steraloids, Inc. (New-port, RI) and included tauro-alpha-muricholic acid (T- $\alpha$ -MCA), tauro-beta-muricholic acid (T- $\beta$ -MCA), tauro-omega-muricholic acid (T- $\omega$ -MCA), alpha-muricholic acid ( $\alpha$ -MCA), beta-muricholic acid ( $\beta$ -MCA), taurohyocholic acid (THCA), glyoursodeoxycholic acid (GUDCA), tau-roursodeoxycholic acid (TUDCA), hyocholic acid (HCA), taurohyoxydeoxycholic acid (THDCA), taurocholic acid (TCA), cholic acid (CA), ursodeoxycholic acid (UDCA), hyodeoxycholic acid (HDCA), glycodeoxycholic acid (GDCA), taurodeoxycholic acid (TDCA), chenodeoxy-cholic acid (CDCA), and deoxycholic acid (DCA).

### 3.2.2. Measurements of CCS of Bile Acids

The  $^{DT}CCS_{N_2}$  values for 50 bile acids were determined based on the Agilent 6560 standardized single field CCS protocol established by Stow et al.(20) This protocol allows for the most consistent determination of CCS values with precisions generally lower than <0.2% RSD (n=3 taken on 3 separate days). Injection procedures were similar to a previously described method,(21) in which bile acid standards were first diluted to 10  $\mu$ g/ml in acetonitrile and stored in glass autosampler vials at 4°C. Aliquots of 10  $\mu$ L were injected at 100  $\mu$ L/min via a 100  $\mu$ L sample loop directly to the Agilent Jet Stream electrospray ionization source (i.e. no LC column

was used). Source settings included drying gas at 300°C and 4 L/min, sheath gas at 200°C and 8 L/min, nebulizer pressure at 12 psi, and electric potential of the entrance capillary and nozzle held at 2800 V and 1750 V, respectively. The mobile phase was comprised of 50:50 acetonitrile/water with 0.1% formic acid. The initial flow rate of 800  $\mu\text{L}/\text{min}$  was decreased to 30  $\mu\text{L}/\text{min}$  from 0.15 min to 0.16 min, where it was held at 30  $\mu\text{L}/\text{min}$  until 0.90 min. From 0.90 min to 1.00 min, the flow rate was increased to 800  $\mu\text{L}/\text{min}$  and maintained for 1.00 min to wash the column and prevent sample carryover.(21) In the 2.00 min data acquisition, features from each sample injection were detected from 0.20 min to 1.00 min. CCS values were collected in this elution window in both positive and negative ionization mode, with a 1350 V bias and nitrogen at 3.94 Torr and 26°C in the IM drift tube. Data was collected once per day for three days to yield three replicates per sample. All bile acid standards were analyzed individually and methods were in agreement with CCS data handling protocol described by Picache et al. with relative standard deviations  $\leq 0.2\%$ .(9) CCS values measured in this work have been submitted to the Unified CCS Compendium for community access.

### 3.3. Discussion

The bile acids in this study were found to ionize readily via electrospray ionization. While  $[\text{M}-\text{H}]^-$  was the predominant adduct in negative ionization mode, other negative adducts were observed at lower relative abundance including  $[\text{M}+\text{Cl}]^-$ ,  $[\text{M}+\text{COOH}]^-$ , and  $[\text{M}+\text{COONa}]^-$ . In positive ionization mode, coordination of a proton or sodium ion were common, with proton-coordinated species solely appearing with neutral losses, including loss of  $\text{H}_2\text{O}$  and/or  $\text{H}_2\text{SO}_4$ . Although  $[\text{M}+\text{H}-\text{H}_2\text{SO}_4]^+$  could be denoted  $[\text{M}+\text{H}-\text{H}_2\text{O}-\text{SO}_3]^+$ , neutral loss of  $\text{SO}_3$  was not experimentally observed, independent of water loss. Multimeric species were observed at high abundance in both polarities, although the scope of this work was limited to measurement of CCS

values of singly charged, monomeric bile acids. The multiple adducts observed in positive ionization mode for  $\beta$ -muricholic acid are depicted in the IM-MS plot in **Figure 3.2**. In this mass spectrum, the  $[M+H]^+$  adduct is present in very low relative abundance whilst the  $[M+Na]^+$  adduct is prominent. As for most bile acids in this study, neutral water loss was common, with  $[M+H-H_2O]^+$ ,  $[M+H-2H_2O]^+$ ,  $[M+H-3H_2O]^+$  adducts present in high relative abundance. Due to hydroxyl and/or sulfate groups being the main differentiating features between bile acids, the common appearance of such a wide variety of adducts across both polarities make it extremely challenging to distinguish functionalized bile acids from one another in complex mixtures.

Nomenclature, molecular formula, R substituents,  $m/z$ , and CCS values for the unsulfated bile acids (including both glycine and taurine species) are found in **Table 3.1**. Bile acid sub-classes are based on glycine and taurine conjugation of the carbon 24 carboxyl group, bond saturation, and sulfation. **Figure 3.3** depicts the mobility-mass conformational space of the  $[M-H]^-$  bile acid adduct. The grouping within each plotted series indicates how the various subcategories denoted by marker color and shape cluster in different regions of conformational space. CCS values for sulfated conjugated bile acids can be found in **Appendix B1**. Similar to other classes in the Unified CCS Compendium, bile acids cluster in CCS vs.  $m/z$  space based on their structural similarity and degree of packing in the gas phase. As is observed for most classes of molecules, we observe a general increase in CCS with  $m/z$ . The sub-class that has the smallest range in cross section is the glycine conjugated bile acids with a range of  $2.6 \text{ \AA}^2$ , while the sub-classes with the largest ranges are the unconjugated sulfated bile acids (mass range 456.25 Da – 488.24 Da) and the unsaturated bile acids (mass range 374.28 Da – 406.27 Da) at  $9.8 \text{ \AA}^2$  and  $9.1 \text{ \AA}^2$ , respectively. This is similar to results reported by Zheng et al. in that smaller unsaturated bile acids separate more readily than saturated bile acids in CCS

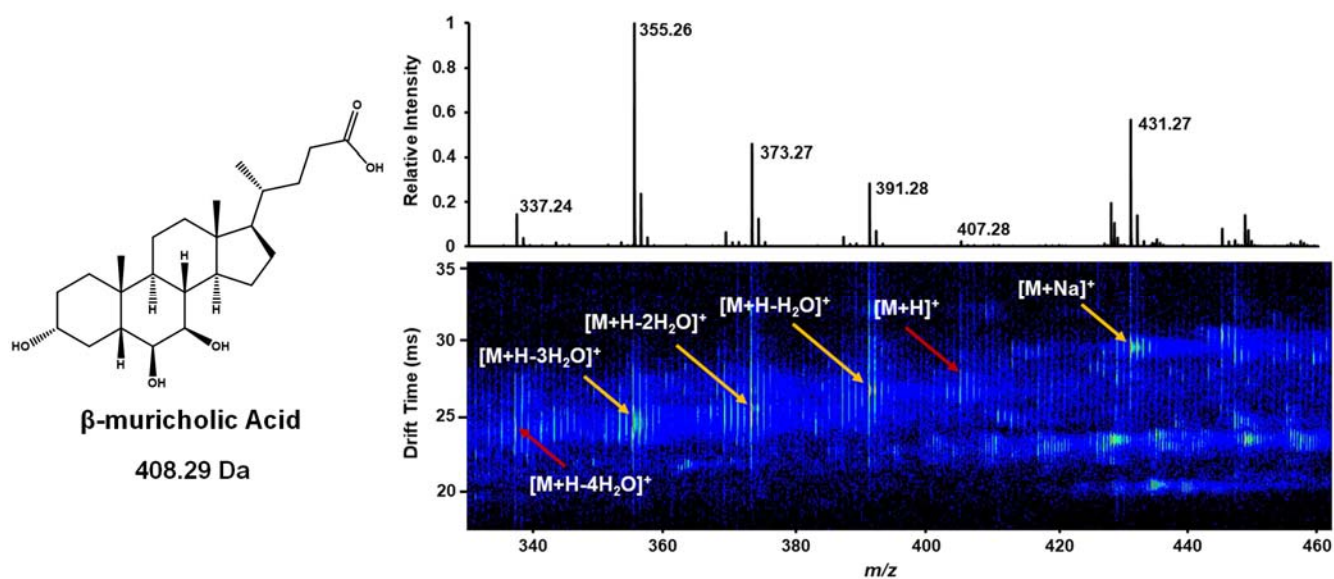


**Figure 3.2.** Representative IM-MS spectrum of  $\beta$ -muricholic acid in positive ionization mode. Multiple adduct forms were observed in both polarities, with water loss commonly exhibited for proton coordinated species in positive ionization mode. Cross sections are reported for species denoted by yellow arrows; however, species denoted by red arrows are not reported due to low intensity.

**Table 3.1.** A list of negative mode CCS measurements for [M-H]<sup>-</sup> adducts of bile acids reported in this study. Values for species in positive ionization mode are reported in the accompanying supplemental materials (**Appendix Table B1**). Bile acids are grouped by subclass, and entries within each subclass are sorted by increasing *m/z* ratio. Structural nomenclature and composition of the R groups are displayed in the table along with chemical formula, *m/z*, and CCS. Numeration of the R groups refers to positions shown in Figure 1. At each R position, the substituent was either hydrogen (-H), alpha or beta hydroxyl ( $\alpha$ - or  $\beta$ -OH), or doubly bonded oxygen (=O). Precision is reported as the %RSD for n=3 measurements made on three separate days.

Sub-class	Name	Chemical Formula	R1	R2	R3	R4	<i>m/z</i>	[M-H] <sup>-</sup> CCS (Å <sup>2</sup> )	% RSD
Unsaturated	dehydrolithocholic acid	C24H38O3	=O	-H	-H	-H	374.57	205.4	0.037
	3,7-dioxy-5 $\beta$ -choanoic acid	C24H36O4	=O	-H	=O	-H	388.26	206.0	0.042
	3,6-diketocholic acid	C24H36O4	=O	=O	-H	-H	388.55	200.8	0.147
	dehydrodeoxycholic acid	C24H36O4	=O	-H	-H	=O	388.55	209.5	0.208
	3-oxo-12 $\alpha$ -cholic acid	C24H38O4	=O	-H	-H	$\alpha$ -OH	390.56	200.6	0.149
	apocholic acid	C24H38O4	$\alpha$ -OH	-H	-H	$\alpha$ -OH	390.58	202.9	0.127
	7 $\alpha$ , 12 $\alpha$ , dihydroxy-5 $\beta$ -cholanolic acid	C24H40O4	-H	-H	$\alpha$ -OH	$\alpha$ -OH	392.58	200.5	0.052
	3 $\beta$ , 7 $\alpha$ , dihydroxy-5 $\beta$ -cholanolic acid	C24H39DO4	$\beta$ -OH, $\alpha$ -D	-H	$\alpha$ -OH	-H	393.59	202.6	0.107
	3,7,12-tri-betacholanolic acid	C24H34O5	=O	-H	=O	=O	402.53	209.6	0.149
	7,12-dioxolithocholic acid	C24H36O5	-OH	-H	=O	=O	404.55	204.1	0.220
	12-dehydrocholic acid	C24H38O5	$\alpha$ -OH	-H	$\alpha$ -OH	=O	406.27	204.0	0.128
	7-ketodeoxycholic acid	C24H38O5	$\alpha$ -OH	-H	=O	$\alpha$ -OH	406.27	204.0	0.161
	3-oxocholic acid	C24H38O5	=O	-H	$\alpha$ -OH	$\alpha$ -OH	406.27	205.4	0.029
Unconjugated	lithocholic acid	C24H40O3	$\alpha$ -OH	-H	-H	-H	376.58	198.8	0.210
	ursodeoxycholic acid	C24H40O4	$\alpha$ -OH	-H	$\beta$ -OH	-H	392.58	198.1	0.116
	hyodeoxycholic acid	C24H40O4	$\alpha$ -OH	$\alpha$ -OH	-H	-H	392.58	199.1	0.114
	murideoxycholic acid	C24H40O4	$\alpha$ -OH	$\beta$ -OH	-H	-H	392.58	200.1	0.147
	chenodeoxycholic acid	C24H40O4	$\alpha$ -OH	-H	$\alpha$ -OH	-H	392.58	202.2	0.068
	hyocholic acid	C24H40O5	$\alpha$ -OH	$\alpha$ -OH	$\alpha$ -OH	-H	407.57	202.6	0.058
	$\alpha$ -muricholic acid	C24H40O5	$\alpha$ -OH	$\beta$ -OH	$\alpha$ -OH	-H	408.57	203.7	0.078
	$\beta$ -muricholic acid	C24H40O5	$\alpha$ -OH	$\beta$ -OH	$\beta$ -OH	-H	408.57	200.6	0.112
	cholic acid	C24H40O5	$\alpha$ -OH	-H	$\alpha$ -OH	$\alpha$ -OH	408.57	202.9	0.059
Glycine Conjugated	glycolithocholic acid	C26H43NO4	$\alpha$ -OH	-H	-H	-H	432.31	199.4	0.030
	glycoursodeoxycholic acid	C26H43NO5	$\alpha$ -OH	-H	$\beta$ -OH	-H	448.31	201.0	0.095
	glycodeoxycholic acid	C26H43NO5	$\alpha$ -OH	-H	-H	$\alpha$ -OH	448.31	199.7	0.062
	glycocholic acid	C26H43NO6	$\alpha$ -OH	-H	$\alpha$ -OH	$\alpha$ -OH	464.30	202.1	0.109
Taurine Conjugated	taurohyodeoxycholic acid	C26H45NO6S	$\alpha$ -OH	$\alpha$ -OH	-H	-H	498.29	206.2	0.051
	tauroolithocholic acid	C26H45NO5S	$\alpha$ -OH	-H	-H	-H	482.30	206.3	0.042
	taurochenodeoxycholic acid	C26H45NO6S	$\alpha$ -OH	-H	$\alpha$ -OH	-H	498.29	207.1	0.054
	taurocholic acid	C26H45NO7S	$\alpha$ -OH	-H	$\alpha$ -OH	$\alpha$ -OH	514.29	207.4	0.074
	taoursodeoxycholic acid	C26H45NO6S	$\alpha$ -OH	-H	$\beta$ -OH	-H	498.29	207.5	0.054
	taurohyocholic acid	C26H45NO7S	$\alpha$ -OH	$\alpha$ -OH	$\alpha$ -OH	-H	514.29	208.3	0.077
	tauro- $\alpha$ -muricholic acid	C26H45NO7S	$\alpha$ -OH	$\beta$ -OH	$\alpha$ -OH	-H	514.29	209.3	0.070
	tauro- $\omega$ -muricholic acid	C26H45NO7S	$\alpha$ -OH	$\alpha$ -OH	$\beta$ -OH	-H	514.29	209.3	0.062
	tauro- $\beta$ -muricholic acid	C26H45NO7S	$\alpha$ -OH	$\beta$ -OH	$\beta$ -OH	-H	514.29	209.5	0.077



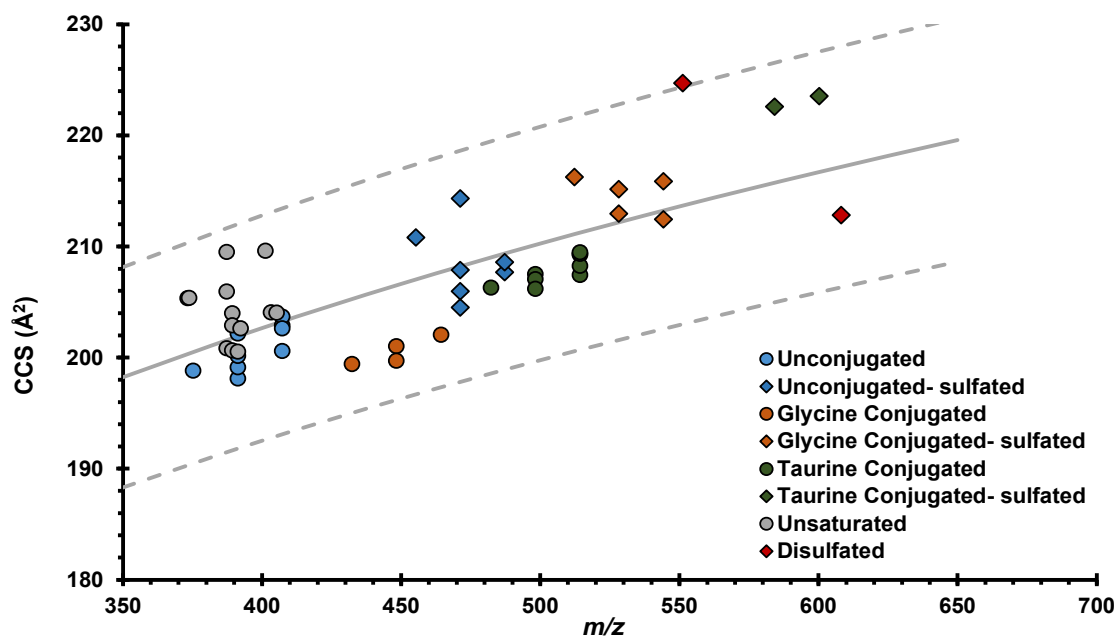


**Figure 3.3.** A conformation space CCS vs  $m/z$  plot of the  $[M-H]^-$  adduct of bile acid standards in negative ionization mode. Marker color indicates the bile acid subgroup. Bile acid and conjugated bile acids are represented by circles while sulfonated bile acids are denoted by diamonds. The solid gray line represents the bile acid trendline for all species, and the dotted lines depict the bounds of the 95% confidence interval. All but one bile acid value fell within this correlation, regardless of conjugation and sulfonation.

space.(8) Zheng et al reported glycine and taurine conjugated bile acids ( $m/z$  449.31 and  $m/z$  514.28, respectively) were the most difficult to separate.(8) This can be associated to the narrow range of the bile acids after glycine or taurine conjugation. It was reported that glycine conjugated bile acids had a smaller CCS range than unconjugated bile acids ( $2.7 \text{ \AA}^2$  for glycine conjugated and  $7.0 \text{ \AA}^2$  for unconjugated).(8)

Using these reported CCS values, we can create correlations similar to those used by Picache et al. in the Unified CCS Compendium by mapping expected mobility-mass space for bile acids.(9) Using the measured experimental bile acid data, a correlation is plot-*ted* using a power fit. This correlation is representative of bile acids and bile acid conjugates. By reporting a bile acid correlation (**Figure 3.3**) and utilizing it to compare predicted and experimental CCS values in future studies, we can increase the confidence in bile acid annotations. All of our values fall within 5% of the calculated correlation, with the only exception being disulfated chenodeoxycholic acid.

Bile acids conjugated with glycine did not exhibit the same increase in CCS with  $m/z$  as other bile acids, an unexpected result. While glycine conjugated values still fell within the confidence interval of the bile acid correlation, the CCS was observed to decrease with increasing  $m/z$ , indicating interaction of glycine with another portion of the structure. This hypothesis is further supported by the lower range in CCS values of glycine conjugated bile acids. **Figure 3.4** shows molecular models of cholic acid and its glycine conjugated counterpart, glycocholic acid. The fused ring sterol core common to these bile acids has no rotational freedom, therefore it is the R groups that introduce variability in CCS. In glycocholic acid, the glycine tail can form a hydrogen-bond with nitrogen (**Figure 3.4B**). The resulting pseudo-5 membered ring prevents the tail from freely rotating and results in a more compact structure than that observed for bile acids with unconstrained tails.

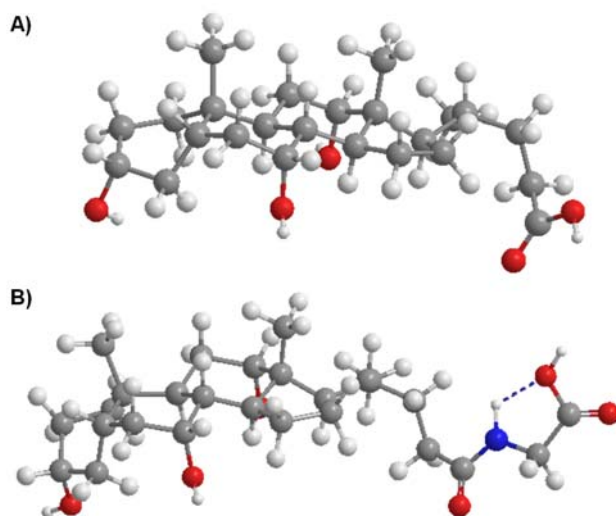


**Figure 3.4.** Ball and stick model of (A) cholic and (B) glycocholic acid. The sterol ring structure is the same in both cholic acid and glycocholic acid, however the tail structure (and their interactions with the core) affect the cross section. With cholic acid (A), the tail has no interactions with the sterol ring, however, based on molecular modelling, with glycocholic acid (B), the tail structure folds in and forms a hydrogen bond with the nitrogen, stabilizing the tail and limiting its motion. Colored spheres represent atoms, with gray carbon, red oxygen, blue nitrogen, and white hydrogen.

Another observation of structural interest is that CCS increases with bile acid unsaturation. As double bonds are introduced, the  $m/z$  decreases by 2, 4, and 6 nominal mass units (corresponding to 1, 2, and 3 double bonds, respectively). With this, an increase in CCS is observed. **Figure 3.5** highlights two pairs of molecules that differ only in the presence of double bonds: (1) lithocholic acid and dehydrolithocholic acid, and (2) cholic acid and 7,12-dioxolithocholic acid. This increase in CCS may be the result of the change in a ring carbon's hybridization. Re-hybridization around the ring strains the chair structure of the six-member ring making the ring adopt a half chair conformation with wider internal bond angles, resulting in a larger CCS value. The position of the double bond also affects how it influences the structure. A double bond between two ring carbons has a larger effect than between a ring carbon and an oxygen. The position of the double bond affects the strain in the sterol cores, and therefore results in a CCS increase.

### 3.4. Conclusion

Bile acids provide a crucial role in digestion and metabolism but are typically difficult to distinguish in LC-MS approaches. To improve the accurate annotation of these molecules, we report CCS values of bile acids and their adducts. In-depth analysis of CCS sub-class correlations afford a glimpse into the structural changes that allow separation via ion mobility. This subset of bile acids provides a step forward for discrimination of these molecules in untargeted metabolomic studies.

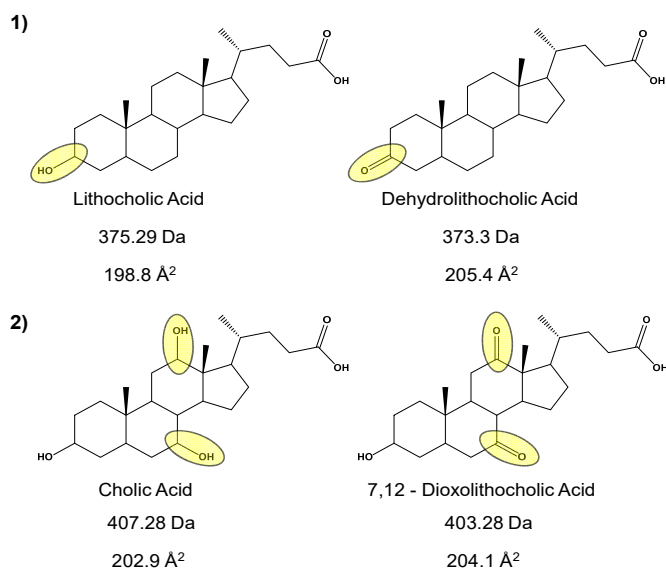


**Figure 3.5.** Comparison of (1) lithocholic acid with dehydrolithocholic acid and (2) cholic acid with 7,12-dioxolithocholic acid. The difference between each pair is highlighted in yellow. The addition of the double bond removes two hydrogens, reducing the  $m/z$  ratio, however the experimental CCS increases with this change. This is also observed with cholic acid and 7,12-dioxolithocholic acid in which two double bonds are introduced and the resultant CCS value increases.

### 3.5 Acknowledgements

This chapter contains the published research article: James C. Poland, Katrina L. Leaptrot, Stacy D. Sherrod, C. Robb Flynn, and John A. McLean, "Collision Cross Section Conformational Analyses of Bile Acids via Ion Mobility-Mass Spectrometry," Submitted to *Journal of the American Society for Mass Spectrometry*, **2020**

Financial support for aspects of this research was provided by the National Institutes of Health (R03CA222452, R21DA043960 and R01DK105847). JCP also thanks Vanderbilt University, the Institute of Chemical Biology, and the Fisk-Vanderbilt Masters to PhD Bridge program for financial support.

### 3.6. References

- (1) Li T., Chiang J.Y.L.; Bile acids as metabolic regulators. *Curr Opin Gastroenterol.* **2015**, 31, 2, 159-165
- (2) Hylemon P.B., Zhou H., Pandak W.M., Ren S., Gil G., Dent P.; Bile acid as regulatory molecules. *J Lipid Res.* **2009**, 50, 1509-1520
- (3) Hofmann A.F., Sjövall J., Kurz G., Radomska A., Schteingart C.D., Tint G.S., Vlahcevic R., Setchell K.D.R.; A proposed nomenclature for bile acids. *J Lipid Res.* **1992**, 33, 599-604
- (4) Ajouz H., Mukherji D., Shamseddine A.; Secondary bile acids: an underrecognized cause of colon cancer. *World Journal of Surgical Oncology.* **2014**, 12
- (5) Jovanovich A., Isakova T., Block G., Stubbs J., Smits G., Chonchol M., Miyazaki M.; Deoxycholic acid, a metabolite of circulating bile acids, and coronary artery vascular calcification in CKD. *Am J Kidney Dis.* **2018**, 71, 1, 27-34
- (6) Griffiths W.J., Sjövall J.; Bile acids: analysis in biological fluids and tissues. *J Lipid Res.* **2010**, 51, 23-41
- (7) Zheng X., Aly N.A., Zhou Y., Dupuis K.T., Bilbao A., Paurus V.L., Orton D.J., Wilson R., Payne S.H., Smith R.D., Baker E.S.; A structural examination and collision cross section database for over 500 metabolites and xenobiotics using drift tube ion mobility spectrometry. *Chem Sci.* **2017**, 8, 7724-7736

- (8) Zheng X., Smith F.B., Aly N.A., Cai J., Smith R.D., Patterson A.D., Baker E.S.; Evaluating the structural complexity of isomeric bile acids with ion mobility spectrometry. *Anal Bioanal Chem.* **2019**, 411, 4673-4682
- (9) Picache J.A., Rose B.S., Balinski A., Leaptrot K.L., Sherrod S.D., May J.C., McLean J.A.; Collision cross section compendium to annotate and predict multi-omic compound identities. *Chem Sci.* **2019**, 10, 983-993
- (10) Fenn L.S., McLean J.A.; Biomolecular structural separations by ion mobility-mass spectrometry. *Anal Bioanal Chem.* **2008**, 391, 905-909
- (11) McLean J.A.; The mass-mobility correlation redux: the conformational landscape of anhydrous biomolecules. *J Am Soc Mass Spectrom.* **2009**, 20, 1775-1781
- (12) Fenn, L.S., Kliman M., Mahsut A., Zhao S.R., McLean J.A.; Characterizing ion mobility-mass spectrometry conformation space for the analysis of complex biological samples. *Anal Bioanal Chem.* **2009**, 392, 235-244
- (13) Paglia G., Angel P., Williams J.P., Richardson K., Olivos H.J., Thompson J.W., Menikarachchi L., Lai S., Walsh C., Moseley A., Plumb R.S., Grant D.F., Palsson B.O., Langridge J., Geromanos S, and Astarita G.; Ion Mobility-Derived Collision Cross Section As an Additional Measure for Lipid Fingerprinting and Identification. *Anal Chem* **2015**, 87 (2), 1137-1144
- (14) May J.C., Goodwin C.R., McLean J.A.; Ion mobility-mass spectrometry strategies for untargeted systems, synthetic, and chemical biology, *Curr Opin Biotechnol.* **2015**, 31, 117-121
- (15) Schrimpe-Rutledge A.C., Codreanu S.G., Sherrod S.D., McLean J.A.; Untargeted metabolomics strategies: challenges and emerging directions, *J Am Soc Mass Spectrom.* **2016**, 27, 1897-1905
- (16) May J.C., Gant-Branum R.L., McLean J.A.; Targeting the untargeted in molecular phenomics with structural mass spectrometry, *Curr Opin Biotechnol.* **2016**, 39, 192-197
- (17) Sherrod S.D., McLean J.A.; Systems-wide high-dimensional data acquisition and informatics using structural mass spectrometry strategies, *Clin Chem.* **2016**, 62, 77-83
- (18) Nichols, C.M., Dodds J.N., Rose B.S., Picache J.A., Morris C.B., Codreanu S.G., May J.C., Sherrod S.D., Mclean J.A.; Untargeted discovery in primary metabolism: collision cross section as a molecular descriptor in ion mobility-mass spectrometry. *Anal Chem.* **2018**, 90 (24), 14484-14492
- (19) Poland J.C., Schrimpe-Rutledge A.C., Sherrod S.D., Flynn C.R., McLean J.A.; Utilizing untargeted ion mobility-mass spectrometry to profile changes in the gut metabolome following biliary diversion surgery, *Anal Chem.* **2019**, 91, 14417-14423

- (20) Stow S.M., Causon T.J., Zheng X., Kurulugama R.T., Mairinger T., May J.C., Rennie E.E., Baker E.S., Smith R. D., McLean J.A.; Feldsted J C. An Interlaboratory Evaluation of Drift Tube Ion Mobility-Mass Spectrometry Collision Cross Section Measurements. *Anal Chem.* **2017**, 89, 9048-9055
- (21) Nichols C.M., May J.C., Sherrod S.D., McLean J.A.; Automated flow injection method for the high precision de-termination of drift tube ion mobility collision cross sections. *Analyst.* **2018**, 143, 1556-1559



## CHAPTER IV

### UTILIZING UNTARGETED ION MOBILITY-MASS SPECTROMETRY TO PROFILE CHANGES IN THE GUT METABOLOME FOLLOWING BILIARY DIVERSION SURGERY

#### **4.1. Introduction**

Worldwide obesity has reached epidemic levels, contributing to a decline in the well-being of many people and drastically increasing public health costs.(1,2) Obesity is continually increasing in severity and has been associated with health problems such as diabetes, chronic inflammation, fatty liver disease and cancer. Efforts toward understanding this complex disease have found contributions related to genetic predisposition, lifestyle, environment, ethnicity, gender, and even composition of the gut microbiota.(2) Strategies to combat obesity include diet and lifestyle changes, medication, and bariatric surgery. Of these interventions, bariatric surgery – namely Roux-en-Y gastric bypass (RYGB) – is more effective than intensive medical therapy at achieving sustained excess weight loss of about 47% at 5 years and 10 years post-operation.(3,4) These surgeries also have a desirable, yet unexplained side-effect of improving type-2 diabetes (T2D) by reducing glycated hemoglobin by ~31% at 1 year and ~21% at 5 years post-operation.(3,5) RYGB results in dramatic and sustained weight loss and improved glycemic control via a multitude of mechanisms, one of which is the increased distal delivery of gallbladder bile in the intestinal lumen and altered enterohepatic circulation of bile acids.(6,7) Bile acids are synthesized in the liver from a cholesterol precursor and expelled by the gallbladder into the intestines where they aid in lipid absorption. This suite of molecules also facilitate their own production through signaling, are involved in glucose metabolism, and act as hormones.(8) We have previously reported, using mouse models, that RYGB results in satiety, weight loss, changes

in the gut microbiome, and fat malabsorption in animals fed a high-fat diet.(9) Each of these changes confounds our understanding of how bile acids modulate enteral glucose handling. To assess the effects of altered bile flow on intestinal nutrient handling, we developed a murine bile diversion model in which the common bile duct is sutured closed and the gallbladder bile is surgically redirected to the duodenum (GB-D), jejunum (GB-J), or 4 cm from the distal ileum (GB-IL<sub>dist</sub>) by anastomosis without any other alterations to gastrointestinal anatomy or alimentary flow.(9,10) Further, bile diversion 10 cm from the ileocecal valve, a procedure we termed proximal GB-IL (GB-IL<sub>prox</sub>), achieved significant improvements in enteral glucose handling without fat absorption.(7) In these studies, we aimed to identify the bile acids and other fecal metabolites that differ between the GB-IL<sub>dist</sub> and GB-IL<sub>prox</sub> procedures. In particular, we developed a method to determine which lipids and bile acids may be selectively transported by the 6 cm portion (between IL<sub>dist</sub> and IL<sub>prox</sub>) of the murine gastrointestinal tract (**Figure 4.1**). Targeted metabolomic methods have previously been utilized to study bile acids, however, these methods are limited in scope and do not measure unexpected endogenous metabolites that may also be affected.(11,12) Considering the multifaceted role of bile acids, the global effects of their dysregulation are also of interest.

The detection of bile acids has previously been reported in plasma but this workflow requires clean-up, such as solid phase extraction, and derivatization, which is time consuming and inherently limits the nature and amount of molecules analyzed.(7,9) Herein, we report a global, untargeted ultra-performance liquid chromatography-ion mobility-mass spectrometry (UPLC-IM-MS/MS) method to rapidly detect a suite of endogenous metabolites, including bile acids, extracted from feces with minimal sample preparation. The additional dimension of IM separation allows for the discrimination of co-eluting and isobaric metabolites in complex mixtures, which

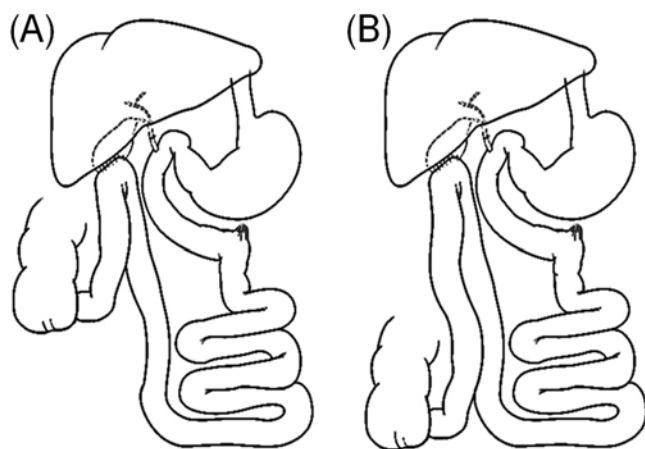


**Figure 4.1.** Schematics of the distal GB-IL<sub>dist</sub> (A) and proximal GB-IL<sub>prox</sub> (B) bile diversion surgeries

enables high confidence characterization and identification.(13-18) IM-MS profiling has previously been demonstrated to separate multiple biological classes in complex biological samples.(19-24) The approach described herein, is an optimized UPLC-IM-MS/MS method that capitalizes on the increased separation capacity (LC dimension combined with IM dimension) to fully characterize extracted fecal metabolites. We demonstrate the utility of this method by investigating the qualitative changes of endogenous metabolites observed in biliary diversion surgery and controls. In addition to describing previously identified metabolite fluctuations, we also observed unexpected metabolic pathways that may also be affected by bile diversion. These conclusions both support and expand upon current knowledge of affected metabolites, and suggest a wide breadth of biological consequences resultant of biliary diversion.

## **4.2 Experimental Methods**

The untargeted metabolomic scheme utilized in this work is shown in **Figure 4.2** and is further described in the following sections.

### **4.2.1. Standards and Chemicals.**

Optima grade acetonitrile and water were purchased from Fisher Scientific (Loughborough, UK). Ammonium acetate was purchased from Sigma Aldrich (Dorset, UK). Formic acid was purchased from Fluka (Buchs, Switzerland). Bile acid standards, including: tauro-alpha-muricholic acid (T- $\alpha$ -MCA), tauro-beta-muricholic acid (T- $\beta$ -MCA), tauro-omega-muricholic acid (T- $\omega$ -MCA), alpha-muricholic acid ( $\alpha$ -MCA), beta-muricholic acid ( $\beta$ -MCA), taurohyocholic acid (THCA), glycooursodeoxycholic acid (GUDCA), tauroursodeoxycholic acid (TUDCA), hyocholic acid (HCA), taurohyoxydeoxycholic acid (THDCA), taurocholic acid

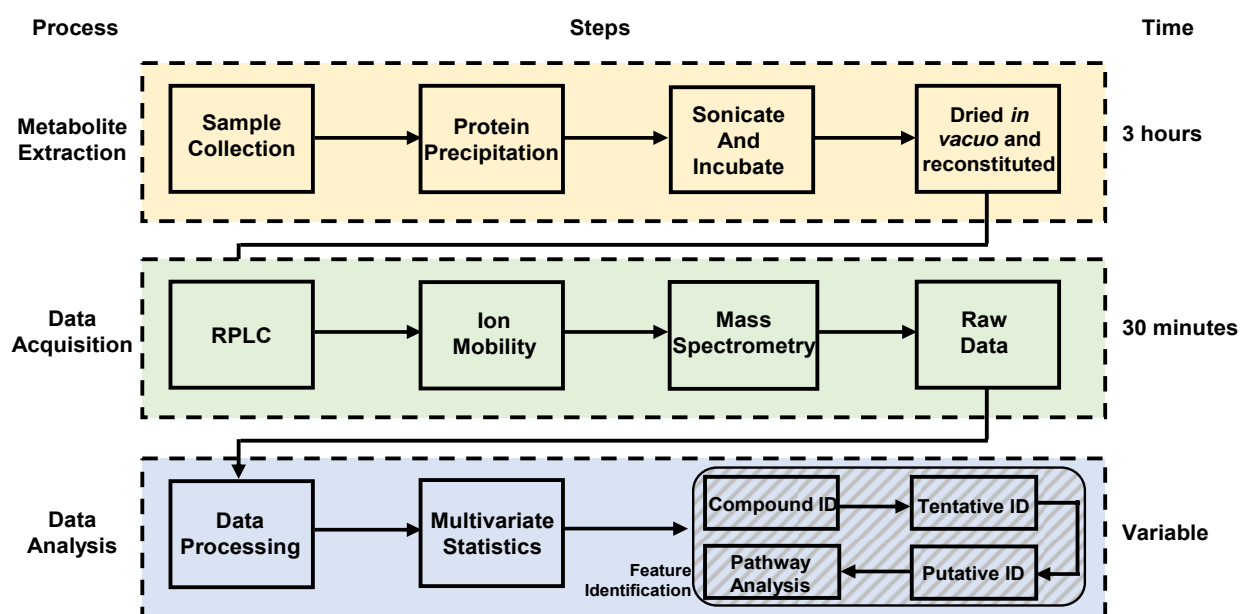


**Figure 4.2.** Flowchart depicting the individual steps taken for each of the processes of metabolite extraction, data acquisition, and data analysis utilized in this work. Representative times for each process are shown.

(TCA), cholic acid (CA), ursodeoxycholic acid (UDCA), hyodeoxycholic acid (HDCA), glycodeoxycholic acid (GDCA), taurodeoxycholic acid (TDCA), chenodeoxycholic acid (CDCA), and deoxycholic acid (DCA) were purchased from Steraloids, Inc. (Newport, RI). Standard solutions of these twenty bile acids were prepared at concentrations of 0.5 nM, 10 nM, 50 nM, 100 nM, 500 nM, 1,500 nM, 5,000 nM, and 10,000 nM in a solution of 20% (v/v) acetonitrile (ACN) and water.

#### **4.2.2. Surgery and Fecal Collection.**

Male C57BL/6J mice (Jackson Labs; Bar Harbor, ME) were housed at 23°C on a 07:00-19:00 light cycle and were fed a high fat diet (60% kcal from fat; Bio-Serv, Frenchtown, NJ), starting at six weeks of age for 12 weeks prior to being randomly allocated to a surgical group. The GB-IL<sub>dist</sub> procedure, where the gallbladder was anastomosed 4 cm from the cecum, was carried out as previously described.<sup>(9)</sup> The GB-IL<sub>prox</sub> surgery was performed in an identical manner with the exception of gallbladder anastomosis 10 cm from the ileocecal valve.<sup>(9,10)</sup> Fecal pellets were collected by hand and stored at -80°C prior to sample preparation.

#### **4.2.3. Fecal Metabolite Extraction, Preparation and UPLC-IM-MS Analysis.**

Fecal pellet samples were thawed on ice prior to extraction. A 25 mg sample of fecal material was mixed with 75:25 (v:v) ACN:H<sub>2</sub>O (1 mL). Samples were sonicated for 30 seconds on ice to break up solid particulates, then vortexed and incubated at -20°C for 2 hours. Following incubation, the solution was centrifuged (4°C, 12,000 rpm, 10 min) and the supernatant was removed. Aliquots were subsequently dried in vacuo using a speedvac (Thermo Scientific) and stored at -80°C until analysis. Prior to analysis, dried extracts were reconstituted in 100 µL of 80:20

(v:v) ACN:H<sub>2</sub>O. To assess instrument reproducibility, a pooled sample was made by combining 20 µL of each individual resuspension sample to serve as a quality control (QC) sample. Reconstituted metabolite extracts were transferred to auto sampler vials for UPLC-IM-MS analysis.

Ultra-Performance Liquid Chromatography-Ion Mobility-Mass Spectrometry (UPLC-IM-MS). Chromatographic separation was performed using a Nano Acquity (Waters Corporation, Manchester, UK) fitted with an Acquity UPLC HSS column (T3, 1.8 µM). The IM-MS instrument (Synapt G2, Waters, Milford, MA, USA) was controlled by MassLynx (version 4.1, Waters).(25) Source conditions were optimized for individual bile acids via direct infusion prior to LC optimization. Bile acids were measured in negative mode with a capillary voltage of 2.2 kV. A bile acid mixture was prepared and chromatography gradients were tested to determine optimal chromatographic conditions for LC separation of the twenty bile acid standards (**Figure 4.3**). Solvent A consisted of 80:20 (v:v) H<sub>2</sub>O:ACN with 10 mM ammonium acetate and solvent B was 20:80 (v:v) H<sub>2</sub>O:ACN with 10mM ammonium acetate. In the analysis of the fecal extracts, the total analysis time was 30 minutes with a flow rate of 75 µL/min. The solvent gradient started at 5% solvent B and increased to 15% B from 0 to 15 min, increased to 25% B from 15 to 20 min, increased to 75% B from 20 to 22 min, and then decreased to 5% B from 22 to 24 min where it was held for the remainder of the run from 24 to 30 min. A heated column jacket sleeve controlled the temperature at 45°C.

To determine IM drift times (DT), used to calculate collision cross sections (CCS), for bile acids were collected individually via direct infusion on three different days. The flow rate was set to 10 µl/min with the electrospray voltage set to 2.3 kV. Desolvation temperature is set to 325 °C. The traveling wave ion mobility cell was operated at a pressure of 3.35 (mbar) N<sub>2</sub> with a wave

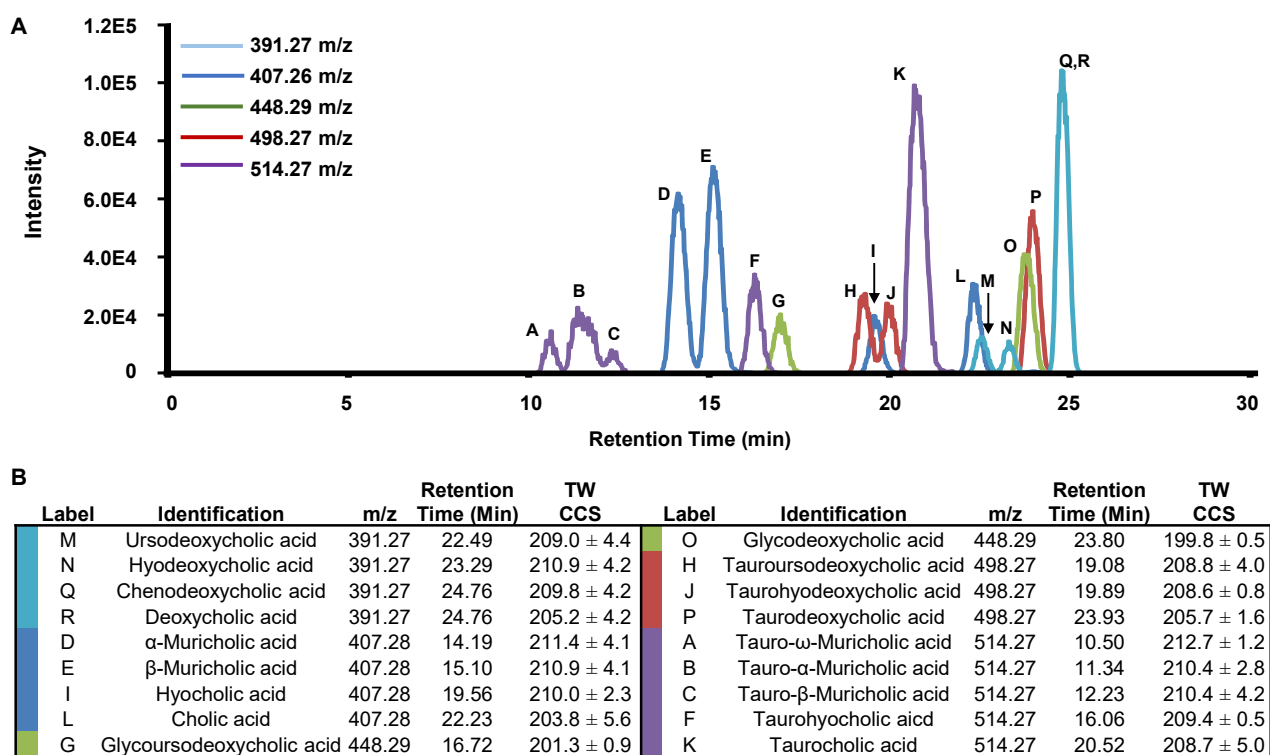


**Figure 4.3.** (A) Overlays of the negative-polarity extracted ion chromatograms of the bile acid standards separated using the optimized method. The colors represent the specific  $m/z$  extracted ion chromatograms shown. (B) Experimental evidence for reference standards including  $m/z$  retention time, and CCS are shown. Labels in (A) correspond to the specific bile acid codes in (B).



velocity of 650 m/s and a transfer wave height of 4 V. The trap and transfer cells were operated at  $2.90 \times 10^{-2}$  and  $1.00 \times 10^{-6}$  mbar, respectively. A calibration solution containing 10  $\mu$ l/ml polyalanine was acquired prior to the bile acid data acquisition each day, and CCS were calculated using DriftScope v2.5.

The MS was operated in both negative and positive electrospray ionization MS<sup>E</sup> modes for both reference standards and fecal samples. The source temperature was maintained at 100 °C, and desolvation temperature at 300 °C. Ion mobility separation in the drift cell was performed in nitrogen gas at a flow rate of 90 mL/min. The traveling wave cell was operated at a pressure of 3.29 (mbar) with a wave velocity of 650 m/s and a transfer wave height of 4 V. The trap and transfer cells were operated at  $2.18 \times 10^{-2}$  and  $2.29 \times 10^{-2}$  mbar, respectively. Mass calibration was performed using sodium iodide. Lockspray was collected at masses of 554.26 Da and 556.27 Da, corresponding to leucine enkephalin [M-H]<sup>-</sup> and [M+H]<sup>+</sup>, respectively, and applied during data analysis. In fragmentation mode, all ions were activated in the collision induced dissociation cell (i.e. MS<sup>E</sup> was utilized).

#### 4.2.4. Data Analysis

Data analysis was performed using Progenesis QI software (version 2.3, Nonlinear Dynamics, New-castle, UK). Default parameters were used for retention time alignment, peak picking, and peak deconvolution. Spectra were normalized to all compounds. Data were filtered for covariance (CV) <30% in QC pool technical replicate injections. A prioritized compound list was generated via a one-factor ANOVA, with GB-D samples set as the control group against GB-IL<sub>prox</sub> and GB-IL<sub>dist</sub> groups. Compounds were considered significant if p-value  $\leq 0.01$  and fold change  $\geq |2.0|$ . Significant compounds were selected for metabolite identification.

Metabolites were identified using an established classification system as previously described by Schrimpe-Rutledge and coworkers.(26) In brief, metabolites were assigned a confidence level based on a scale of 5→1 (1 being the most confident) with increased confidence in annotation requiring increased supporting evidence (e.g., accurate mass, fragmentation pattern, and retention time matching with standards). This approach incorporates separation descriptors (RT, DT) as well as structural descriptors (MS, MS/MS). Measurements for each applicable descriptor were used to score annotations and provide a confidence metric. Following this system, identifications were made based on similarity to reference data found in in-house and online databases (Metlin, NIST, Chempidder). Scores were calculated by Progenesis based on mass error (<20 ppm), isotope similarity, and fragmentation spectra when applicable. In cases where multiple metabolites were possible candidates for a single feature, the metabolite(s) with the highest score was selected as the tentative annotation. IM drift time was used to distinguish bile acids in cases in which they co-eluted.

Data is available at the NIH Common Fund's National Metabolomics Data Repository (NMDR) website, the Metabolomics Workbench, <https://www.metabolomicsworkbench.org> where it has been assigned Project ID (PR000836). The data can be accessed directly via it's Project DOI: (10.21228/M8MQ2G). This work is supported by NIH grant U2C-DK119886.

## **4.3. Results and Discussion**

### **4.3.1. Bile Acid Separation Optimization.**

One of the primary challenges in the mass spectrometric analysis of bile acids is the large redundancy of isobaric species that are commonly encountered.(27) While ion mobility separations can separate many isobaric species,(28-30) LC-IM-MS offers increased peak capacity

and an additional analytical descriptor and thus was chosen for the untargeted fecal metabolite analyses of these complex mixtures.(31-33)

In addition to LC retention times, MS/MS fragmentation spectra and IM CCS values were collected for each of the reference standards (**Figure 4.3B**). Fragmentation patterns from collision induced dissociation (CID) of most isomeric bile acids are indistinguishable, thus identifications based on fragmentation data alone is difficult. However, CCS measurements were often able to differentiate isomers and were used to aid in identifications. Extracted ion chromatograms of the matrix-free bile acids standards are shown in Figure 4.3A. The majority of the bile acid isomers (18/20) were resolved by the RPLC gradient presented, including the stereoisomers of  $\alpha$ -,  $\beta$ -, and  $\omega$ -muricholic acid as well as their conjugates. Although chenodeoxycholic acid and deoxycholic acid co-eluted, these analytes were separated in the ion mobility dimension (i.e., distinct CCS values) and hence could be experimentally distinguished (**Appendix Figure C.1**). Experimental data acquired from the bile acids was used to generate a bile acid database containing collision cross section (CCS), retention time (RT), and accurate mass. In these studies, this annotated in-house database was used to assign co-eluting bile acids with increased confidence. Traveling wave collision cross sections (TWIM) and relative standard deviation can be found in supplemental data (**Appendix Table C.1**). The calculated TWIM CCS values are observed to be higher than the reported drift tube ion mobility values found in the compendium.(23) These results have an average percent difference <6% which is in agreement with results reported by Ridenour et al, in that an average percent difference of 7% can be expected when your mobility cell is calibrated with molecules structurally different than your analytes(34).

#### **4.3.2. Global, Untargeted Analysis of Fecal Metabolite Profiling.**

In a preliminary study, the optimized bile acid method was applied to control mouse fecal samples. In addition to being able to identify 9 bile acids (and bile acid-like molecules), this global, untargeted method facilitated the detection of a variety of compounds including lipids, amino acids, and peptides (**Appendix Table C.2.**). These findings demonstrated that the optimized bile acid separation method is applicable for comparative analyses complex biological investigations.

#### **4.3.3. Application of the Untargeted LC-IM-MS Method to Mouse Feces following Bile Diversion Surgery.**

Three groups of mice underwent biliary diversion surgery to various degrees. The first group was a control in which an incision was made but no diversions were performed (group labeled as GB-D), the second group received bile diversion 10 cm from the ileocecal valve (group labeled as GB-IL<sub>prox</sub>), and the third group received the bile diversion 4 cm from the ileocecal valve (group labeled as GB-IL<sub>dist</sub>). The metabolite extraction protocol was performed on collected feces for each group (n = 5 mice per sample group). Using the described UPLC-IM-MS method, the complex mix of fecal metabolites were chromatographically resolved, detected, and annotated.

Many compounds emerged as statistically significant in pairwise comparisons against the GB-D group (GB-IL<sub>prox</sub> vs. GB-D and GB-IL<sub>dist</sub> vs. GB-D). In positive ion mode, 9,255 compounds were detected with 1,093 compounds meeting the significance criteria (p-value  $\leq 0.01$  and a fold change  $\geq |2.0|$ ) between the GB-D and GB-IL<sub>dist</sub> groups, and 102 significant between the GB-D and GB-IL<sub>prox</sub> groups. Of the 1,801 compounds detected in negative mode, 181 compounds met significance criteria between GB-D and GB-IL<sub>dist</sub>, while only 12 were found to be significant between GB-D and GB-IL<sub>prox</sub> groups. A PCA score plot is shown in **Figure 4.4A** revealing minimal separation between GB-D and GB-IL<sub>prox</sub>. However, the separation between the former groups and the GB-IL<sub>dist</sub> cluster reveal a unique GB-IL<sub>dist</sub> metabolomic profile. Positive ion

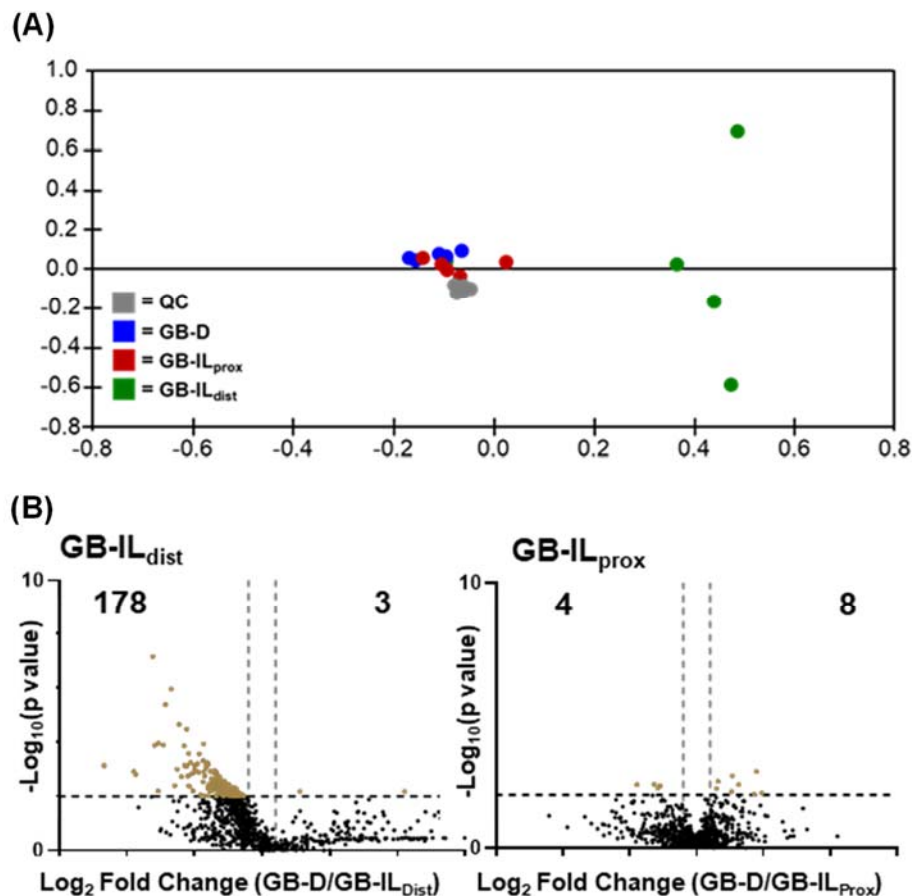


**Figure 4.4.** (A) The unsupervised principal component analysis (PCA) displaying biological replicates of the fecal sample of each sample group. Each point represents one biological replicate while color represent a complete sample group. The GB-D and GB-IL<sub>prox</sub> samples show close similarities by clustering near each other, while GB-IL<sub>dist</sub> samples segregate in distinct clusters. (B) Pair-wise comparison was performed between the diet-induced obese mice (GB-D) and surgical GB-IL<sub>dist</sub> or GB-IL<sub>prox</sub> mice to create volcano plots from the untargeted metabolomics data. Compounds of interest were prioritized using significance criteria ( $p$ -value  $\leq 0.01$  and fold change  $\geq 2$ ), visualized in the upper, outer corners of the volcano plots. (Negative mode data shown).

mode data is shown in **Appendix Figure C.2.** revealing a similar trend in group separation.

Compounds were prioritized using pairwise comparisons relative to GB-D to determine significant dysregulation of the sample groups. **Figure 4.4B** (and **Appendix Figure C.2.**) displays volcano plots that highlight significant compounds in pairwise comparisons of GB-D versus GB-IL<sub>dist</sub> or GB-IL<sub>prox</sub> samples. The subsets of significantly dysregulated metabolites were searched against the in-house bile acid database to evaluate potential changes in bile acid abundance; relative bile acid intensities were compared between groups (**Figure 4.5**). Similar to the results outlined in the PCA, the bile acid profile of the GB-D group and the GB-IL<sub>prox</sub> group were similar, however the GB-IL<sub>dist</sub> group has several differences. Specifically,  $\alpha$ -muricholic acid and chenodeoxycholic acid show a significant decrease, while cholic acid and taurocholic acid are increased. In addition to noticeable changes in the composition of bile acids and their derivatives, the abundances of other metabolites were observed to be statistically significant, these include: vitamin derivatives, fatty acids, and cholesterol derivatives. Lists of tentatively identified metabolites are included in **Appendix Tables C.3.–C.6.**

To associate altered metabolite abundances with their respective biological pathways, predictive network activity analysis was performed using Mummichog.(18,26,35) The Mummichog algorithm uses the accurate mass of m/z features to map candidate metabolites to metabolic networks, calculating local enrichment of metabolites to distinguish those networks from a stochastic distribution of likely false activity. In these analyses, we were able to correlate metabolic function with dysregulation in bile acid biosynthesis, vitamin A, D3, and E metabolism, arachidonic acid metabolism, leukotriene metabolism, and steroid hormone bio-synthesis with the GB-IL<sub>dist</sub> surgery (**Figure 4.6**). These results are consistent with measured fluctuations of specific metabolites as significant changes were observed in bile acid concentration and lipid soluble

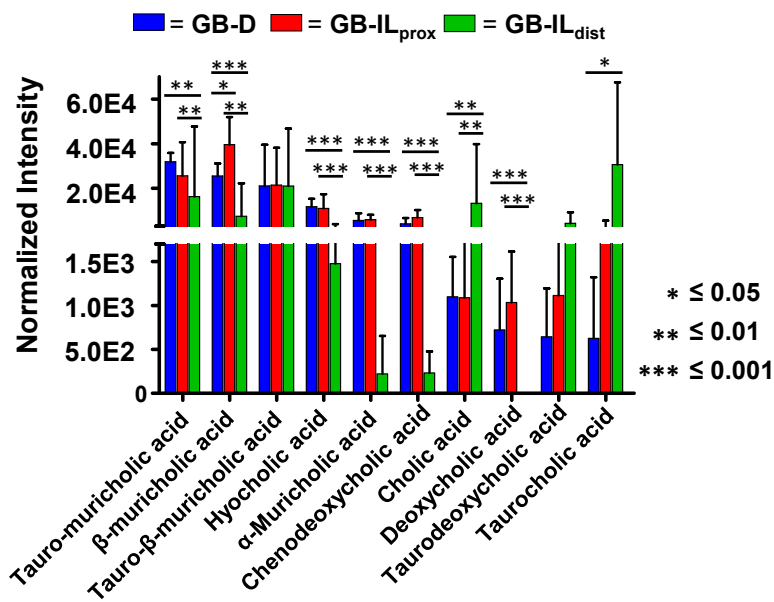


**Figure 4.5.** Observed bile acids and their normalized intensities among the biological sample groups.

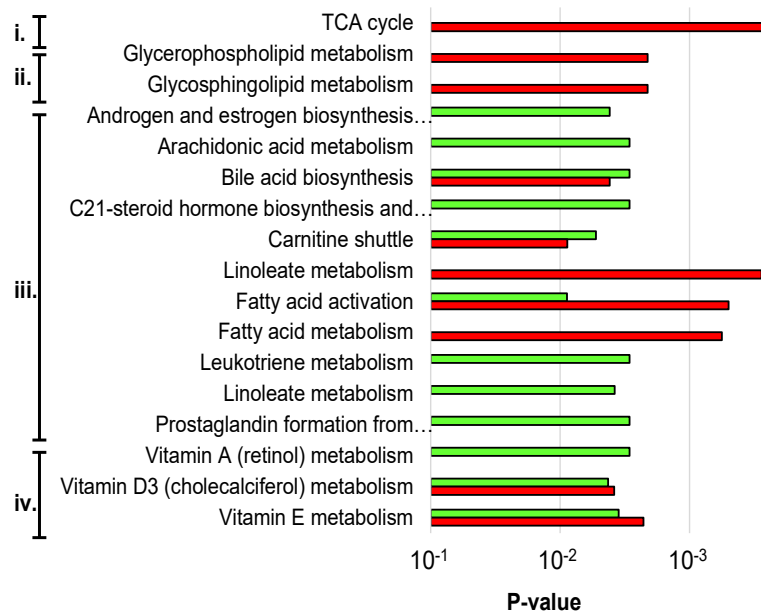


**Figure 4.6.** Top predicted pathways altered as a result of GB-IL<sub>prox</sub> (Red) and GB-IL<sub>dist</sub> (Green). Related pathways are labelled as: i. carbohydrate metabolism, ii. glycan biosynthesis and metabolism, iii. lipid metabolism, and iv. vitamin metabolism. (Full pathway names can be found in **Supplemental Table ST7**).



molecules. The enterohepatic circulation system was perturbed after biliary diversion surgery, so it was anticipated to affect numerous small molecules involved in emulsion and mixed micelle formation. The decrease in total fecal bile acids and the increase in lipid content also point to emulsion or mixed micelle formation. Additional significant changes were also observed for pathways not directly involved with bile acid circulation, for example steroid hormone biosynthesis. These results suggest that the developed global, untargeted method can be used to elucidate perturbed pathways without a priori knowledge.

Alterations and fluctuations in the bile acid biosynthesis and conjugation pathways in the GB-IL<sub>dist</sub> sample group were in agreement with knowledge that enterohepatic circulation is affected. Bile acids form emulsions with phospholipids and triacylglycerols prior to absorption through the small intestines. Disrupting this process greatly reduces lipid and lipophilic molecule absorption. It is important to note that 95% of bile acids are recycled via enterohepatic circulation; fecal samples were received four weeks after the procedure, which may account for this observed decrease. Considering that the emulsion and mixed micelle formation is disturbed, many of the bile acids would be excreted, and hence there would be a drastic decrease observed after four weeks, because fewer bile acids would be recycled over time. Bile acids are synthesized from cholesterol, and disruption of the enterohepatic circulation can result in decreasing endogenous cholesterol and cholesterol derived metabolites, as the body might attempt to account for the loss by synthesizing larger quantities. These results could explain why steroid hormone biosynthesis emerged as a significantly altered pathway (**Appendix Figure C.3.**), as increasing bile acid production would draw more from the overall cholesterol pool. With more cholesterol being utilized for the synthesis of bile acids, other hormones derived from cholesterol were affected.

#### 4.4. Conclusion

In conclusion, we report a UPLC-IM-MS method that can be used to identify relative changes in bile acid abundance, as well as detect dysregulation of other small molecules that may contribute to observed phenotypical changes in the gut. The described method was able to observe expected pathways in the gastrointestinal system, and also reveal pathways that have not been previously explored. Taken together, these data demonstrate the utility in using UPLC-IM-MS analyses for studying gastrointestinal disease/treatment.

#### 4.5. Acknowledgements

This chapter contains the published research article: James C. Poland, Alexandra C. Schrimpe-Rutledge, Stacy D. Sherrod, Charles Robb Flynn and John A. McLean, “Utilizing Untargeted Ion Mobility-Mass Spectrometry to Profile Changes in the Gut Metabolome Following Biliary Diversion Surgery,” *Analytical Chemistry*, **2019**, 22, 14417-14423

Financial support for aspects of this research was provided by The National Institutes of Health (Grants NCI RO1DK105847 and RO3CA222452). This work was supported in part using the resources of the Center of Innovative Technology at Vanderbilt University. The Metabolomic Workbench is supported by NIH grant U2CDK119886. JCP also thanks Vanderbilt University, the Institute of Chemical Biology, and the Fisk-Vanderbilt Masters to PhD Bridge program for financial support.

#### 4.6. References

1. Wang Y., Beydoun M. A.; The Obesity Epidemic in the United States—Gender, Age, Socioeconomic, Racial/Ethnic, and Geographic Characteristics: A Systematic Review and Meta-Regression Analysis. *Epidemiol Rev*, **2007**, 29 (1), 6-28.

2. Goodwin P. J.; Stambolic V. Impact of the Obesity Epidemic on Cancer. *Annu Rev Med*, **2015**, 66 (12), 281-296.
3. Schauer P. R.; Bhatt D. L.; Kirwan J. P.; Wolski K.; Arminian A.; Brethauer S. A.; Navaneethan S. D.; Singh R. P.; Pothier C. E.; Nissen S. E.; Kashyap S. R. Bariatric Surgery versus Intensive Medical Therapy for Diabetes — 5-Year Outcomes. *New Eng J Med*, **2017**, 376, 641-651.
4. Golzarand M.; Toolabi K.; Farid R. The bariatric surgery and weight losing: a meta-analysis in the long- and very long-term effects of laparoscopic adjustable gastric banding, laparoscopic Roux-en-Y gastric bypass and laparoscopic sleeve gastrectomy on weight loss in adults. *Surg Endosc*, **2017**, 31 (11), 4331-4345.
5. Schauer P. R.; Kashyap S. R.; Wolski K.; Brethauer S. A.; Kirwan J. P.; Pothier C. E.; Thomas S.; Abood B.; Nissen S. E.; Bhatt D. L. Bariatric Surgery versus Intensive Medical Therapy in Obese Patients with Diabetes. *New Eng J Med*, **2012**, 366, 1597-1576.
6. Albaugh V. L.; Flynn C. R.; Tamboli R. A.; Abumrad N. N. Recent advances in metabolic and bariatric surgery. *F1000research*, **2016**, 5(F1000 Faculty Rev):978.
7. Albaugh V. L.; Wei Y.; Xiong Y.; Ping J.; Abumrad N. N.; Flynn C. R. Proximal bile diversion to ileum partitions fat malabsorption from glycemic control. *Mol Metab*, **2019**, submitted
8. Staels B.; Fonseca V. A. Bile Acids and Metabolic Regulation. *Diabetes Care*, **2009**, 32, 237-245.
9. Flynn C. R.; Albaugh V. L.; Cai S.; Cheung-Flynn J.; Williams P. E.; Brucker R. M.; Bordenstein S. R.; Guo Y.; Wasserman D. H.; Abumrad N. N. Bile diversion to the distal small intestine has comparable metabolic benefits to bariatric surgery. *Nat. Commun.*, **2015**, 6, Article Number 7715.
10. Albaugh V. L.; Banan B.; Antoun J.; Xiong Y.; Guo Y.; Ping J.; Alikhan M.; Clements B.A.; Abumrad N. N.; Flynn C. R. Role of Bile Acids and GLP-1 in Mediating the Metabolic Improvements of Bariatric Surgery. *Gastroenterology*, **2019**, 154 (4), 1041-1051.
11. Bobeldijk I.; Hekman M.; de Vries-van der Weij J.; Coulier L.; Ramaker R.; Kleemann R.; Kooistra T.; Rubingh C.; Freidig A.; Verheij E. Quantitative profiling of bile acids in biofluids and tissues based on accurate mass high resolution LC-FT-MS: Compound class targeting in a metabolomics workflow. *J of Chromatogr B*, **2008**, 871, 306-313.
12. Garcia-Canaveras J. C.; Donato M. T.; Castell J. V.; Lahoz A. Targeted profiling of circulating and hepatic bile acids in human, mouse, and rat using a UPLC-MRM-MS-validated method. *J Lipid Res*, **2012**, 53, 2231-2241.

- 13 Hines, K. M.; Ashfaq, S.; Davidson, J. M.; Opalenik, S. R.; Wikswo, J. P.; McLean, J. A. Biomolecular Signatures of Diabetic Wound Healing by Structural Mass Spectrometry. *Anal. Chem.* **2013**, 85 (7), 3651-3659.
- 14 Goodwin C. R.; Sherrod S. D.; Marasco C. C.; Bachman B. O.; Schramm-Sapyta N.; Wikswo J. P.; McLean J. A. Phenotypic Mapping of Metabolic Profiles Using Self-Organizing Maps of High-Dimensional Mass Spectrometry Data. *Anal. Chem.* **2014**, 86, 6563-6571.
- 15 Hines, K. M., Ballard, B. R., Marshall, D. R., McLean, J. A.; Structural mass spectrometry of tissue extracts to distinguish cancerous and non-cancerous breast diseases. *Mol. Biosys.* **2014**, 10 (11), 2827-2837.
- 16 May, J. C., Goodwin, C. R., McLean, J. A.; Ion mobility-mass spectrometry strategies for untargeted systems, synthetic, and chemical biology. *Curr. Opin. Biotech.* **2015**, 31, 117-121.
- 17 Sherrod, S. D.; McLean, J. A. Systems-Wide High-Dimensional Data Acquisition and Informatics Using Structural Mass Spectrometry Strategies. *Clin. Chem.* **2016**, 62 (1), 77-83.
- 18 May, J. C., Gant-Branum, R. L., McLean, J. A.; Targeting the untargeted in molecular phenomics with structurally-selective ion mobility-mass spectrometry. *Curr. Opin. Biotech.* **2016**, 39, 192-197.
- 19 Fenn, L. S., McLean, J. A.; Biomolecular structural separations by ion mobility-mass spectrometry. *Anal. Bioanal. Chem.* **2008**, 391 (3), 905-909.
- 20 McLean, J. A.; The mass-mobility correlation redux: The conformational landscape of anhydrous biomolecules. *J. Am. Soc. Mass Spectrom.* **2009**, 20 (10), 1775-1781.
- 21 Fenn, L. S., Kliman, M., Mahsut, A., Zhao, S. R., McLean, J. A.; Characterizing ion mobility-mass spectrometry conformation space for the analysis of complex biological samples. *Anal. Bioanal. Chem.* **2009**, 394 (1), 235-244.
- 22 May J. C., Goodwin C. R., Lareau N. M., Leaptrot K. L., Morris C. B., Kurulugama R. T., Mordehai A., Klein C., Barry W., Darland E., Overney G., Imatani K., Stafford G.C., Fjeldsted J. C., McLean J. A.; Conformational Ordering of Biomolecules in the Gas Phase: Nitrogen Collision Cross Sections Measured on a Prototype High Resolution Drift Tube Ion Mobility-Mass Spectrometer. *Anal. Chem.* **2014**, 86 (4), 2107-2116.
- 23 Picache J. A., Rose B. S., Balinski A., Leaptrot K. L., Sherrod S. D., May J. C., McLean J. A.; Collision cross section compendium to annotate and predict multi-omic compound identities. *Chem Sci*, **2019**, 10, 983-993.
- 24 Leaptrot K. L., May J. C., Dodds J. N., McLean J. A.; Ion mobility conformational lipid atlas for high confidence lipidomics. *Nat. Commun.* **2019**, 10, 985.

- 25 May J. C., McLean J. A.; Ion Mobility-Mass Spectrometry: Time-Dispersive Instrumentation. *Anal. Chem.* **2015**, 87 (3), 1422-1436.
- 26 Schrimpe-Rutledge A. C.; Codreanu S. G.; Sherrod S. D.; McLean J. A.; Untargeted Metabolomics Strategies—Challenges and Emerging Directions. *J. Am. Soc. Mass Spectrom.* **2016**, 27, 1897-1905.
- 27 May, J. C., McLean, J. A.; Advanced Multidimensional Separations in Mass Spectrometry: Navigating the Big Data Deluge. *Ann. Rev. Anal. Chem.* **2016**, 9, 387-409.
- 28 Fenn, L. S., McLean, J. A.; Structural resolution of carbohydrate positional and structural isomers based on gas-phase ion mobility-mass spectrometry. *Phys. Chem. Chem. Phys.* **2011**, 13 (6), 2196-2205.
- 29 Kliman, M., May, J. C., McLean, J. A.; Lipid analysis and lipidomics by structurally selective ion mobility-mass spectrometry. *Biochim. Biophys. Acta.* **2011**, 18 (11), 935-945.
- 30 Dodds, J. N., May, J. C., McLean, J.A.; “Investigation of the Complete Suite of the Leucine and Isoleucine Isomers: Toward Prediction of Ion Mobility Separation Capabilities.” *Anal. Chem.* **2017**, 89 (1), 952-959.
- 31 Valentine, S. J., Kulchania, M., Barnes, C. A. S., Clemmer, D. E.; Multidimensional separations of complex peptide mixtures: a combined high-performance liquid chromatography/ion mobility/time-of-flight mass spectrometry approach. *Int. J. Mass Spectrom.* **2001**, 212 (1-3), 97-109.
- 32 McLean, J. A., Ruotolo, B. T., Gillig, K. J., Russell, D. H.; Ion mobility–mass spectrometry: a new paradigm for proteomics. *Int. J. Mass Spectrom.* **2005**, 240, 301-315.
- 33 Dodds, J. N.; May, J. C.; McLean, J. A. Correlating Resolving Power, Resolution, and Collision Cross Section: Unifying Cross-Platform Assessment of Separation Efficiency in Ion Mobility Spectrometry. *Anal. Chem.* **2017**, 89 (22), 12176-12184.
- 34 Ridenour W.B.; Kliman M., McLean J. A.; Caprioli R. M.; Structural characterization of phospholipids and peptides directly from tissue and sections by MALDI traveling-wave ion mobility-mass spectrometry. *Anal. Chem.* **2010**, 82, 5, 1881-1889
- 35 Li S.; Park Y.; Duraisingham S.; Strobel F. H.; Khan N.; Soltow Q. A.; Jones D. P.; Pulendran B. Predicting Network Activity from High Throughput Metabolomics. *PLoS Comput. Biol.* **2013**, 9 (7)

## CHAPTER V

### CONCLUSIONS AND FUTURE DIRECTIONS FOR ION MOBILITY-MASS SPECTROMETRY BASED METHODS TO PROBE THE GUT MICROBIOME

#### 5.1. Summary

As the field of systems biology matures, the need of a rapid separation technique emerges as a necessity to analyze molecules from vast chemical classes simultaneously. The technique is required to have high throughput, good separation capacity, and high sensitivity. In systems biology, it is recognized that changing molecules will have wide ranging effects. In order to fully understand the interconnectivity of biological molecules, multiple classes will need to be analyzed simultaneously, including, lipids, peptides, nucleotides, and other small molecules. This becomes an arduous task as these classes have different chemical motifs and conditions in which these molecular classes are extracted can vary widely. For example, lipidomic and metabolomic analyses are typically processed separately. In addition to them having different extraction protocols, traditional instrument conditions and buffers used are incompatible. To address this, we use buffers compatible to both fields, allowing the solvation of non-polar lipids without sacrificing more polar metabolites. However, redundancy of  $m/z$  ratio becomes more of a challenge with an increase in small molecules dissolved. This is where ion mobility–mass spectrometry excels. This technique addresses the redundancy by providing an additional dimension of separation focusing on the structural uniqueness of these classes. This supports the integration of multi-omic analysis by allowing the simultaneous analysis of multiple biological classes.

The separation capability of ion mobility mass spectrometry was discussed in Chapter I. The ability to nestle ion mobility between traditional liquid chromatography and mass spectrometry techniques enhances the ability to separate molecules that are difficult to distinguish by either techniques alone. It provides complementary size and mass separations into a single platform that functions on the millisecond time scale. As mentioned in the previous paragraph, there is great chemical diversity between biological classes. This diversity makes use of a traditional separation technique difficult, as different classes require the selection of various columns (reverse phase, HILIC, chiral, etc). In contrast, during IM-MS analysis, classes of biological molecules separate into different conformational spaces. Biological molecules travel through a mobility cell at speeds correlating to the number of inert gas collisions they experience. This allows the separation of molecules dependent on their gas-phase packing efficiency. This increase in separation capacity allows for the integration of all biological classes within one experimental method.

Previous applications of IM-MS in the fields of proteomics, metabolomics, and lipidomics have been discussed in Chapter I. Cases that highlight multidimensional separation are shown to enhance the feature identification as well as reduce redundancy for molecules with similar  $m/z$  and polarity. This allows the data to drive the biology. Instead of focusing on just one area of the metabolome, you can survey across all molecules and discover interesting features to focus on in later analyses.

Current trends and the direction that the field is heading was discussed in Chapter I, and a proof-of-concept application of these trend discussed in Chapter II. This presented the first true use of an IM-MS method in the investigation of the mechanism of action for cisplatin. A simple liquid chromatography method was developed for IM-MS analysis of metabolites after exposure

to cisplatin. This work was performed in parallel to proteomic, transcriptomic, and biological assays and then stitched back together. The extraction protocols did not call for any metabolite derivatization, so most small molecules were preserved and could be analyzed simultaneously. This work demonstrated the ability of a LC-IM-MS/MS metabolomics in an multi-omic study to determine perturbed pathways. In this, the field of systems biology has a model with which ion mobility mass spectrometry based metabolomics plays a central role.

Shifting gears from the workflow developed in Chapter II, Chapter III focused on the analysis of a class bile acids, small molecules found primarily in the enterohepatic circulation system. Many bile acids are isomers of each other and therefore difficult to distinguish in mass spectrometry as they have identical  $m/z$  and their polarities make them difficult to separate using liquid chromatography techniques as well. However, due to the gas phase interactions between the sterol and the tail, ion mobility allows these bile acids to be distinguished. This study validated that ion mobility is useful for separating problematic isomers. Bile acid cross sections are then used to populate a CCS compendium to aid in the identification of compounds in complex biological mixtures.

Building upon the workflows developed in Chapter II and conformational understanding gained in Chapter III, Chapter IV focused on the application of this methodology in a gastrointestinal system. The workflow developed was a global, untargeted metabolomic workflow that utilizes four descriptors (retention time, drift time,  $m/z$ , and fragmentation) to identify changes that are the result of biliary diversion surgery on mice. Fecal profiles of healthy controls were constructed from this metabolomic data and compared to two experimental surgical groups. In this, biological changes that result from bile acid dysregulation was discovered. A noted effect is how it alters the production of cholesterol derived steroids. Ion mobility provided increase



separation capacity allowing isobaric bile acid species to be distinguished. This is novel in that this untargeted method allowed metabolites outside of the scope of the experiment to be detected and further studied. This supports the notion that ion mobility- mass spectrometry methods that focus on metabolomics can be used to drive systems biology.

Workflows described in this dissertation support the separation and analysis of metabolites derived from a complex sample aimed towards using this as a tool to understanding the microbiome. In particular, the ability to build and compare fecal profiles demonstrates the potential for this to be used to better understand the malabsorption of small molecules.

## **5.2. Future Directions**

As mentioned throughout this dissertation, future direction lies in assigning confident metabolite identification and using it to strengthen systems biology studies. This will have to incorporate a multi-omic approach. Metabolomics pairs nicely with proteomic and genomic studies as they can be performed parallel. This aids understanding how changes in one omic fields influence others. Aspects of this type of research has been performed more recently. In this section, I will highlight some studies that have used similar methods in multi-omic experiments to analyze the cause of gastrointestinal perturbations.

The utility of an untargeted metabolomic method for identifying changing gastrointestinal metabolites has been demonstrated in Chapter IV. The gut metabolome profiles, together with other omic data, can to be used to understand the interactions between the host and microbiota flora. This has been seen in studies by Yu Gu et al. (1) In this study, metabolomic data generated using gas chromatography is combined with 16s rDNA profiling of the cecum contents of mice. In it, metabolomic differences were found between obesity-prone mice and obesity-resistant mice. These differences were mostly lipids, or metabolites involved in glycolysis, amino acid

metabolism, and the TCA cycle. It is important to note that in order to use the gas chromatography system, metabolites had to be derivatized prior to being run, therefore it is possible that many small molecules may have been missed after the derivatization process. There is a distinct microbiota profile that was found to be correlated to obesity. When looked at together, the increase of a particular class of bacteria, Parasutterella from the Proteobacteria phylum, correlated with many of the altered metabolites, suggesting that this class is essential to obesity.

This can also be used to understand the gastrointestinal disorders. One such study by Dr. Katrine Whiteson and colleagues studied the effects of the gut microbial, virome, metabolome after fecal transplantation in children affected by ulcerative colitis.(2) Samples from healthy adult patients are compared to children before and four weeks after fecal transplantation. DNA and small molecules are extracted directly from fecal samples. Untargeted metabolomics via gas chromatography is utilized to profile the metabolome. In their results, this group found that as many 3 of the 4 patients metabolomic profiles shifted towards the donor profiles after fecal transplantation. Clinical recovery increased as patients metabolome moved closer to the donor. In the one patient that did not have significant metabolomic alteration, lower clinical improvement was also seen, even though their microbiome had shifted towards the donor. This gives credence to the fact that the microbiome alone is not responsible for the development of this disorder, but also that metabolomic studies can support the understanding of the gut environment.

In our lab we collected preliminary data focused on the effect that changing diet has on both the gut metabolome and the microbiota. In this study, performed in collaboration with Dr. Bordenstein at Vanderbilt University, we have performed a multi-omic study combining metabolomic, genomic, bacteriomic data to build gastrointestinal profiles before and after diet change. The LC-IM-MS developed utilized in Chapter IV is used on human fecal samples to

yield metabolomic profiles. 16s rDNA is utilized to profile the changes in the microbiota. In this study, the effects that a changing diet has on the microbiota is explored. Patients go from a western diet, to a plant based diet for six days, and then back to a western diet. Fecal samples are collected at before, during, and after the diet change. Using the techniques described in this dissertation, a method to analyze extracted metabolites. **Figure 5.1** shows self-organizing maps created to track metabolomic changes for individual patients through the course of the study. Although the data has been collected, and some profiles made, we are still in the process of analyzing the full dataset, and have not begun to correlate metabolomic changes with genomic and microbiota data. These studies bridge our method with the future of multiomic microbiome analysis.

### **5.3. Conclusions**

Liquid chromatography, ion mobility, and mass spectrometry techniques have been explored in the support of systems biology. The history and current uses of ion mobility as separation technique has been explained with an emphasis on the biological fields of lipidomics, proteomics, and metabolomics. Focusing on metabolomics, IM-MS aids in the classification unknown molecules into biological classes based on their coordination on a mobility plot (using the  $m/z$  and CCS values together). This provides increased confidence in the validation of small molecules and the identification assigned to them, allowing for more biological information to be gleaned from metabolomic analysis, besides simply identifying biomarkers.

Chapter II focused on utilizing metabolomic data in a multi-omic study. In it, four descriptors were assigned (retention time, drift time,  $m/z$ , and fragmentation) and used to more accurately assign identification to small molecules. These identified molecules combined with proteomic and genomic data to build a mechanism of action for cells exposed to cisplatin. The method described in Chapter II served as a proof of concept studied, and was then used in to

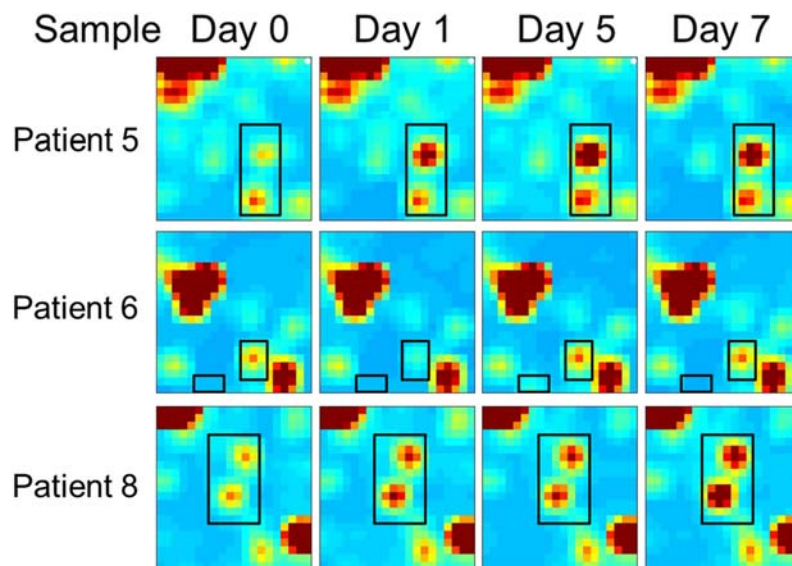


**Figure 5.1.** Displayed preliminary data of gut metabolites visualized as self-organizing maps (SOM). These are created using the GEDI software in which features that have similar patterns are grouped together and communal changes over time are observed. Boxed areas represent features that changed in relation to an individual over time.

develop a method for Chapters IV, focusing on probing the gut metabolome. These same descriptors are used to assign identification to features of interest, with the cross section of bile acids determined in Chapter III. The untargeted LC-IM-MS workflow designed in this dissertation is novel in that it is focusing on the metabolomic differences of the gut and the effects these changes will have on both the host and the microbiota community. The complex interactions between the bacteria that populate the gastrointestinal tract and the organism in which they reside can only be understood through a multi-omic approach, and this method provides the means in which the metabolomic arm can be accomplished. In this, little alteration to extracted small molecules is needed and a board range of biological classes are covered.

#### **5.4. References**

1. Gu Y., Zheng N., Jia W., Zhang W., Li H.; Metabolic and Gut Microbial Characterization of Obesity-Prone Mice under High-Fat Diet. *J. Proteome Res* **2019**, 18, 1703-1714.
2. Nusbaum D. J., Sun F., Ren J., Zhu Z., Ramsy N., Pervolarakis N., Kunde S., England W., Gao B.; Fiehn O., Michail S., Whiteson K.; Gut Microbial and Metabolomic Profiles after Fecal Microbiota Transplantation in Pediatric Ulcerative Colitis Patients. **2018**, 94, 9

## APPENDIX A

### REFERENCES OF ADAPTATION FOR CHAPTERS

- Chapter I. Caleb C. Morris, **James C. Poland**, Jody C. May, John A. McLean, “Fundamentals of Ion Mobility-Mass Spectrometry for the Analysis of Biomolecules,” Invited chapter for inclusion in “Methods in Molecular Biology,” Giuseppe Astarita and Giuseppe Paglia, Eds. *Springer Nature*, **2020**, chapter 1, 1-34
- Chapter II. Jeremy L. Norris, Melissa A. Farrow, Danielle B. Gutierrez, Lauren D. Palmer, Nicole Muszynski, Stacy D. Sherrod, James C. Pino, Jamie L. Allen, Jeffrey M. Spraggins, Alex L. R. Lubbock, Ashley Jordan, William Burns, **James C. Poland**, Carrie Romer, M. Lisa Manier, Yuan-wei Nei, Boone M. Prentice, Kristie L. Rose, Salisha Hill, Raf Van de Plas, Tina Tsui, Nathaniel M. Braman, M. Ray Keller, Stacey A. Rutherford, Nichole Lobdell, Carlos F. Lopez, D. Borden Lacy, John A. McLean, John P. Wikswo, Eric P. Skaar, and Richard M. Caprioli, “Integrated, High-Throughput, Multiomics Platform Enables Data-Driven Construction of Cellular Responses and Reveals Global Drug Mechanisms of Action,” *Journal of Proteome Research*, **2017**, 16 (3) 1364-1375
- Chapter III. **James C. Poland**, Katrina L. Leaptrot, Stacy D. Sherrod, C. Robb Flynn, and John A. McLean, “Collision Cross Section Conformational Analyses of Bile Acids via Ion Mobility-Mass Spectrometry,” Submitted to for *Journal of the American Society for Mass Spectrometry*, **2020**
- Chapter IV. **James C. Poland**, Alexandra C. Schrimpe-Rutledge, Stacy D. Sherrod, Charles Robb Flynn, and John A. McLean, “Utilizing Untargeted Ion Mobility-Mass Spectrometry to Profile Changes in the Gut Metabolome following Biliary Diversion Surgery,” *Analytical Chemistry*, **2019**, 22, 14417-14423

## APPENDIX B

### SUPPLEMENTARY MATERIAL FOR CHAPTER II

#### **B.1. Supplemental Materials for Structural Understanding of Bile Acids through Collision Cross Section Measurements**

**Table B.1.** Bile acid CCS values measured in this work. [M-H]<sup>-</sup> CCS values (reported with standard deviation from n=3 measurements taken on 3 separate days) were measured in negative ionization mode while all other adducts were measured in positive ionization mode

Molecule	Molecular Formula	Molecule Weight (Da)	[M-H] <sup>-</sup> A	[M+Na] <sup>+</sup> A	[M+H-H <sub>2</sub> O] <sup>+</sup> A	[M+H-2H <sub>2</sub> O] <sup>+</sup> A	[M+H-H <sub>2</sub> SO <sub>4</sub> ] <sup>+</sup> A	[M+H-H <sub>2</sub> SO <sub>4</sub> -H <sub>2</sub> O] <sup>+</sup> A	[M+H-H <sub>2</sub> SO <sub>4</sub> -2H <sub>2</sub> O] <sup>+</sup> A	[M+H-2(H <sub>2</sub> SO <sub>4</sub> )] <sup>+</sup> A
12-dehydrocholic acid	C24H38O5	406.27	204.0±0.3	204.6±0.3	191.2±0.3	186.6±0.0	--	--	--	--
3,6-diketocholic acid	C24H36O4	388.26	200.8±0.3	218.8±0.3	188.8±0.3	184.7±0.3	--	--	--	--
3,7,12-tri-betacholanic acid	C24H34O5	402.24	209.6±0.3	201.2±0.2	188.5±0.2	185.3±0.3	--	--	--	--
3,7-dioxy-5β-choanoic acid	C24H36O4	388.26	206.0±0.1	201.8±0.3	185.0±0.2	182.2±0.1	--	--	--	--
3-oxo-12α-cholic acid	C24H38O4	390.28	200.6±0.3	192.1±0.2	191.5±0.3	182.1±0.3	--	--	--	--
3-oxocholic acid	C24H38O5	406.27	205.4±0.1	201.5±0.1	186.2±0.2	182.5±0.2	--	--	--	--
3β, 7α, dihydroxy-5β-cholanic acid	C24H39DO4	406.27	202.6±0.2	210.0±0.2	--	186.5±0.0	--	--	--	--
7,12-dioxolithocholic acid	C24H36O5	404.26	204.1±0.4	204.8±0.1	194.9±0.3	185.5±0.2	--	--	--	--
7-ketodeoxycholic acid	C24H38O5	406.27	204.0±0.3	204.5±0.2	204.8±0.3	186.6±0.2	--	--	--	--
7α, 12α, dihydroxy-5β-cholanic acid	C24H40O4	392.30	200.5±0.1	203.7±0.2	--	186.4±0.1	--	--	--	--
Apocholeic acid	C24H38O4	390.28	202.9±0.3	202.4±0.2	190.7±0.2	184.5±0.3	--	--	--	--
α-Muricholic acid	C24H40O5	408.29	203.7±0.2	222.8±0.1	--	187.4±0.2	--	--	--	--
β-Muricholic acid	C24H40O5	408.29	200.6±0.2	222.6±0.1	201.3±0.2	192.4±0.1	--	--	--	--
Chenodeoxycholic acid	C24H40O4	392.29	202.2±0.1	202.8±0.2	--	186.9±0.2	--	--	--	--
Dehydrodeoxycholic acid	C24H36O4	388.26	209.5±0.4	197.5±0.1	188.0±0.2	182.2±0.2	--	--	--	--
Dehydrolithocholic acid	C24H38O3	373.28	205.4±0.1	201.4±0.1	--	--	--	--	--	--
Hyocholic acid	C24H40O5	408.29	202.6±0.1	218.4±0.2	199.6	203.3±0.1	--	--	--	--
Hyodeoxycholic acid	C24H40O4	392.29	199.1±0.2	219.1±0.2	--	186.8±0.1	--	--	--	--
Lithocholic acid	C24H40O3	376.30	198.8±0.4	214.8±0.3	191.6±0.3	--	--	--	--	--
Murideoxycholic acid	C24H40O4	392.29	200.1±0.3	222.5±0.3	--	--	--	--	--	--
Glycocholic acid	C26H43NO6	465.31	202.1±0.2	202.8±0.1	197.4±0.2	196.9±0.2	--	--	--	--
Glycodeoxycholic acid	C26H43NO5	449.31	199.7±0.1	207.6±0.4	207.2±0.2	204.2±0.2	--	--	--	--
Glycolithocholic acid	C26H43NO4	433.32	199.4±0.1	211.6±0.2	209.2±0.2	--	--	--	--	--
Glycoursodeoxycholic acid	C26H43NO5	449.31	201.0±0.2	211.1±0.3	--	202.8±0.5	--	--	--	--
Taurochenodeoxycholic acid	C26H45NO6S	499.30	207.1±0.1	--	--	218.7±0.1	--	--	--	--
Taurocholic acid	C26H45NO7S	515.29	207.4±0.2	211.1±0.2	204.6±0.2	200.7±0.1	--	--	--	--
Taurohyocholic acid	C26H45NO7S	515.29	208.3±0.2	213.3±0.2	206.2±0.1	206.7±0.3	--	--	--	--
Taurohyodeoxycholic acid	C26H45NO6S	499.30	206.2±0.1	206.7±0.2	204.5±0.1	204.5±0.2	--	--	--	--
Tauroolithocholic acid	C26H45NO5S	483.30	206.3±0.1	214.2±0.3	219.3±0.3	--	--	--	--	--
Tauroursodeoxycholic acid	C26H45NO6S	499.30	207.5±0.1	216.4±0.3	--	202.6±0.2	--	--	--	--
Tauro-α-muricholic acid	C26H45NO7S	515.29	209.3±0.1	213.1±0.4	--	201.2±0.3	--	--	--	--
Tauro-β-muricholic acid	C26H45NO7S	515.29	209.5±0.2	218.3±0.3	203.2±0.2	203.3±0.3	--	--	--	--
Tauro-ω-muricholic acid	C26H45NO7S	515.29	209.3±0.0.1	221.9±3.1	209.2±0.2	201.9±0.2	--	--	--	--
Ursodeoxycholic acid	C24H40O4	392.29	198.1±0.2	--	--	186.8±0.1	--	--	--	--



Molecule	Molecular Formula	Molecule Weight (Da)	[M-H] <sup>-</sup> A	[M+Na] <sup>+</sup> A	[M+H-H <sub>2</sub> O] <sup>+</sup> A	[M+H-2H <sub>2</sub> O] <sup>+</sup> A	[M+H-H <sub>2</sub> SO <sub>4</sub> ] <sup>+</sup> A	[M+H-H <sub>2</sub> SO <sub>4</sub> -H <sub>2</sub> O] <sup>+</sup> A	[M+H-H <sub>2</sub> SO <sub>4</sub> -2H <sub>2</sub> O] <sup>+</sup> A	[M+H-2(H <sub>2</sub> SO <sub>4</sub> )] <sup>+</sup> A
Chenodeoxycholic acid 3-sulfate	C24H40O7S	472.25	204.5±0.1	--	--	--	--	186.7±0.2	--	--
Chenodeoxycholic acid 7-sulfate	C24H40O7S	472.25	214.3±0.3	--	--	--	--	186.6±0.1	--	--
Cholic acid 12-sulfate	C24H40O8S	488.24	207.7±0.3	--	--	--	--	190.3±0.1	186.4±0.1	--
Cholic acid 3-sulfate	C24H40O8S	488.244	208.6±0.3	--	--	--	--	189.6±0.2	186.1±0.2	--
Deoxycholic acid 17-sulfate	C24H40O7S	472.25	206.0±0.2	--	--	--	--	187.4±0.2	--	--
Deoxycholic acid 3-sulfate	C24H40O7S	472.25	207.9±0.3	--	--	--	--	187.4±0.2	--	--
Lithocholic acid 3-sulfate	C24H40O6S	456.25	210.8±0.2	--	--	--	191.6±0.1	--	--	--
Glycocholic acid 12-sulfate	C26H43NO9S	545.27	212.4±0.0	207.8±0.2	--	--	--	204.5±0.2	196.9±0.1	--
Glycocholic acid 3-sulfate	C26H43NO9S	545.27	215.9±0.3	--	--	--	211.4±0.2	200.6±0.2	196.6±0.2	--
Glycochenodeoxycholic acid 3-sulfate	C26H43NO8S	529.27	215.2±0.3	--	--	--	203.6±0.3	201.9±0.3	--	--
Glycodeoxycholic acid 12-sulfate	C26H43NO8S	529.27	212.9±0.2	--	--	--	202.8±1.2	204.5±0.5	--	--
Glycolithocholic acid 3-sulfate	C26H43NO7S	513.28	216.2±0.3	--	--	--	209.0±0.1	--	--	--
Taurochenodeoxycholic acid 3-sulfate	C26H45NO9S2	579.25	215.6±0.3	--	--	--	--	202.5±0.3	--	--
Taurolithocholic acid 3-sulfate	C26H45NO8S2	563.26	214.7±0.3	219.5±0.2	--	--	219.4±0.1	--	--	--
Chenodeoxycholic acid, disulfate	C24H40O10S2	552.21	224.7±0.1	--	--	--	--	--	--	186.9±0.1
Glycochenodeoxycholic acid disulfate	C26H43NO11S2	609.23	223.7±0.3	--	--	--	--	--	--	206.5±1.1

## APPENDIX C

### SUPPLEMENTARY MATERIAL FOR CHAPTER III

#### C.1. Supplemental Materials for Utilizing Untargeted Ion Mobility-Mass Spectrometry to Profile Changes in the Gut Metabolome following Biliary Diversion Surgery

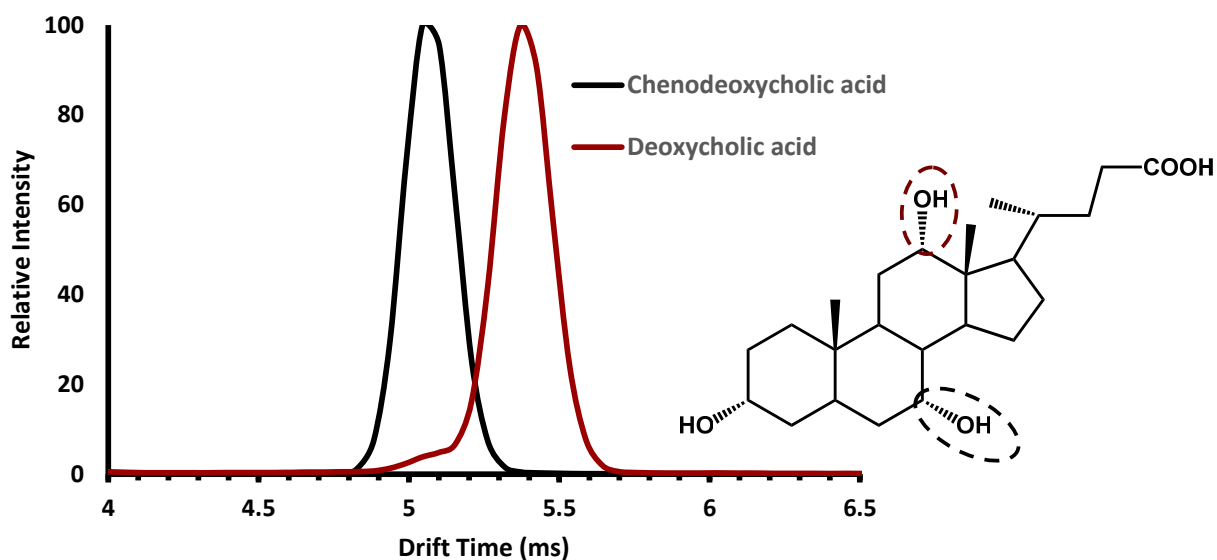


**Figure C.1.** Arrival time distribution for chenodeoxycholic acid and deoxycholic acid in negative ion mode. This demonstrates the ability of ion mobility to separate this pair of isomeric bile acids. The structure is displayed to illustrate the location of the hydroxyl group that differentiates chenodeoxycholic acid and deoxycholic acid.

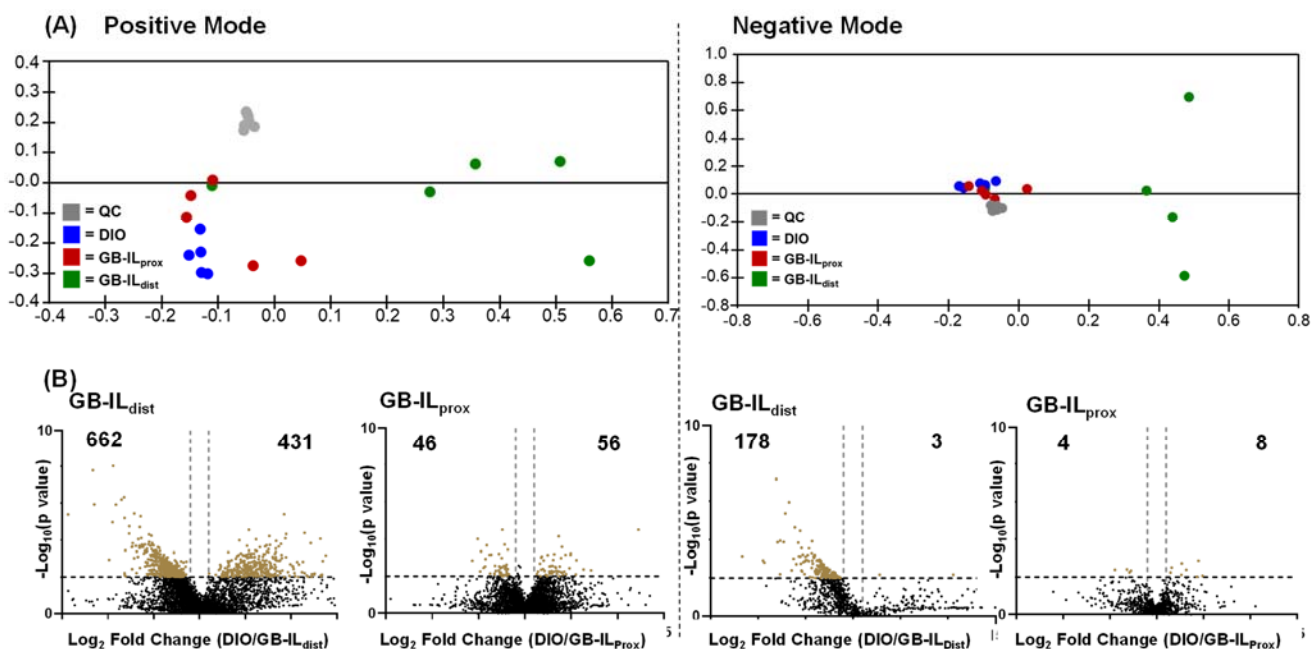


**Figure C.2.** (A) The unsupervised principal component analysis (PCA) displaying biological replicates of the fecal sample of each sample group. Each point represents one biological replicate while color represent a complete sample group. The Sham and GB-IL<sub>prox</sub> samples show close similarities by clustering near each other, while GB-IL<sub>dist</sub> samples segregate completely. (B) Pair-wise comparison is performed between the diet induced obese mice (DIO) and surgical GB-IL<sub>dist</sub> or GB-IL<sub>prox</sub> mice to create volcano plots from the untargeted metabolomics data. Compounds of interest are prioritized using significance criteria ( $p\text{-value} \leq 0.01$  and fold change  $\geq 2$ ), visualized in the upper, outer corners of the volcano plots.

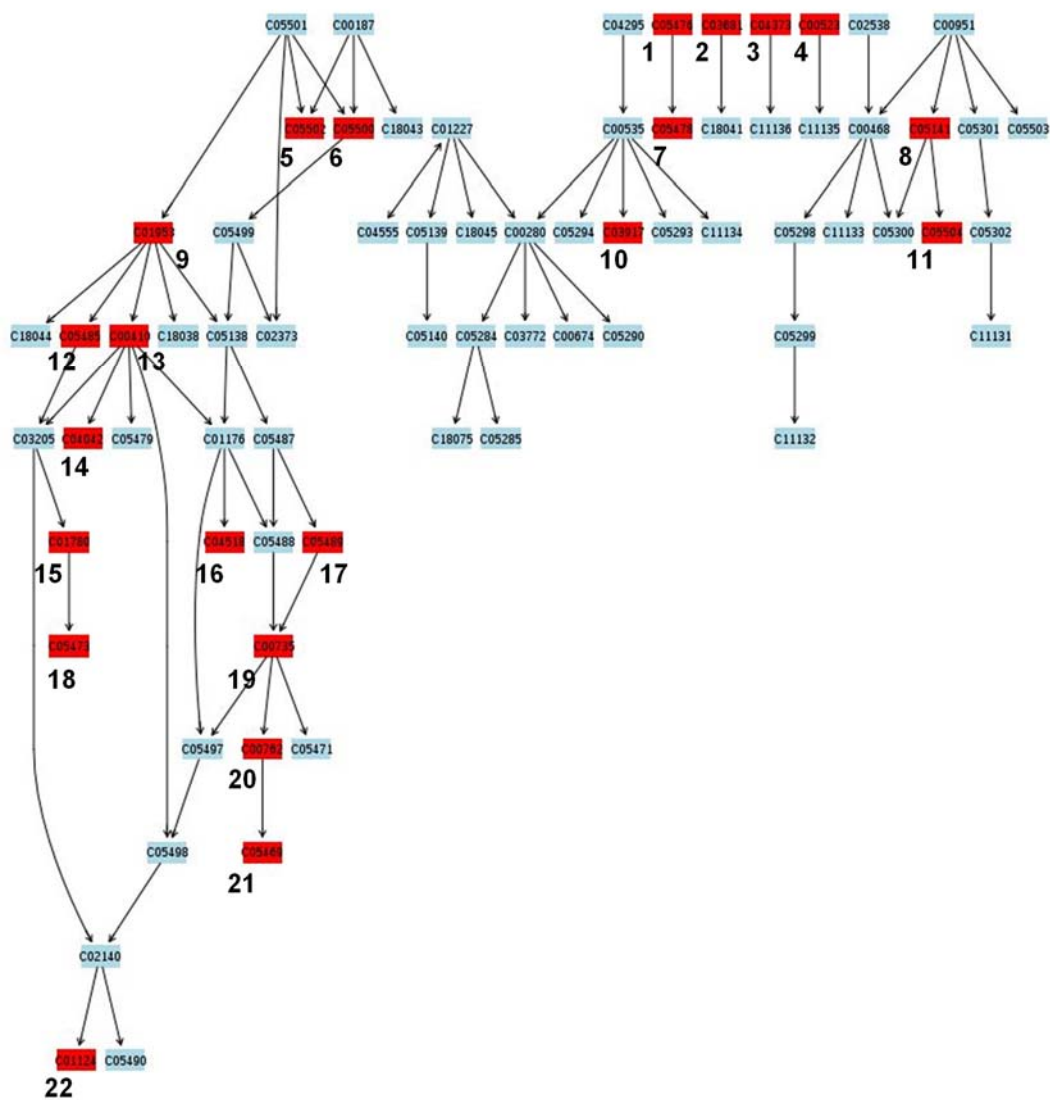


**Figure C.3.** Overview of the steroid hormone biosynthesis pathway. Metabolites shaded red are tentatively annotated as a molecule of interest. Significant metabolites in this pathway include: 1. Tetrayhdocorticosterone; 2. 5a-Pregnane-3,20-dione; 3. Etiocolanolone; 4. Androsterone; 5. 22b-Hydroxycholesterol; 6. 20a-Hydroxycholesterol; 7. 3a,21-Dihydroxy-5b-pregnane-11,20-dione; 8. Estriol; 9. Pregnenolone; 10. Dihydrotestosterone; 11. 16-Glucuronide-estriol; 12. 21-Hydroxypregnenolone; 13. Progesterone; 14. 20a-Dihydroprogesterone; 15. Aldosterone; 16. 17a, 20a-Dihydroxypregn-4-en-3-one; 17. 11b,17a,21-Trihydroxypreg-nenolone; 18. 11b,21-Dihydroxy-3,20-oxo-5b-pregnan-18-al; 19. Cortisol; 20. Cortisone; 21. 17a,21-Dihydroxy-5b-pregnane-3,11,20-trione; 22. 18-Hydroxycorticosterone.

**Table C.1.** Supplemental table showing name, m/z, retention time, adduct type, travelling wave collision cross section, and relative standard deviation of bile acid standards.

Bile Acid	m/z	R.T. (min)	Adduct	TWIM CCS $\text{\AA}^2$	RSD
Ursodeoxycholic acid	391.27	22.49	[M-H] <sup>-</sup>	209.02	2.07
Hyodeoxycholic acid	391.27	23.29	[M-H] <sup>-</sup>	210.93	1.97
Chenodeoxycholic acid	391.27	24.76	[M-H] <sup>-</sup>	209.78	1.98
Deoxycholic acid*	391.27	24.76	[M-H] <sup>-</sup>	205.18	2.05
$\alpha$ - muricholic acid	407.28	14.19	[M-H] <sup>-</sup>	211.35	1.92
$\beta$ - muricholic acid	407.28	15.10	[M-H] <sup>-</sup>	210.92	1.91
Hyocholic acid	407.28	19.56	[M-H] <sup>-</sup>	210.02	1.09
Cholic acid	407.28	22.23	[M-H] <sup>-</sup>	203.78	2.71
Glycourosodeoxycholic acid	448.29	16.72	[M-H] <sup>-</sup>	201.29	0.42
Glycodeoxycholic acid	448.29	23.80	[M-H] <sup>-</sup>	199.79	0.25
Tauroursodeoxycholic acid	498.27	19.08	[M-H] <sup>-</sup>	208.83	1.89
Taurohyodeoxycholic acid	498.27	19.89	[M-H] <sup>-</sup>	208.62	0.38
Taurodeoxycholic acid	498.27	23.93	[M-H] <sup>-</sup>	205.7	0.78
Tauro- $\omega$ -muricholic acid	514.27	10.50	[M-H] <sup>-</sup>	212.74	0.58
Tauro- $\alpha$ -muricholic acid	514.27	11.34	[M-H] <sup>-</sup>	210.36	1.34
Tauro- $\beta$ -muricholic acid	514.27	12.23	[M-H] <sup>-</sup>	210.39	1.96
Taurohyocholic acid	514.27	16.06	[M-H] <sup>-</sup>	209.44	0.24
Taurocholic acid	514.27	20.52	[M-H] <sup>-</sup>	208.67	2.33

**Table C.2.** Truncated tentative annotations of the top 30 most abundant compounds isolated from fecal metabolite extractions. Annotations are made based on accurate mass and fragmentation, compared to online databases

Compound	Description	Formula	Adducts
5.21_652.6629m/z	N-Tetracosanoylsphinganine	C42H85NO3	M+H
5.58_589.3036m/z	Urobilin	C33H40N4O6	M+H
6.26_389.2701m/z	3-Oxocholeic acid	C24H38O5	M+H-H2O
6.56_408.2892n	Cholic acid	C24H40O5	M+H-2H2O, M+H-H2O, M+Na, 2M+Na
7.16_389.2703m/z	3-Oxocholeic acid	C24H38O5	M+H-H2O
7.27_408.2892n	Cholic acid	C24H40O5	M+H-2H2O, M+H-H2O, M+Na
6.40_390.2787n	12-Ketodeoxycholic acid	C24H38O4	M+H-2H2O, M+K, M+Na, M+H-H2O
6.78_406.2728n	3-Oxocholeic acid	C24H38O5	M+H-2H2O, M+H
1.98_402.2476m/z	Gln-Val-Arg	C16H31N7O5	M+H
5.48_507.2741m/z	1-Hexadecanoyl-sn-glycero-3-phospho-(1'-sn-glycerol)	C22H45O9P	M+Na
18.20_305.2489m/z	15-OxoEDE	C20H34O3	M+H-H2O
7.28_357.2782m/z	Docosahexaenoic acid ethyl ester	C24H36O2	M+H
5.74_277.2178m/z	8,10-Octadecadiynoic acid	C18H28O2	M+H
1.81_434.2256m/z	1-Tridecanoyl-sn-glycero-3-phosphoethanolamine	C18H38NO7P	M+Na
7.65_432.3242n	Cholest-5-en-26-oic acid, 3 $\beta$ ,7 $\alpha$ -hydroxy	C27H44O4	M+H-H2O, M+Na, M+H-2H2O
1.98_271.1668n	Pro-Arg	C11H21N5O3	M+H-H2O, M+H
6.50_399.3270m/z	7 $\alpha$ ,24(S)-Dihydroxy-4-cholesten-3-one	C27H44O3	M+H-H2O
1.98_175.1199m/z	DL-Arginine	C6H14N4O2	M+H
6.45_397.3105m/z	Cholest-5-en-26-oic acid, 3 $\beta$ ,7 $\alpha$ -hydroxy	C27H44O4	M+H-2H2O
4.75_642.3849m/z	His-Leu-Leu-Val-Phe-OME	C33H51N7O6	M+H
6.59_430.3173m/z	1-(9Z-Octadecenyl)-sn-glycero-3-phosphoethanolamine	C23H48NO6P	M+H-2H2O
1.98_288.2051m/z	Ile-Arg	C12H25N5O3	M+H
6.80_390.2776n	12-Ketodeoxycholic acid	C24H38O4	M+H-H2O, M+H, M+K, M+H-2H2O
1.98_473.2835m/z	Glycolic acid hexaethoxylate 4-tert-butylphenyl ether	C24H40O9	M+H
6.97_442.3522m/z	Oleyloxyethylphosphorylcholine	C25H52NO5P	M+H-2H2O
6.50_555.3102m/z	2-O-(beta-D-galactopyranosyl-(1->6)-beta-D-galactopyranosyl) 2S-hydroxytridecanoic acid	C31H48O6	M+H
6.42_235.1710m/z	trans-delta-2-11-Methyl dodecenoic Acid	C13H24O2	M+Na
7.56_591.3187m/z	Deoxycholic acid 3-glucuronide	C15H24O5	M+Na
1.98_260.1987m/z	Ile-Lys	C12H25N3O3	M+H
1.98_389.2430m/z	Palmitoleoyl 3-carbacyclic Phosphatidic Acid	C10H17NO2	M+H

Compound	Description	Formula	Adducts	Anova (p)	Fold Change.	MSMS
4.76_424.2346m/z	8-{4-[1-Oxido-4-(2-pyrimidinyl)-1-piperazinyl]butyl}-8-azaspiro[4.5]decane-7,9-dione 8-{4-[4-(5-Hydroxy-2-pyrimidinyl)-1-piperazinyl]butyl}-8-azaspiro[4.5]decane-7,9-dione 2-Hydroxy-8-{4-[4-(2-pyrimidinyl)-1-piperazinyl]butyl}-8-azaspiro[4.5]decane-7,9-dione 6-Hydroxy-8-{4-[4-(2-pyrimidinyl)-1-piperazinyl]butyl}-8-azaspiro[4.5]decane-7,9-dione	C21H31N5O3	M+Na	7.10E-05	+ 12.69	yes
7.30_557.3256m/z	phe-ile, leu-phe ile-phe phe-leu	C15H22N2O3	2M+H	1.98E-04	+ 4.58	Yes*
1.58_492.2346m/z	Trp-His-Lys His-Trp-Lys	C23H31N7O4	M+Na	3.71E-04	+ 3.57	Yes*
5.98_862.6757m/z	(6Z,9Z,12Z,15Z,25R)-31-Amino-28-hydroxy-28-oxido-22-oxo-23,27,29-trioxa-28lambda~5~-phosphahentriaconta-6,9,12,15-tetraen-25-yl tetracosanoate (2R)-3-[[2-Aminoethoxy](hydroxy)phosphoryl]oxy}-2-[(7Z,10Z,13Z,16Z)-7,10,13,16-docosatetraenoxy]propyl tetracosanoate	C51H94NO8P	M+H-H2O	3.99E-04	+ Infinity	Yes
7.19_444.3315m/z	Glucosylsphingosine Galactosylsphingosine D-Glucosyl-.beta.1-1'-D-erythro-sphingosine	C24H47NO7	M+H-H2O	7.04E-04	+ 14.02	Yes
4.85_374.2065m/z	8,8'-Bis[(2E)-3,7-dimethyl-2,6-octadien-1-yl]-7,7'-dimethoxy-3,3'-dimethyl-9H,9'H-1,1'-bicarbazole-2,2'-diol	C48H56N2O4	M+H+Na	7.24E-04	- 5.57	Yes*
4.05_416.7422m/z	(3Z,6Z,9Z,12Z,15Z,23R)-29-Amino-26-hydroxy-26-oxido-20-oxo-21,25,27-trioxa-26lambda~5~-phosphanonacosa-3,6,9,12,15-pentaen-23-yl (4Z,7Z,10Z,13Z,16Z,19Z)-4,7,10,13,16,19-docosahexaenoate; (2R)-3-[[2-Aminoethoxy](hydroxy)phosphoryl]oxy}-2-[(5Z,8Z,11Z,14Z,17Z)-5,8,11,14,17-icosapentaenoxy]propyl (4Z,7Z,10Z,13Z,16Z,19Z)-4,7,10,13,16,19-docosahexaenoate	C47H72NO8P	M+H+Na	1.37E-03	- 47.63	Yes*
6.71_529.2944m/z	(2Z)-N-(4-Aminobutyl)-3-(4-hydroxy-3-methoxyphenyl)acrylamide val-phe	C14H20N2O3	2M+H	2.42E-03	+ 3.95	Yes
6.10_441.2337m/z	Retinoyl-β-glucuronide	C26H36O8	M+H-2H2O	2.73E-03	+ 4.76	Yes
7.01_381.1586n	3,7-Dimethoxy-6-hydroxy-10-oxyphenanthroindolizidine	C22H23NO5	M+H-2H2O, M+Na, M+H-H2O	2.75E-03	+ 9.34	Yes*
7.44_440.3366m/z	Di-n-dodecyl phosphite	C24H50O3P	M+Na	2.90E-03	+ 6.78	Yes*
7.59_559.3418m/z	1,2-Didodecanoyl-sn-glycero-3-phosphate	C27H53O8P	M+Na	3.24E-03	+ 4.11	Yes*
6.53_829.7927m/z	1-(Octadecyloxy)-3-(tetradecanoyloxy)-2-propanyl (11Z)-11-icosenoate 2-(Octadecyloxy)-3-(tetradecanoyloxy)propyl (11Z)-11-icosenoate 1-(Octadecyloxy)-3-(palmitoyloxy)-2-propanyl (11Z)-11-octadecenoate 1-(Octadecyloxy)-3-(palmitoyloxy)-2-propanyl (9Z)-9-octadecenoate 3-(Octadecyloxy)-2-(palmitoyloxy)propyl (11Z)-11-octadecenoate 3-(Octadecyloxy)-2-[(9Z)-9-tetradecenoyloxy]propyl icosanoate	C55H106O5	M+H-H2O	3.46E-03	- 10.27	Yes*
22.53_365.1971m/z	(1S,2S)-1-(4-Methoxyphenyl)-1,2-propanediol; 7a-Hydroxy-3,6-dimethyl-5,6,7,7a-tetrahydro-1-benzofuran-2(4H)-one 2-Ethoxy-4-(methoxymethyl)phenol Ethyl vanillyl ether 2-Furylmethyl 3-methylbutanoate 2,6-Dimethoxy-4-ethylphenol 3-Methylbutyl 2-furoate	C10H14O3	2M+H	3.69E-03	+ 4.44	Yes*
6.71_553.2949m/z	N-(3-Aminopropyl)-3-(3,4-dihydroxyphenyl)-N-{4-[(3-{3-(3,4-dihydroxyphenyl)propanoyl}amino)propyl]amino}butyl} propanamide N-{4-[(3-Aminopropyl)amino]butyl}-3-(3,4-dihydroxyphenyl)-N-(3-{3-(3,4-dihydroxyphenyl)propanoyl}amino)propyl}propanamide N,N'-1,4-Butanediylobis[N-(3-aminopropyl)-3-(3,4-dihydroxyphenyl)propanamide] N,N'-[1,4-Butanediylobis(imino-3,1-propanediyl)]bis[3-(3,4-dihydroxyphenyl)propanamide]	C28H42N4O6	M+Na	4.00E-03	+ 4.34	Yes
1.53_309.1059n	N-Acetyl-alpha-neuraminic acid 4-Carboxy-2-(tyrosylamino)butanoate Sialic acid Neu5Ac 5-Oxidanydil-5-oxidanylidenorvalyltyrosine	C11H19NO9	M+Na, M+K	4.08E-03	- 3.89	Yes
6.67_428.2995m/z	N-(1,3-Dihydroxypropan-2-yl)-9S,11R,15S-trihydroxy-5Z,13E-prostadienoyl amine	C23H41NO6	M+H	5.03E-03	+ 8.68	Yes*

5.11_494.2656m/z	N-[4-(Hydroxymethyl)-3-{[4-(3-pyridinyl)-2-pyrimidinyl]amino}-1,5-cyclohexadien-1-yl]-4-[(4-methyl-1-piperazinyl)methyl]benzamide	C29H33N7O2	M+H-H2O	5.10E-03	- 10.47	Yes
20.12_306.2559n	Linolenic acid ethyl ester	C20H34O2	M+H-2H2O, M+K	5.43E-03	+ 3.89	Yes*
6.97_555.3108m/z	2,3-Dihydroxy-29-methoxy-29-oxoolean-12-en-28-oic acid	C31H48O6	M+K	6.09E-03	+ 6.12	Yes
8.36_537.3181m/z	ile-his	C12H20N4O3	2M+H	6.26E-03	+ 6.53	Yes*
21.23_439.3560m/z	3,22-Dihydroxyolean-12-en-23-al	C30H48O3	M+H-H2O	7.04E-03	+ 9.63	Yes
4.71_705.3793m/z	1-(4-Hydroxy-3-methoxyphenyl)-3,5-diacetoxyoctane	C19H28O6	2M+H	7.54E-03	+ 2.48	Yes*
6.67_471.3167n	(.+/-)-Terfenadine	C32H41NO2	M+H, M+K	7.75E-03	+ 3.31	Yes*
8.97_517.3179n	(2R)-2-Hydroxy-3-[(6Z,9Z,12Z)-6,9,12-octadecatrienoxy]propyl 2-(trimethylammonio)ethyl phosphate	C26H48NO7P	M+H, M+Na	8.25E-03	+ 4.11	Yes
8.29_615.2436m/z	1-(5,6,7a,8-Tetrahydro-7H-[1,3]benzodioxolo[6,5,4-de]benzo[g]quinolin-7-yl)ethanone	C19H17NO3	2M+H	9.57E-03	+ 5.53	Yes*

**Table C.3.** Tentative annotations of significant compounds in a pairwise comparison of DIO and GB-ILprox in positive mode. Annotations are made based on accurate mass and fragmentation and compared to online databases. Features with positive fold changes are higher in the control, while negative fold changes denotes features that are higher in the experimental group. Infinity signifies that the feature is detectable in one sample group and undetectable in the other. The MSMS column indicates if the molecule did or did not have fragmentation spectra associated with it (Yes/No). Yes\* denotation means some fragments are consistent with, but not indicative of, metabolite identity.



**Table C.4.** Tentative annotation table of significant compounds in a pairwise comparison of DIO and GB-ILprox in negative mode. Annotations are made based on accurate mass and fragmentation and compared to online databases. Features with positive fold changes are higher in the control, while negative fold changes denotes features that are higher in the experimental group. Infinity signifies that the feature is detectable in one sample group and undetectable in the other. The MSMS column indicates if the molecule did or did not have fragmentation spectra associated with it (Yes/No). Yes\* denotation means some fragments are consistent with, but not indicative of, metabolite identity.

Compound	Description	Formula	Adducts	Anova (p)	Fold Change	MSMS
4.24_459.1722m/z	Asp-pro 1-[4-(1,2,3,4-Tetrahydroxybutyl)-1H-imidazol-2-yl]ethanone N-(1-Carboxycyclopropyl)glutamine 1-(3-Amino-3-carboxypropyl)-5-oxoproline	C9H14N2O5	2M-H	4.11E-03	- 8.88	No
1.96_492.2463m/z	N-[4-(Hydroxymethyl)-3-{{4-(3-pyridinyl)-2-pyrimidinyl}amino}-1,5-cyclohexadien-1-yl]-4-[(4-methyl-1-piperazinyl)methyl]benzamide	C29H33N7O2	M-H2O-H	5.52E-03	+ 7.51	No
7.15_421.2593m/z	CerP(d18:1/2:0) (2S,3R,6aS,12bS,12cS,14aS)-2-(2-Hydroxy-2-propanyl)-12b,12c-dimethyl-3,4b,5,6,6a,7,12,12b,12c,13,14,14a-dodecahydro-2H-chromeno[5',6':6,7]indeno[1,2-b]indol-3-ol	C20H40NO6P	M-	5.65E-03	- 2.77	Yes*
23.27_243.1963m/z	a-Hydroxymyristic acid 3-[(2-Isopropyl-5-methylcyclohexyl)oxy]-2-methyl-1,2-propanediol 2-Hydroxymyristic acid (3R)-3-hydroxymyristic acid Ethyl 3-hydroxydodecanoate	C14H28O3	M-H	8.46E-03	- 29.56	Yes
22.83_287.2226m/z	10,16-Dihydroxyhexadecanoic acid	C16H32O4	M-H	9.49E-03	- 19.64	Yes

Compound	Description	Formula	Adducts	Anova (p)	Fold Change	MSMS
5.68_738.3823m/z	Tris(4-tert-butyl-3-hydroxy-2,6-dimethylbenzyl) isocyanurate	C42H57N3O6	M+K	3.24E-09	+ Infinity	Yes*
6.81_773.5196m/z	(2R)-3-({[(2S)-2,3-Dihydroxypropoxy](hydroxy)phosphoryl]oxy)-2-(palmitoyloxy)propyl stearate (19R,25S)-22,25,26-Trihydroxy-22-oxido-16-oxo-17,21,23-trioxa-22lambda~5~-phosphahexacosan-19-yl stearate	C40H79O10P	M+Na	1.67E-07	+ Infinity	Yes*
6.32_637.2777m/z	Asn-Trp trp-asn tyr-his his-tyr	C15H18N4O4	2M+H	3.68E-07	+ Infinity	Yes*
5.88_594.4187m/z	1,2-Diundecanoyl-sn-glycero-3-phosphocholine 1-Dodecanoyl-2-tridecanoyl-sn-glycero-3-phosphoethanolamine	C30H60NO8P	M+H	4.59E-07	+ 297.79	Yes*
7.11_654.3666m/z	6-{2-[(1E)-6-Amino-3-(3-amino-3-carboxypropyl)-6-carboxy-1-hexen-1-yl]-3,5-bis(3-amino-3-carboxypropyl)-1-pyridiniumyl}norleucine	C30H49N6O10+	M+H	6.35E-07	+ Infinity	Yes*
5.35_309.1815m/z	8-Hydroxy-5-{2-hydroxy-3-[(2-methyl-2-propanyl)amino]propoxy}-3,4-dihydro-2(1H)-quinolinone 3-Oxohexadecanoic acid 8-Oxohexadecanoic acid 9-Oxohexadecanoic acid 11-Oxohexadecanoic acid	C16H24N2O4	M+H	1.17E-06	+ 560.31	Yes*
8.30_325.2531m/z	3-[(8E)-8-Pentadecen-1-yl]phenol	C21H34O	M+Na	4.96E-06	+ 85.71	Yes
5.95_625.3204m/z	4-[(6,7-Dimethoxy-2-methyl-1,2,3,4-tetrahydro-1-isoquinolinyl)methyl]-2-[[6-methoxy-1-(4-methoxybenzyl)-2-methyl-1,2,3,4-tetrahydro-7-isoquinolinyl]oxy]phenol	C38H44N2O6	M+H	6.17E-06	+ 293.04	Yes*
11.31_570.3555m/z	(2R)-2-Hydroxy-3-[(11Z,14Z)-11,14-icosadienoyloxy]propyl 2-(trimethylammonio)ethyl phosphate	C28H54NO7P	M+Na	9.37E-06	- Infinity	Yes
10.95_515.4507m/z	2-[(5Z,8Z,11Z)-5,8,11-Icosatrienoyloxy]-3-[(9Z,12Z)-9,12-nonadecadienoyloxy]propyl tetracosanoate 2-[(5Z,8Z,11Z)-5,8,11-Icosatrienoyloxy]-3-[(11Z,14Z)-11,14-nonadecadienoyloxy]propyl tetracosanoate 3-[(5Z,8Z,11Z)-5,8,11-Icosatrienoyloxy]-2-[(9Z,12Z)-9,12-nonadecadienoyloxy]propyl tetracosanoate 3-[(8Z,11Z,14Z)-8,11,14-Icosatrienoyloxy]-2-[(9Z,12Z)-9,12-nonadecadienoyloxy]propyl tetracosanoate 3-[(5Z,8Z,11Z)-5,8,11-Icosatrienoyloxy]-2-[(11Z,14Z)-11,14-nonadecadienoyloxy]propyl tetracosanoate 3-[(13Z)-13-Docosenoxyloxy]-2-[(9Z,12Z)-9,12-nonadecadienoyloxy]propyl (13Z,16Z)-13,16-docosadienoate 1-[(13Z)-13-Docosenoxyloxy]-3-[(9Z,12Z)-9,12-nonadecadienoyloxy]-2-propanyl (13Z,16Z)-13,16-docosadienoate	C66H118O6	M+H+Na	1.20E-05	- Infinity	Yes*
4.78_158.1176m/z	Threonine, butyl ester; Homoserine, butyl ester	C8H15NO2	M+H-H2O	1.89E-05	+ 91.62	No
6.24_707.4361m/z	(8β)-N-(1-Hydroxy-2-butanyl)-1,6-dimethyl-9,10-didehydroergoline-8-carboxamide	C21H27N3O2	2M+H	2.64E-05	+ Infinity	Yes*
18.59_291.2687m/z	Dihomolinoleic acid (20:2(n-6)) Eicosadienoic Acid	C20H36O2	M+H-H2O	3.53E-05	- Infinity	Yes
18.17_543.4762m/z	(2S)-1-Hydroxy-3-(pentadecanoyloxy)-2-propanyl (9Z,12Z)-9,12-octadecadienoate	C36H66O5	M+H-2H2O	4.59E-05	- 706.28	Yes*
5.93_195.0902n	Acetyl-L-carnitine 2-Methyl-1,2,3,4-tetrahydro-4,6,7-isoquinolinetriol 3-Hydroxy-2-phenylpropyl carbamate Metirosine Methyl tyrosinate N-[2-(3,4-Dihydroxyphenyl)ethyl]acetamide Isopentenyladenine	C10H13NO3	M+H-H2O, M+H	4.86E-05	+ 45.45	Yes*
5.93_168.1023m/z	(2R,3S)-3-Hydroxy-8-methyl-8-azabicyclo[3.2.1]octane-2-carboxylic acid (2S,3S)-3-Hydroxy-8-methyl-8-azabicyclo[3.2.1]octane-2-carboxylic acid; Ecgonine 2,2-Bis(hydroxymethyl)-3-quinclidinone	C9H15NO3	M+H-H2O	5.70E-05	+ 38.21	Yes*
18.29_331.2637m/z	Anacardic Acid 16-Hydroxykauran-18-yl acetate Carbocyclic thromboxane A2	C22H36O3	M+H-H2O	5.91E-05	- 198.13	Yes

	Tridecyl 3-(4-hydroxyphenyl)propanoate					
7.93_410.2580m/z	(19R,25S)-22,25,26-Trihydroxy-22-oxido-16-oxo-17,21,23-trioxa-22lambda~5~-phosphahexacosan-19-yl (4Z,7Z,10Z,13Z,16Z)-4,7,10,13,16-docosapentaenoate (19R,25S)-22,25,26-Trihydroxy-22-oxido-16-oxo-17,21,23-trioxa-22lambda~5~-phosphahexacosan-19-yl (7Z,10Z,13Z,16Z,19Z)-7,10,13,16,19-docosapentaenoate (7Z,19R,25S)-22,25,26-Trihydroxy-22-oxido-16-oxo-17,21,23-trioxa-22lambda~5~-phosphahexacos-7-en-19-yl (7Z,10Z,13Z,16Z)-7,10,13,16-docosatetraenoate (7Z,21R,27S)-24,27,28-Trihydroxy-24-oxido-18-oxo-19,23,25-trioxa-24lambda~5~-phosphaoctacos-7-en-21-yl (5Z,8Z,11Z,14Z)-5,8,11,14-icosatetraenoate (9Z,21R,27S)-24,27,28-Trihydroxy-24-oxido-18-oxo-19,23,25-trioxa-24lambda~5~-phosphaoctacos-9-en-21-yl (5Z,8Z,11Z,14Z)-5,8,11,14-icosatetraenoate (6Z,9Z,21R,27S)-24,27,28-Trihydroxy-24-oxido-18-oxo-19,23,25-trioxa-24lambda~5~-phosphaoctacos-6,9-dien-21-yl (5Z,8Z,11Z)-5,8,11-icosatrienoate (6Z,9Z,21R,27S)-24,27,28-Trihydroxy-24-oxido-18-oxo-19,23,25-trioxa-24lambda~5~-phosphaoctacos-6,9-dien-21-yl (8Z,11Z,14Z)-8,11,14-icosatrienoate	C44H77O10P	M+H+Na	8.67E-05	+ 101.94	Yes*
11.92_355.1779m/z	Biocytin	C16H28N4O4S	M+H-H2O	8.90E-05	- 73.45	Yes*
18.17_189.1640m/z	2-Methyl-1,3-cyclohexadiene 5,6-dihydrotoluene	C7H10	2M+H	1.00E-04	- 20.41	No
11.87_220.1836n	1,1,4,7-Tetramethyl-1a,2,3,5,6,7,7a,7b-octahydro-1H-cyclopropa[e]azulen-7-ol (3R,4aS,8aR)-1,1,3,6-Tetramethyl-3-vinyl-3,4,4a,7,8,8a-hexahydro-1H-isochromene (3Z,7Z)-1,5,5,8-Tetramethyl-12-oxabicyclo[9.1.0]dodeca-3,7-diene (4Z,7Z)-1,5,9,9-Tetramethyl-12-oxabicyclo[9.1.0]dodeca-4,7-diene 4,5-Epoxy-4,11,11-trimethyl-8-methylenebicyclo[7.2.0]undecane; 4-Nonylphenol (2Z)-2-Methyl-5-[(1S,2R,4R)-2-methyl-3-methylenebicyclo[2.2.1]hept-2-yl]-2-penten-1-ol	C15H24O	M+H-H2O, M+H	1.08E-04	- 332.30	Yes
20.36_103.0531m/z	4-Methylbenzaldehyde Phenylacetaldehyde 4-Vinylphenol	C8H8O	M+H-H2O	1.40E-04	- Infinity	Yes
21.35_365.1978m/z	(1S,2S)-1-(4-Methoxyphenyl)-1,2-propanediol 7a-Hydroxy-3,6-dimethyl-5,6,7,7a-tetrahydro-1-benzofuran-2(4H)-one 2-Ethoxy-4-(methoxymethyl)phenol Ethyl vanillyl ether	C10H14O3	2M+H	1.61E-04	- 475.24	No
11.85_221.2273m/z	Octadiene	C8H14	2M+H	1.62E-04	- Infinity	Yes
8.30_214.1121m/z	N-(3-oxo-hexanoyl)-homoserine lactone	C22H32N2O5	M+H	1.73E-04	+ 62.49	Yes*
4.99_184.0978m/z	Pantothenic acid	C10H13N5O	M+H-2H2O	1.83E-04	+ 36.42	No
11.83_184.1465n	10-Hendecenoic acid 10-Undecenoic acid 3-Acetoxy-1-nonene Allyl octanoate (3Z)-3-Octen-1-yl propionate trans-2-Hexenyl valerate trans-2-Hexenyl Isovalerate Methyl decenoate 2,3-Undecanedione	C11H20O2	M+H- 2H2O, M+Na, M+H-H2O	1.91E-04	- 159.43	Yes*
12.18_424.3173n	Unoprostone isopropyl ester	C25H44O5	M+H-H2O, M+Na	1.92E-04	+ 32.08	Yes*
6.60_626.3352m/z	(5 $\alpha$ ,7 $\alpha$ )-17-(Cyclopropylmethyl)-7-(2-hydroxy-3,3-dimethyl-2-butanyl)-6-methoxy-18,19-dihydro-4,5-epoxy-6,14-ethenomorphinan-3-yl $\beta$ -D-glucopyranosiduronic acid	C35H49NO10	M+H-H2O	1.97E-04	+ 40.91	Yes

**Table C.5.** Truncated tentative annotations of the 30 most significant compounds (passed on p-value) in a pairwise comparison of DIO and GB-IL<sub>dist</sub> in positive ion mode. Annotations are made based on accurate mass and fragmentation and compared to online databases. Features with positive fold changes are higher in the control, while negative fold changes denotes features that are higher in the experimental group. Infinity signifies that the feature is detectable in one sample group and undetectable in the other. The MSMS column indicates if the molecule did or did not have fragmentation spectra associated with it (Yes/No). Yes\* denotation means some fragments are consistent with, but not indicative of, metabolite identity.

Compound	Description	Formula	Adducts	Anova (p)	Fold Change	MSMS
1.22_251.0231m/z	3-Acetylthiophene; 5-Methyl-2-thenaldehyde; 2-Acetylthiophene	C6H6OS	2M-H	6.87E-08	+ 269.50	Yes*
4.11_315.1347m/z	N-[4-(5-Amino-2,2-dimethyl-4-oxo-3,4-dihydro-2H-chromen-6-yl)-1-hydroxy-4-oxo-2-butanyl]acetamide	C17H22N2O5	M-H2O-H	1.11E-06	+ 105.27	No
21.81_389.3523m/z	2-Methyltetracosane	C25H52	M+K-2H	4.25E-06	+ 138.87	Yes*
2.09_317.2252m/z	6,10,14-Trimethyl-2-methylenepentadecanal	C19H36O	M+K-2H	2.26E-05	+ 70.17	Yes*
21.79_457.2570m/z	6-O-[Bis(diisopropylamino)acetyl]hexonic acid; (3S)-3-[(2E)-2-Butenoxy]-4-(trimethylammonio)butanoate	C20H40N2O8	M+Na-2H	3.36E-05	+ 46.88	Yes
6.19_591.3181m/z	GPSer(17:2/5:0); GPSer(18:2/4:0); GPSer(2:0/20:2); GPSer(20:2/2:0); GPSer(4:0/18:2); GPSer(5:0/17:2)	C28H50NO10P	M-	1.14E-04	+ 201.62	Yes*
2.47_351.2171m/z	(5Z,9alpha,11alpha,13E,15S)-9,11,15,20-Tetrahydroxyprosta-5,13-dien-1-oic acid; (5R,6Z,8E,12R,14Z)-5,12,20,20-Tetrahydroxy-6,8,14-icosatrienoic acid; (5Z,9alpha,11alpha,13E,15S)-9,11,15,20-Tetrahydroxyprosta-5,13-dien-1-oic acid; (9alpha,11alpha,13E,15S)-9,11,15-Trihydroxy-6-oxoprost-13-en-1-oic acid	C20H34O6	M-H2O-H	1.17E-04	+ 19.82	Yes*
22.14_455.2468m/z	Butyl (9E)-18-(sulfoxy)-9-octadecenoate	C22H42O6S	M+Na-2H	1.32E-04	+ 157.58	Yes
20.19_453.2314m/z	2-amino-1,7,9-trimethylimidazo(4,5-g)quinoxaline	C12H13N5	2M-H	1.35E-04	+ 246.11	Yes
4.60_633.1983m/z	novobiocin; tetragastrin	C31H36N2O11	M+Na-2H	2.11E-04	+ Infinity	No
2.24_319.1658m/z	2-Oxoretinal; 3-[(1Z,5Z)-1-(4-Methoxyphenyl)-6-methyl-1,5,7-octatrien-4-yl]-2,2-dimethyloxirane; 3,4-Didehydroretinoic acid; Norethindrone	C20H26O2	M+Na-2H	2.69E-04	+ 42.30	Yea
4.14_465.3215m/z	PE(P-18:0/0:0)	C23H48NO6P	M-	2.81E-04	+ 25.10	Yes*
1.96_492.2463m/z	N-[4-(Hydroxymethyl)-3-[[4-(3-pyridinyl)-2-pyrimidinyl]amino]-1,5-cyclohexadien-1-yl]-4-[(4-methyl-1-piperazinyl)methyl]benzamide	C29H33N7O2	M-H2O-H	4.04E-04	+ Infinity	No
2.28_381.1124m/z	4-[2-(4-Allyl-2-methoxyphenoxy)-1-hydroxypropyl]-2-methoxyphenol; 4,4'-(3,4-Dimethyltetrahydrofuran-2,5-diyl)bis(2-methoxyphenol); (6E,10E)-6-Formyl-10-methyl-3-methylene-2-oxo-2,3,3a,4,5,8,9,11a-octahydrocyclodeca[b]furan-4-yl (2Z)-2-methyl-2-butenolate; 6-Hydroxy-6,9-dimethyl-3-methylene-2-oxo-2,3,3a,4,5,6,9a,9b-octahydroazuleno[4,5-b]furan-5-yl (2E)-2-methyl-2-butenolate; 12-Hydroxy-7,20-epoxyabieta-8,12-diene-11,14,20-trione	C20H24O5	M+K-2H	4.97E-04	+ 20.22	Yes
10.86_471.2418m/z	(3α,5β,7α)-7-Hydroxy-3-(sulfoxy)cholan-24-oic acid	C24H40O7S	M-H	5.86E-04	+ 38.61	Yes*
1.85_255.1112m/z	2-Oxo-1-pyrrolidinecarboxamide; Dihydrothymine; 3-Methyl-2,5-piperazinedione	C5H8N2O2	2M-H	5.96E-04	+ 16.46	No
6.90_593.3333m/z	GPSer(14:1/8:0); GPSer(15:1/7:0); GPSer(16:1/6:0); GPSer(17:1/5:0); GPSer(18:1/4:0); GPSer(2:0/20:1); GPSer(20:1/2:0); GPSer(4:0/18:1); GPSer(5:0/17:1); GPSer(6:0/16:1); GPSer(7:0/15:1); GPSer(8:0/14:1)	C28H52NO10P	M-	7.29E-04	+ 3238.95	No
22.16_435.2754m/z	5-Methoxydimethyltryptamine; 4-[2-(Propylamino)ethyl]-1,3-dihydro-2H-indol-2-one	C13H18N2O	2M-H	7.35E-04	+ 51.69	Yes*
9.58_471.3111m/z	(3Z,7Z)-1,5,5,8-Tetramethyl-12-thiabicyclo[9.1.0]dodeca-3,7-diene; (3Z,7Z)-3,7,10,10-Tetramethyl-12-thiabicyclo[9.1.0]dodeca-3,7-diene; 5-Isopropyl-2-methyl-8-methylene-11-thiatriacyclo[5.3.1.0~2,6~]undecane	C15H24S	2M-H	7.37E-04	+ 17.85	Yes*
15.70_407.3646m/z	(+)-S,S-Ethambutol; 7-Isopropyl-1,4-dimethyl-1,2,3,4,5,6-hexahydroazulene;	C10H24N2O2	2M-H	7.50E-04	+ 46.41	Yes*

	2,4-Diisopropenyl-1-methyl-1-vinylcyclohexane; 2-Methyl-3-methylene-2-(4-methyl-3-penten-1-yl)bicyclo[2.2.1]heptane; 3,7,11,11-Tetramethylbicyclo[8.1.0]undeca-2,6-diene; 1,4,4-Trimethyl-8-methylene-1,5-cycloundecadiene; 1-Isopropyl-3a-methyl-6-methylenedecahydrocyclopenta[3,4]cyclobuta[1,2]cyclopentene; 4-Methylene-1-(6-methyl-5-hepten-2-yl)bicyclo[3.1.0]hexane; 1-Methyl-4-(6-methyl-6-hepten-2-yl)-1,4-cyclohexadiene					
6.21_469.2263m/z	7-Sulfocholic acid	C24H40O8S	M-H2O-H	7.63E-04	+ 31.68	yes
5.31_438.1952m/z	(1S,9S)-9-{{(2S)-1-Ethoxy-1-oxo-4-phenyl-2-butanyl}amino}-10-oxooctahydro-6H-pyridazino[1,2-a][1,2]diazepine-1-carboxylic acid	C22H31N3O5	M+Na-2H	8.54E-04	+ 17.20	Yes
12.93_810.5273n	(2R)-3-[(Hydroxy{[(1s,3R)-2,3,4,5,6-pentahydroxycyclohexyl]oxy};phosphoryl)oxy]-1,2-propanediyl dihexadecanoate	C41H79O13P	M-H, M+Na-2H	9.68E-04	+ 76.54	Yes*
22.54_531.3549m/z	Desipramine; (18E)-18-Ethylidene-8,14-diazapentacyclo[9.5.2.0~1,9~.0~2,7~.0~14,17~]octadeca-2,4,6-triene	C18H22N2	2M-H	1.08E-03	+ 11.38	Yes*
1.77_351.2171m/z	(5Z,8S,9R,10E,12S)-8-Acetyl-9-formyl-12-hydroxy-5,10-heptadecadienoic acid; (5Z,8beta,11beta,12alpha)-11-Hydroxy-9,15-dioxoprost-5-en-1-oic acid; (5R,6R,7E,9E,11Z)-5,6-Dihydroxy-15-oxo-7,9,11-icosatrienoic acid; (5R,6R,7E,9E,11Z,13E,15R)-5,6,15-Trihydroxy-7,9,11,13-icosatetraenoic acid; Prostaglandin H2; Prostaglandin D2; 15-dehydro-prostaglandin E1; 15-oxo-prostaglandin F2alpha; (9alpha,11alpha,13E,15S)-9,11,15-Trihydroxy-6-oxoprost-13-en-1-oic acid; (5Z,9alpha,11alpha,13E,15S,17Z)-9,11,15-Trihydroxyprosta-5,13,17-trien-1-oic acid	C20H32O5	M-H	1.14E-03	+ 13.09	Yes
18.23_389.2693m/z	12-Ketodeoxycholic Acid; 2-[(8E)-8-Heptadecen-1-yl]-4,6-dihydroxybenzoic acid	C12H38O4	M-H	1.14E-03	+ 29.50	Yes*
2.26_255.1516m/z	(3E,7Z)-4,8,12-Trimethyl-1,3,7,11-tridecatetraene; 1,2-Dimethyl-4-[(4E)-6-methyl-4-hepten-1-yl]-1,3-cyclohexadiene	C16H26	M+K-2H	1.15E-03	+ 31.66	No
2.17_381.2278m/z	Sarcostin	C21H34O6	M-H	1.20E-03	+ 19.62	Yes*
7.75_591.3186m/z	3-[2-[[[3-(2-carboxyethyl)-5-[(3-ethyl-4-methyl-5-oxo-1,2-dihydropyrrol-2-yl)methyl]-4-methyl-1H-pyrrol-2-yl]methyl]-5-[(4-ethyl-3-methyl-5-oxo-1,2-dihydropyrrol-2-yl)methyl]-4-methyl-1H-pyrrol-3-yl]propanoic acid	C33H44N4O6	M-H	1.20E-03	+ 700.46	Yes*
6.11_471.2403m/z	1,4-Anhydro-6-O-dodecanoyl-2,3-bis-O-(2-hydroxyethyl)-D-glucitol	C22H42O8	M+K-2H	1.23E-03	+ 14.08	Yes*

**Table C.6.** Tentative annotations of the 30 most significant compounds (based on p-value) in a pairwise comparison of DIO and GB-IL<sub>dist</sub> in negative mode. Annotations are made based on accurate mass and fragmentation and compared to online databases. Features with positive fold changes are higher in the control, while negative fold changes denotes features that are higher in the experimental group. Infinity signifies that the feature is detectable in one sample group and undetectable in the other. The MSMS column indicates if the molecule did or did not have fragmentation spectra associated with it (Yes/No). Yes\* denotation means some fragments are consistent with, but not indicative of, metabolite identity.

**Table C.7.** Affected pathways as predicted with *Mummichog*

GB-IL <sub>dist</sub> Pathway Analysis				
Pathway	Overlap	Pathway Size	P-Value	Mode
Arachidonic acid metabolism	68	71	2.91E-03	+
Prostaglandin formation from arachidonate	56	61	2.91E-03	+
C21-steroid hormone biosynthesis and metabolism	74	86	2.91E-03	+
Bile acid biosynthesis	52	59	2.91E-03	+
Vitamin A (retinol) metabolism	34	36	2.91E-03	+
Leukotriene metabolism	47	53	2.91E-03	+
Putative anti-Inflammatory metabolites formation from EPA	21	22	2.99E-03	+
Vitamin E metabolism	29	35	3.53E-03	+
Linoleate metabolism	17	19	3.80E-03	+
Androgen and estrogen biosynthesis and metabolism	52	69	4.14E-03	+
Vitamin D3 (cholecalciferol) metabolism	10	10	4.26E-03	+
Drug metabolism - cytochrome P450	29	37	4.96E-03	+
Carnitine shuttle	19	23	5.28E-03	+
Fatty acid activation	16	20	8.85E-03	+
Bile acid biosynthesis	31	42	2.57E-03	-
Prostaglandin formation from arachidonate	32	49	3.40E-03	-
Leukotriene metabolism	28	42	3.42E-03	-
Linoleate metabolism	12	15	3.66E-03	-
GB-IL <sub>prox</sub> Pathway Analysis				
Pathway	Overlap	Pathway Size	P-Value	Mode
Vitamin E metabolism	15	34	2.27E-03	+
Vitamin D3 (cholecalciferol) metabolism	5	10	3.83E-03	+
Bile acid biosynthesis	15	53	4.13E-03	+
Carnitine shuttle	7	23	8.81E-03	+
TCA cycle	3	4	2.71E-04	-
De novo fatty acid biosynthesis	5	15	2.78E-04	-
Fatty acid activation	4	13	5.01E-04	-
Bile acid biosynthesis	8	44	5.48E-04	-
Fatty Acid Metabolism	3	7	5.62E-04	-
Vitamin E metabolism	5	28	1.86E-03	-
Glycerophospholipid metabolism	4	20	2.11E-03	-
Glycosphingolipid metabolism	4	20	2.11E-03	-
Xenobiotics metabolism	3	15	5.55E-03	-

APPENDIX D  
CURRICULUM VITAE

**James C. Poland, Ph.D.**

Vanderbilt University Department of Chemistry  
7330 Stevenson Center, Station B 35-1822  
Nashville, TN, 37235  
Lab: (615)343-4563  
j.c.poland@vanderbilt.edu  
jcpoland06@gmail.com

**Education**

**Vanderbilt University**  
Ph.D. in Chemistry

Nashville, TN  
Expected May 2020

Dissertation: Method Development towards Probing the Gut Metabolome using Reverse Phase  
Liquid Chromatography - Ion Mobility - Mass Spectrometry  
Advisor: Dr. John A. McLean

**Fisk University**  
Masters of Art in Chemistry

Nashville, TN  
July 2013

Thesis: Synthesis and Characterization of Functional Polymers for Tissue Engineering and  
Fuel Cell Applications  
Advisor: Dr. Natalie Arnett

**Delaware State University**  
Bachelors of Science in Chemistry  
Advisor: Dr. Peter DiMaria

Dover, DE  
December 2008

**Research Experience**

**Graduate Research Assistant**  
*Vanderbilt University, Nashville, TN*  
Advisor: Dr. John A. McLean

August 2013-May 2020

Development of separation technologies for the simultaneous analysis of various biological class  
in metabolomic studies with applications in gut microbiome studies.

**Graduate Research Assistant**

August 2011-June 2013

*Fisk University, Nashville, TN*

Advisor: Dr. Natalie Arnett

Synthesis and characterization of functional polymers with tissue engineering and hydrogen fuel cell applications

**Research Assistant**

January 2008- July 2011

*Delaware State University, Dover, DE*

Advisor: Dr. Peter DiMaria

In vivo biochemical characterization of a potential *Antonospora locustae* tgs1 gene**Independent Undergraduate Research**

August 2006 – June 2007

Advisor: Dr. Preston Hayward

Determination of equivalent weight of Nafion before and after use to determine rate of degradation

**Publications:**

- 4 **James C. Poland**, Katrina L. Leaptrot, Stacy D. Sherrod, C. Robb Flynn, and John A. McLean, “Collision Cross Section Conformational Analysis of Bile Acids via Ion Mobility-Mass Spectrometry,” Submitted to *Journal of the American Society for Mass Spectrometry*, **2020**
- 3 **Poland, J. C.**; Schrimpe-Rutledge, A.; Sherrod, S. D.; Flynn C. R.; McLean, J. A. “Utilizing an Untargeted Ion Mobility-Mass Spectrometry Method to Profile Changes in the Gut Metabolome after Biliary Diversion Surgery,” *Analytical Chemistry*, **2019**
- 2 Morris, C. B.; **Poland, J. C.**; McLean, J. A. “Fundamentals of Ion Mobility-Mass Spectrometry for the Analysis of Biomolecules.” *Methods in Molecular Biology*, Giuseppe Astarita and Giuseppe Paglia, Eds. Springer Nature, **2020**, Chapter 1, page 1-34
1. Norris, J. L.; Farrow, M. A., Gutierrez, D. B.; Palmer, L. D.; Muszynski, N.; Sherrod, S. D.; Pino, J. C.; Allen, J. L.; Spraggins, J. M.; Lubbock A. L. R.; Jordan, A., Burns, W.; **Poland, J. C.**; Romer, C.; Manier M. L.; Nei, Y.; Prentice, B. M.; Rose, K. L.; Hill, S.; Van de Plas, R.; Tsui, T.; Braman, N. M.; Keller, M. R.; Rutherford, S. A.; Lobdell, N.; Lopez, C. F.; Lacy, D. B.; McLean, J. A.; Wikswo, J. P.; Skaar, E. P.; and Caprioli, R. M. “Integrated, High-Throughput, Multiomics Platform Enables Data-Driven Construction of Cellular Responses and Reveals Global Drug Mechanisms of Action.” *Journal of Proteome Research*, **2017** 16 (3), 1364-1375

**Presentations****Orals**



6. **Poland J. C.**; Schrimpe-Rutledge, A. C.; Flynn, C. R.; McLean, J. A. “Utilizing an Untargeted Ion Mobility-Mass Spectrometry Method to Profile the Gut Microbiome” Vanderbilt Institute of Chemical Biology Student Research Symposium, Nashville, TN (August 2017).
5. **Poland J. C.**; McLean, J. A. “Metabolomic Analysis of Lung Epithelial Cells using Ion Mobility-Mass Spectrometry” 3rd Annual Bridge Research Celebration Day, Nashville TN. (August 2015)
4. **Poland, J. C.**; Zlibut, E.; Arnett, N. “Synthesis and Characterization of novel xylitol based elastomers for tissue engineering.” 244th ACS National Meeting & Exposition, Philadelphia PA (August 2012)
3. **Poland, J. C.**; Muller, J.; DiMaria, P. “The in vivo biochemical characterization of a potential *Antonospora locustae* tgs1 gene.” Louis Stokes, AMP Annual Symposium for the Greater Philadelphia Region, Philadelphia, PA (August 2010)
2. **Poland, J. C.**; DiMaria, P.; “A Microsporidial Protein is an Enzyme that Hypermethylates RNA Cap Structures.” Leadership Alliance National Symposium, Philadelphia, PA (July 2008)
1. **Poland, J. C.**; Morgan, E.; Hayward, P. “The determination of the equivalent weight of Nafion before and after use.” Leadership Alliance National Symposium, Philadelphia, PA (July 2007)

## Posters

15. Poland, J. C.; Brooks, A. W.; Sherrod S. D.; Bordenstein, S. R.; McLean, J. A. “Towards developing a multiomic approach to understanding human gut-microbe interactions” 66th Conference on Mass Spectrometry and Allied Topics, San Diego, CA (June 2018)
14. Poland, J. C.; Schrimpe-Rutledge, A. C.; Flynn, C. R.; McLean, J. A. “Utilizing an Untargeted Ion Mobility-Mass Spectrometry Method to Profile Changes in the Gut Metabolome” 65th Conference on Mass Spectrometry and Allied Topics, Indianapolis, Indiana (June 2017).
13. Gant-Branum, R.; Sherrod, S. D.; Codreanu, S. G.; Schrimpe-Rutledge, A. C.; Poland, J. C.; Holman, J.; Muszynski, N.; Pino, J. C.; Romer, C. E.; Allen, J. L.; Caprioli, R. M.; McLean, J. A. “Rapid Threat Analysis- A workflow to support metabolomics analysis of a cell’s response to an unidentified toxin in 30 days” 65th Conference on Mass Spectrometry and Allied Topics, Indianapolis, Indiana (June 2017).
12. Poland, J. C.; Schrimpe-Rutledge, A. C.; Flynn, C. R.; McLean, J. A. “Mass Spectrometry Based Metabolomics Targeting Changes in Fecal Bile Salt Concentration” Vanderbilt Institute of Chemical Biology Student Research Symposium, Nashville, TN (August 2016)

11. Poland, J. C.; McLean, J. A. "Profiling the Gut Microbiota Metabolome using HPLC coupled to Ion Mobility-Mass Spectrometry" AbbVie Analytical Research Symposium, North Chicago, IL (August 2016)
10. Poland, J. C.; Schrimpe-Rutledge, A. C.; Flynn, C. R.; McLean, J. A. "Profiling the Gut Microbiota Metabolome using HPLC couple to Ion Mobility-Mass Spectrometry to study Obesity." 10th Annual q-bio Conference, Nashville TN, (July 2016).
9. Poland, J. C.; Schrimpe-Rutledge, A. C.; Flynn, C. R.; McLean, J. A. "Profiling the Gut Microbiota Metabolome using HPLC couple to Ion Mobility-Mass Spectrometry to study Obesity." 64th Conference on Mass Spectrometry and Allied Topics, San Antonio TX (June 2016).
8. Morris, J. L.; Farrow, M. A., Gutierrez, D. B.; Palmer, L. D.; Muszynski, N.; Sherrod, S. D.; Pino, J. C.; Allen, J. L.; Spraggins, J. M.; Lubbock A. L. R.; Jordan, A., Burns, W.; Poland, J. C.; Romer, C.; Manier M. L.; Nei, Y.; Prentice, B. M.; Rose, K. L.; Hill, S.; Van de Plas, R.; Tsui, T.; Braman, N. M.; Keller, M. R.; Rutherford, S. A.; Lobdell, N.; Lopez, C. F.; Lacy, D. B.; McLean, J. A.; Wiksw, J. P.; Skaar, E. P.; and Caprioli, R. M. "Data-driven construction of global drug mechanisms enabled by an integrated high-throughput multi-omics platform." 64th Conference on Mass Spectrometry and Allied Topics, San Antonio TX (June 2016).
7. Poland, J. C., Keller, M. R.; Sherrod, S. D.; Mclean, J. A. "Metabolomic Analysis of Lung Epithelial Cells using Ion Mobility-Mass Spectrometry" Vanderbilt Institute of Chemical Biology Student Research Symposium, Nashville TN. (August 2015)
6. Poland, J. C.; Keller, M. R.; Sherrod, S. D.; Mclean, J. A. "Metabolomic Analysis of Lung Epithelial Cells using Ion Mobility-Mass Spectrometry" 2015 Chemistry-Biology Interface Career Development Conference, Nashville TN. (August 2015)
5. Poland, J. C., Keller, M. R.; Sherrod, S. D.; Mclean, J. A. "Metabolomic Analysis of Lung Epithelial Cells using Ion Mobility-Mass Spectrometry" 63rd American Society for Mass Spectrometry Conference on Mass Spectrometry and Applied Topics, St. Louis MO (May 2015).
4. Keller, M. R.; Poland, J. C.; Goodwin, C. R.; Sherrod, S. D.; McLean, J. A. "Development of a Targeted Metabolomics Protocol for Rapid Profiling of Mechanism of Action." Vanderbilt Institute of Chemical Biology Student Research Symposium, Vanderbilt University, Nashville TN, (August 2014)
3. Luitel, K.; Poland, J. C.; Arnett, N. "The Synthesis and Characterization of Disulfonated Bis[4(3-aminophenoxy)phenyl] sulfone Polyamide Copolymers for proton Exchange Membrane Fuel Cells." 16th Annual Fisk Research Symposium, Fisk University, Nashville TN. (April 2014)

2. Poland, J. C.; Zlibut, E.; Luitel, K.; Odiase, P.; Arnett, N. "The polymerization of Sulfonated Poly (aryl ether sulfone) copolymers with applications in Hydrogen Fuel Cells." 15th Fisk Annual Research Symposium, Fisk University, Nashville TN, (April 2013)
1. Poland, J. C.; Zlibut, E.; Arnett, N. "Novel Xylitol-based biodegradable polymers for Tissue Engineering." 14th Fisk Annual Research Symposium, Fisk University, Nashville TN (April 2012)